GENE THERAPY ADVANCEMENTS IN MURINE PHENYLKETONURIA (PKU)

By

Daelyn Yvonne Richards

A DISSERTATION

Presented to the Department of Molecular & Medical Genetics

and the Oregon Health & Science University

School of Medicine

in partial fulfillment of

the requirements for the degree of

Doctor of Philosophy

August 2020

School of Medicine

Oregon Health & Science University

CERTIFICATE OF APPROVAL

This is to certify that the PhD dissertation of

Daelyn Y. Richards

has been approved

_____

Mentor/Advisor

_____

Member

_____

Member

_____

Member

_____

Member

Table of Contents

Index of Figures

Index of Tables

List of Abbreviations

+ CNTL	Positive control
2n	Diploid genome
4n	Tetraploid genome
5-HTP	5-hydroxytryptophan
5’ UTR	5’ untranslated region of a gene
8n	Octoploid genome
AAAH	Aromatic amino acid hydroxylase
AAP	AAV assembly activating protein
AAV	Adeno-associated virus
AAV2	AAV serotype 2
AAV2/8_Ex7RepairTemp_U6G1	AAV8 capsid packaged with AAV2 genome containing *Pah* exon 7 repair template and a human U6 pol III promoter driving expression of guide 1
AAV2/8 LSPmPAHfs	Recombinant AAV2/8 containing LSP driving expression of murine PAH containing a frameshift mutation
AAV5	AAV serotype 5
AAV8	AAV serotype 8
AAV8-LSP-FLAG-PAH	AAV8 packaged with LSP driving murine PAH
AAV9	AAV serotype 9
ABI	Applied Biosystems
ADA	Adenosine deaminase

ADHD	Attention deficit hyperactivity disorder
AGMO	Alkylglycerol monooxygenase
AIDS	Acquired immunodeficiency syndrome
Ala	Alanine
Alb	Murine albumin gene
Alt-EJ	Alternative end joining
ANOVA	Analysis of variance
Arg	Arginine
BBB	Blood brain barrier
BD	Bile duct of hepatic lobule
BH_4	Tetrahydrobiopterin
bp	Base pairs
BSA	Bovine serum albumin
BTBR	Black and Tan Brachyury T+ *Itpr3tf/*J mouse strain
C^{14}-Phe	Phe containing radionuclide carbon-14
cAMP	Cyclic adenosine monophosphate
Cap	AAV capsid proteins
Cap	Capsid genes in AAV genome
Cas	CRISPR associated proteins
CAR	Chimeric antigen receptor
CCR5	C-C motif chemokine receptor 5
cDNA	Coding DNA
CEHPOBA	4-[(2-carboxyethyl)-hydroxyphosphinyl]-3-oxobutyrate

cGMP	Casein glycomacropeptides
C-HA-PAH	C-terminal HA tagged PAH
chr	Chromosome
COSMID	CRISPR off-target sites with mismatches, insertions, and deletions
CMV	Cytomegalovirus promoter
cPKU	Classical PKU defined as blood Phe: >1200 μM
CRISPR	Clustered regularly interspaced short palindromic repeats
crRNAs	CRISPR-RNAs
C-terminal	Carboxyl (COOH) terminus
CV	Central vein of hepatic lobule
D-98S	Human sternal bone marrow cells
dAAV	Dual AAV treatment group receiving an AAV8 expressing *Sp*Cas9 enzyme and an AAV8 containing the *enu2* repair template and guide 1
dAAV+Van	Dual AAV plus vanillin treatment group receiving an AAV8 expressing *Sp*Cas9 enzyme, an AAV8 containing the *enu2* repair template and guide 1, as well as vanillin administration
DAPI	4',6-diamidino-2-phenylindole
D-loop	Displacement loop in DNA
DNA	Deoxyribonucleic acid
DNAJC12	Human DNA J-domain containing protein member C12 gene
DNAJC12	DNA J-domain containing protein member C12

DSB	Double-strand DNA break
EC	Enzyme Commission
ENU or enu	N-ethyl-N-nitrosourea
ERT	Enzyme replacement therapy
EU	European Union
FAH	Fumarylacetoacetate hydrolase
Fah$^{\Delta exon5/\Delta exon5}$	HT1 model mice with homozygous FAH knockout alleles containing a neomycin-expression cassette inserted into the *SphI* restriction enzyme site in *Fah* exon 5
Fah$^{-/-}$	FAH deficient mice
FDA	Food and Drug Administration
FLAG	Sigma Aldrich trademark name for the DYKDDDDK peptide
FLAG-PAH	FLAG peptide on C-terminal PAH
GAPDH	Glyceraldehyde 3-phosphate dehydrogenase
GCH1	GTP cyclohydrolase 1 gene
GFP	Green fluorescent protein
GR	GeneRide^{TM} system trademarked by Logic Bio Therapeutics
GR+UHS	GeneRide^{TM} plus universal hepatocyte selection
GRCm38	*Mus musculus* (house mouse) genome assembly GRCm38 (mm10) from Genome Reference Consortium
GT	Gene therapy
HA	Hepatic arteriole of hepatic lobule

HA	Hemagglutinin
HAT	Hypoxanthine aminopterin thymidine
HDR	Homology directed recombination
HEK293	Human embryonic kidney 293 cells
HGPRT	Hypoxanthinephosphoribosyl transferase
HIV	Human immunodeficiency virus
H+L	Heavy and light immunoglobulin chains
HPA	Hyperphenylalaninemia
HPPD	4-hydroxyphenylpyruvate dioxygenase
HR	Homologous recombination
H.R. 2587	House of Representatives bill # 2587
H.R. 2501	House of Representatives bill # 2501
HSP40	Heat shock protein family 40
HSP70	Heat shock protein family 70
HT1	Hereditary tyrosinemia type I
IEM	Inborn errors of metabolism
IgG	Immunoglobulin g
indels	Insertions or deletions
IQ	Intellectual Quotient
ITR	Inverted terminal repeats in AAV genome
IVS1	Intervening sequence (intron) 1 of a gene
kb	Kilobase
kDa	Kilodaltons

L	Levorotatory form of a molecule
LAT1	Large neutral amino acid transporter type 1
L-dopa or L-DOPA	Levodopa
LMO2	Human LIM domain only 2 oncogene
LNAA	Large neutral amino acids
LPLD	Lipoprotein lipase deficiency
LSP	Liver specific promoter
Lys	Lysine
M	Molar
mg	Milligrams
mg/dL	Milligrams per deciliter
Mild HPA	Hyperphenylalaninemia defined as blood Phe: 120-600 μM
Mild PKU	Mild PKU defined as blood Phe: 600-1200 μM
miRNA	MicroRNA
MIT	Massachusetts Institute of Technology
mL	Milliliters
MMLV	Murine leukemia virus
MNEA	Medical Nutrition Equity Act
MO	Missouri
MOPS	3-(N-morpholino) propanesulfonic acid
MS/MS	Tandem mass spectrometry
MVSC	Molecular Virology Support Core
MW	Molecular weight

NC	Complete genomic molecule in reference sequence
NEB	New England Biolabs
NGS	Next generation sequencing
N-HA-PAH	N-terminal HA tagged PAH
NHP	Non-human primate
NIH	National Institutes of Health
nm	Nanometer
NOS	Nitric oxide synthase
NPKUA	National PKU Alliance
NTBC	2-(2-nitro-4-trifluoromethylbenzoyl)-1,3- cyclohexanedione
N-terminal	Amino (NH_2) terminus
OHSU	Oregon Health & Science University
OMIM	Online mendelian inheritance in man
OTC	Ornithine transcarbamylase
P2A	Porcine teschovirus 2A self-cleaving peptide sequence
P1	Postnatal day 1
P3	Postnatal day 3
P3	Promoter 3
p.304-GFP	Plasmid #304 expressing GFP
PA	Phenylpyruvic acid or phenylpyruvate
pAAV2 LSP_N-HA-PAH	Plasmid containing AAV2 ITRs with LSP driving N-HA-PAH
pAAV2 LSP_C-HA-PAH	Plasmid containing AAV2 ITRs with LSP driving C-HA-PAH
PAGE	Polyacrylamide gel electrophoresis

PAH	Phenylalanine hydroxylase
PAH	Phenylalanine hydroxylase gene (human/simian)
Pah	Phenylalanine hydroxylase gene (mouse)
PAHdb	PAH database
Pah$^{\Delta exon1}$	Mutant PAH allele containing full knockout of *Pah* exon 1
Pah$^{\Delta exon1/\Delta exon1}$	Homozygous PAH ∆*exon1* mouse
Pah$^{+/+}$	WT mouse homozygous for two WT alleles
Pah$^{+/\Delta exon1}$	Heterozygous ∆*exon1* mouse containing a WT allele and a PAH ∆*exon1* allele
Pah$^{+/enu2}$	Heterozygous *enu2* mouse containing a WT allele and a PAH *enu2* allele
Pah^{enu1}	HPA mouse allele # 1 containing ENU-induced mutation in the *Pah* gene (p.V106A)
Pah$^{enu1/enu1}$	HPA mouse model containing homozygous *Pah enu1* alleles
Pah$^{enu1/enu2}$	HPA mouse model containing heteroallelic *Pah enu1* and *Pah enu2* alleles
Pah^{enu2}	HPA mouse allele # 2 containing ENU-induced mutation in the *Pah* gene (p.F263S)
Pah$^{enu2/enu2}$	HPA mouse model containing homozygous *Pah enu2* alleles
Pah^{enu3}	HPA mouse allele # 1 containing ENU-induced mutation in the *Pah* gene (frameshift)
PAL	Phenylalanine ammonia lyase
PAM	Protospacer adjacent motifs

PBS	Phosphate buffered saline
PBT	PBS containing Triton-X
PCBD	Pterin-4 alpha-carbinolamine dehydratase
PCR	Polymerase chain reaction
PEAR	Pair end read merger
PEG	Polyethylene glycol
PEG-PAL	PEGylated PAL
PEI	Polyethylenimine
Phe	Phenylalanine
PK	Protein Kinase
PKU	Phenylketonuria
pLSPmPAH	Plasmid containing LSP driving murine PAH expression
PMI	Personal molecular imager system from BioRad, Inc.
PMSF	Phenylmethylsulfonyl fluoride
PNA	Peptide nucleic acids
Pol III	RNA polymerase III
Pro	Proline
PTS	6-pyruvoyltetrahydropterin synthase
PV	Portal venule of hepatic lobule
QDPR	Quinoid dihydropteridine reductase
qPCR	Quantitative PCR
rAAV2/8_LSP_SpCas9	AAV8 capsid packaged with AAV2 genome containing LSP driving expression of *Sp*Cas9

rAAV2/8 PAH-GR+UHS	Recombinant AAV8 capsid packaged with AAV2 genome containing PAH cDNA in GeneRide™ with an intronic HPPD miRNA against HPPD for universal hepatocyte selection in tyrosinemic conditions
Rep	AAV replication regulatory proteins
Rep	Replication regulatory genes in AAV genome
RNA	Ribonucleic acid
RNAi	RNA interference
RNP	Ribonucleic acid-protein complex
rtAAV	Repair template AAV treatment group receiving an AAV8 containing the *enu2* repair template and guide 1
S.1194	Senate bill # 1194
SA	Succinylacetone
SCID	Severe combined immunodeficiency
SD	Standard deviation
SDS	Sodium dodecyl sulfate
SEM	Standard error of the mean
Ser	Serine
sgRNA	Single-guide RNA
*Sp*Cas9	*Streptococcus pyogenes* Cas9 enzyme
Spf^{ash}	Sparse fur-abnormal skin and hair mouse strain
SPR	Sepiapterin reductase
SSC	Saline sodium citrate

TALENs	Transcription-activator-like-effector nucleases
T-ALL	T-cell acute lymphoblastic leukemia
TE	Tris-ethylenediaminetetraacetic acid
TH	Tyrosine hydroxylase
TILs	Tumor infiltrating lymphocytes 37
TLC	Thin-layer chromatography
TMV	Tobacco mosaic virus
TPH	Tryptophan hydroxylase
tracRNA	Trans-activating CRISPR RNA
Trp	Tryptophan
TTRmin	Minimal transthyretin promoter
Tyr	Tyrosine
UC	University of California
UHS	Universal hepatocyte selection
USA	United States of America
USPTO	United States Patent and Trademark Office
UV	Ultraviolet radiation
μM	Micromolar
μm	Micrometer
Val	Valine
vg	Vector genomes
vg/dg	Vector genomes per diploid liver genome
vg/mL	Vector genomes per milliliter

VP	AAV viral proteins
WT	Wild type
ZFNs	Zinc finger nucleases

Acknowledgements

The story of phenylketonuria (PKU) is interwoven with persistent, strong-willed parents, talented physicians, and innovative scientists that worked in concert to create a world where people born with PKU have a chance at experiencing life to its fullest. Without persevering mothers, dedicated physicians, and passionate scientists determined to execute early detection and effective treatments, functional children and adults living with PKU, and thriving, would not be possible. The work in this dissertation was only possible due to these continued efforts by parents, physicians, and scientists dedicated to furthering PKU research, in particular, the National PKU Alliance. The National PKU Alliance graciously funded this research, and hosted events including Lift the Limits for PKU in Denver, New York City, and Philadelphia in which I was able to share this research with the PKU community, as well the 5th annual National PKU Conference in Atlanta and the Patients and Providers for Medical Nutrition Equity advocacy efforts in Washington D.C. I would personally like to thank three amazing women at the NPKUA: Executive Director Christine S. Brown, who I bunked with at my first-ever PKU Family Camp; Event and Development Coordinator Michelle Pernsteiner, who has personally worked with me on each of the Lift the Limits events I spoke at and become a dear friend; and Registry Coordinator Eileen Blakely, who bunked with me at my fifth PKU Family Camp. I would also like to acknowledge friends and acquaintances from Lift the Limits events: Alison and Tia Reynolds; Dick and Ginny Michaux; Emele, Adam, and Breeze Porter; Michelle, Lucy, Lilly, and Lucas Moffett-Francis; Kathy and Emma Friedl; the entire Heffernan family, and Scott and Jane Pelley.

In addition to the NPKUA, I thank PKU Northwest (PKUNW), which helped me create my own family within the PKU community at PKU Family Camp. In particular I thank the following folks whom I consider my dearest of friends:

The Haber Family- Jeb, Kellie, Max, Owen, and Olive

The Wilkinson Family- Renee, Jay, Juniper, River, and Fox

The Beazer Family- Jenn, Xavier, and Cruz

The Chamberlin Family- Sarah, Zoe, and Izzy

The Stewart Family- Jennifer, Rilynn & Laila Stewart

The Christenson Family- Jennifer, Blaine, Owen & Emery

The Hobbs Family- Michelle, Jeremy, Tilden & Jameson Hobbs

Dan and Sam Petersen

Lauren and Adam Read

Brenda Winiarski (Cook 4 Love)

Sarah Chamberlin, Jenn Beazer, and Michelle Hobbs (How Much Phe)

Lillian Isabella and Sophia Rodriguez

Kurt Sensenbrenner

I thank the PKU Organization of Illinois for letting me share this research with their local PKU community and who welcomed me with open arms. In particular I extend a special thanks to Danae Bartke, the Kowalczyk family, and the glorious Dr. Barbara Burton.

I am so blessed to have found my path in graduate school and am committed to spending my life bettering the world for people with rare disorders. In the next chapter of

my career development at the Elson S. Floyd College of Medicine, I have continued to share my passions for rare disorders and will continue to do so as President of the Washington State University National Organization of Rare Disorders student chapter, “Students for Rare.” At this point in time, my career trajectory includes the pursuit of a joint residency program in pediatric genetics, so I may serve the rare disorders community as a physician scientist.

In addition to the PKU community, I express my gratitude to the following scientific entities for publishing this research: Molecular Therapy: Methods & Clinical Development, Molecular Genetics & Metabolism, the American Society of Gene and Cell Therapy, the Society for Inherited Metabolic Diseases, and the Japanese Society for Inherited Metabolic Diseases. In particular, I thank Dr. Georgianne Arnold for travelling with me to Japan for JSIMD, taking me on some side adventures to tour Hiroshima and Miyajima island, and sharing her intimate knowledge of metabolic genetics with me over a special meal of authentic Japanese cuisine.

I also thank my friends and family that supported me throughout this journey. From my best friend, Angelia Smith, PA, who has always been there for me since we were partners in molecular biology lab uncovering the identity of our mystery bug, *Serratia marcescens*; my anatomy and physiology professor, Dr. Edward DeGrauw, who believed in me and inspired me to pursue my dreams; and my undergraduate research mentor, Dr. Deborah Lutterschmidt, who fueled my passion for research and infused me with confidence to pursue graduate school. During graduate school, I thank Greg Lange

and his family for their support. I appreciate the travels around the globe and the home across the river with, at times, seven dogs, known to the neighborhood as “Camas kennels.”

From the heavens and stars above, I envision my father, Dr. Glen Richards, who inspired my love for science, looking down upon me and beaming with pride for the person I have become. And here and now, I recognize that my mother, Dr. Sue Richards, who passed her passion for rare disorders to me, has everything to do with my path into the field of molecular genetics. She has supported me through all of my ups and downs in life and molded me into the strong woman I am now. To both of my parents, I am forever grateful.

Most recently and excitingly, I acknowledge Alexander Germain, who has been a profound and positive force in my life. His example inspires me to be the best version of myself- to work harder than I ever have before, to think outside the box with double loop thinking, and to keep digging, reading, and researching ways to implement new technologies in ways that others have yet to dream about. He is a ray of light in my life, and he has inspired me to become a better person, both professionally and personally.

To Alex, you have my deepest gratitude, admiration, and my heart.

Cordelia the “pig dog” and I love you dearly.

This list of recognitions would not be complete without mention of my real life superheroes- Dr. Brené Brown, Justice Ruth Bader Ginsburg, and Dr. Jennifer Doudna.

I recognize Dr. Brené Brown, whose work helped me transform my life in ways I never thought were possible. She inspires me to dare greatly, emotionally and intellectually, to live a bold, audacious, and enriching life in the arena. I recognize the late Justice Ruth Bader Ginsburg who was a leader of women's rights. Without her efforts I would not be in the position I am today pursuing a career as a woman physician scientist. Finally, I recognize Dr. Jennifer Doudna who recently won the Nobel Prize and has been an inspiring strong woman scientist in the field of gene editing for me to look up to and aspire to work with one day.

Lastly, I express thanks to Oregon Health & Science University, the Program in Molecular and Cellular Biology, including previous director and first year mentor Dr. Cheryl Maslen, and the Department of Molecular and Medical Genetics, including the Chair, Dr. Susan Hayflick and the graduate directors Dr. McCullough and Dr. Dai. I thank my entire Dissertation Advisory Committee for providing me guidance and supporting all of my dreams. I personally thank the Chair, Dr. John Brigande, who steered the committee and my graduate education with diligence and grace, and took time out of his day to enjoy coffee with me on many an occasion at the Hatfield Cafe. I acknowledge Dr. Markus Grompe for inspiring many of the experiments I pursued throughout graduate school with several of his impressive technological advancements to the field of metabolic gene therapy. In Harding Lab, I cannot put into words the appreciation I have for my "sub-mentors," Shelley Winn and Sandra Dudley, who not only taught me all the ins and outs of surgical and molecular techniques, but also shared simple pleasures of life with me through dining out and daytime workouts.

Additionally, I would like to thank the entire Gillingham Lab, particularly Dr. Melanie Gillingham, who has been a co-mentor and friend every step of the way, as well Garen Gasten and Tiffany DeVine who supported my efforts.

Most of all, I express my deepest gratitude to my inspiration, my hero, my mentor, Dr. Cary Harding. He took me in when I was a shell of my former self and fostered a safe, positive, and encouraging space for me to heal, grow, and flourish. He spent countless hours coaching me, teaching me, and motivating me to be stronger, smarter, and braver so I could face the scientific community (and life!) with confidence and self-assurance. I am indebted to Dr. Harding for his sublime mentorship, which I believe is a reflection of his truly genuine, self-sacrificing, and virtuous nature. Dr. Harding is the reason I have blossomed into the well-rounded, compassionate, and resilient scientist I am today.

This personally owned picture is of Dr. Cary Harding (left) and myself (right) showing our support for “Advancing the Dream for PKU” at the 2017 Fifth Annual National PKU Alliance Conference in Atlanta, Georgia.

Dissertation Abstract

The main focus of this dissertation work was to advance gene therapy research for phenylketonuria (PKU). PKU is an inborn error of metabolism characterized by phenylalanine hydroxylase (PAH) deficiency that results in severe neurological damage if left untreated. PAH functions in the liver to metabolize the essential amino acid phenylalanine (Phe), which is taken up in excess through dietary means. The standard of care for PKU is a highly restricted diet that is void of Phe that one must adhere to for life, however the diet is challenging for all and unrealistic for most. The PKU community has voiced their desire for the development of a gene therapy that would, in essence, be a one-time curative treatment for their disease, allowing for a completely liberated diet without the devastating neurological consequences. Currently, preclinical adeno-associated virus (AAV) mediated PKU gene addition therapy is very promising, with robust and long-term results in adult mice, but the effects are ultimately temporary. The work in this dissertation was aimed at addressing the temporary nature of gene addition therapy by performing genomic manipulations using multiple strategies, with the most success achieved by employing gene editing with the CRISPR/Cas9 system. However, the results were difficult to interpret, as the significant amount of DNA correction and PAH enzyme activity did not lead to the expected normalization of Phe levels. Unfortunately these curious results could not be evaluated further due to the limitations of the longstanding classical PKU mouse model, *Pah*$^{enu2/enu2}$. This model expresses abundant albeit inactive PAH that dampens overall wild type PAH activity through the dominant negative effect phenomenon, lowering gene therapy efficacy *in vivo*, and furthermore, the mutant PAH is cross reactive with PAH antibodies, making immune-

based experiments to quantify and localize gene therapy derived wild type PAH through western blot and immunohistology impossible. It would thus be ideal to have a PKU model that is completely void of PAH protein expression to effectively test and properly analyze different PKU gene therapy approaches. This was the impetus for the generation of a classical PKU knockout mouse presented in this dissertation. Overall, this dissertation has led to the advancement of PKU gene therapy by testing two novel PKU genome editing approaches and generated a superior model with which to test preclinical PKU gene therapy that will be available for academic and industry scientists around the globe.

CHAPTER 1: Introduction

Phenylketonuria

a. Preface: Inborn Errors of Metabolism

The history of our understanding of human metabolic disorders begins at the turn of the twentieth century when physician biochemist, Sir Archibald Garrod, demonstrated that abnormal metabolism, which he theorized was the result of a metabolic block in the body caused by a defective enzyme, could be passed down in a hereditary fashion within families. Garrod's theory of human metabolism came from his research on alkaptonuria, a rare metabolic disorder that was discovered in the mid-1800s due to the unusual feature of blackened oxidized urine. At first, physicians believed it was an atypical form of diabetes, as the urine reduced in Fehling's solution, typically indicating the presence of glucose, yet the Nylander reaction (bismuth hydroxide test) was negative for presence of reducing sugars. It was noted that the oxidation in the Fehling's test was pronounced in the presence of the alkaline reagent, potassium hydroxide. The highly oxidative nature of this mysterious non-sugar compound in alkaline solution led to the term Alkapton, derived from Greek participle "to suck up [oxygen] greedily" and Arabic "alkali" [in alkaline solutions], which was observed to behave similar to hydroxyphenols like pyrogallol and quinone. Eventually the compound was identified as 2,5-dihydroxyphenylacetic acid, or homogentisic acid. The urinary excess of homogentisic acid was postulated to be a product of protein putrefaction in the gut, however, Garrod had other ideas.

During a series of Croonian Lectures to the Royal College of Physicians in London, Garrod described the complexities of human metabolism as an interconnected web containing series of enzymes that served distinct and critical roles in altering molecular components of complex molecules:

"The conception of metabolism [is] gaining ground that each successive step in the building up and breaking down, not merely of proteins, carbohydrates, and fats in general, but even of individual fractions of proteins and of individual sugars, is the work of special enzymes set apart for each particular purpose [1]."

Garrod predicted that the darkened urine was due to a metabolic defect of the aromatic amino acid oxidation of phenylalanine and tyrosine, causing an abnormal buildup of the metabolite homogentisic acid. His first clue was that the condition seemed to be related to diet, as it took fifty-two hours after birth before the blackened urine appeared, which he predicted was likely due to the time necessary for metabolic products to accumulate after orally-derived nutrition. In order to rule out the previous prediction that elevated homogentisic acid was due to gut protein putrefaction, Garrod performed urine studies in a patient after feeding intervals. The study found that the elevation in homogentisic acid occurred seven hours after a meal, indicating that absorption of tyrosine from the diet preceded the conversion of it to homogentisic acid by the body's metabolism, verifying a defect in metabolism. Garrod was able to link a pathological finding to this disease, ochronosis, which is a build-up of homogentisic acid in cartilage,

causing discoloration and hardening of connective tissues within the body. Finally, through studying family pedigrees, Garrod observed that this rare condition occurred more frequently in families with marriages between first-cousins, that the parents of the affected individuals did not exhibit any of the symptoms of the condition, and through discussions with Mendel advocate William Batesman, determined this condition was genetic in nature, transmitted through a recessive inheritance pattern. Garrod compiled his findings in the first published account of recessively inherited metabolic disorders in humans in 1908 describing alkaptonuria, albinism, cystinuria, and pentosuria [1, 2]. He collectively termed these types of disorders inborn errors of metabolism (IEM), which are characterized by recessive transmission of a genetic defect of a single enzyme that results in abnormal metabolism which may be detected in urine, modified by diet, and cause distinct disease characteristics [1, 3, 4].

b. History of PKU

Phenylketonuria (Online Mendelian Inheritance in Man [OMIM] #261600) is among one of the most common IEMs and was discovered by a talented biochemist, Ivar Asbjørn Følling of Oslo, Norway, in 1934 [5, 6]. He was approached by a persistent mother of two severely mentally impaired children, whose husband was a former pupil of Følling's, that was convinced there was an underlying cause to her children's condition. The children, aside from their mental state, presented with spastic extremities, fair skin, and a musty odor in their urine. Følling performed a routine urine test for ketones using ferric chloride, which resulted in an abnormal deep green coloring. This was unusual as the test was only known to turn red-brown in the absence of ketones or purple in the presence of ketones. Using classical organic chemistry techniques (see description below), and 20 liters of the children's urine, Følling found the children excreted high levels of phenylpyruvic acid (PA).

In an interview with Dr. Victoria Cass, Director of Maternal and Child Health for the state of Massachusetts, he describes his discovery:

"I started by isolating the compound in oxygen-rich conditions, which resulted in a black substance at the bottom of my dish, so I knew the substance had been oxidized during the extraction. I repeated the isolation in nitrogenous conditions, and with the pure product, performed organic chemical analysis for the elementary formula, which I found to be C-9, H-8, O-3. I added a weak oxidizing

reagent and found evidence of benzoic acid and oxonic acid, which told me the molecular structures of a benzene ring, a side chain of at least three carbons, and a ketone. Putting it all together, I surmised the mysterious compound in the children's urine was none other than phenylpyruvic acid, which I confirmed with a melting analysis [7]."

To determine if there was a correlation between this finding and the mental impairment, Følling tested urine from 430 patients in mental institutions, 8 of which also had this unusual high level of PA. In his publication of these observations, he suggested the cause of the excess PA was due to a "metabolic block," as Garrod described for alkaptonuria, but in this case referring to the inability to properly metabolize the essential amino acid phenylalanine and titled the disease *imbecillitas phenylpyrouvica* [5, 8]. Another observation he considered noteworthy was that of the 8 individuals with high PA, 3 were sets of sibling pairs from parents that were close relatives, leading to the suspicion of a recessive inheritance pattern of this disease. Følling set out to confirm the metabolic block of phenylalanine and inheritance pattern with biochemical techniques. He developed an assay to perform phenylalanine challenges on blood samples, which confirmed both the metabolic block was the inability to metabolize phenylalanine, and that parents of affected children were carriers of the disease [9-12].

Although Følling made a breakthrough regarding the identification of this disease, which was referred to as Følling's Syndrome in Norway, it was George Jervis, a scientist that "dedicated his life on the problems of developmentally disabled individuals and brought compassion and relief to them and their families [13]," that discovered the cause was due to a mutated liver enzyme responsible for hydroxylating phenylalanine into tyrosine. He accomplished this through rather straight forward experiments showing elevation of tyrosine in blood of normal patients after administration of phenylalanine, whereas PKU patients had no tyrosine response, and confirmed these findings in post-mortem liver samples [14-16]. He went on to show the aberrant metabolic products were not only present in urine, but also in the blood, and developed an assay that was not only able to detect PKU in patients, but also sensitive enough to determine carriers of the disease by focusing on blood tyrosine at various intervals following a Phe bolus challenge of 2 mmoles/kg [17-19].

While Følling and Jervis were committed to unravel the biochemical and genetic nature of Følling's Syndrome, research to identify an effective treatment began with Lionel Penrose, who was the first to coin the term phenylketonuria (PKU) in 1935 [20]. Penrose hypothesized that since PKU was due to a metabolic block of phenylalanine, the restricted dietary intake of protein should ameliorate the devastating neurological consequences of the disease. He implemented a diet that consisted solely of sugar, fruit, oil, and vitamins in PKU patients and monitored their urine with the ferric chloride test. He was excited that the diet was

beginning to show improvement in the urine test, but unfortunately his diet led to malnutrition and the breakdown of muscle mass into endogenous amino acid pools including phenylalanine, worsening the results of the urine test, and the theory of a Phe-restricted diet was, for the moment, abandoned [15]. It would be another decade before an effective treatment was discovered.

Once again, it took the persistence of a mother of a mentally impaired child diagnosed with PKU to motivate a German scientist, Horst Bickel, to implement a novel therapy for her child. It started with the research of a talented chemist, Louis Woolf, who worked at the Hospital for Sick Children in London researching ways to isolate amino acids from milk to feed starving Europeans during World War II. During his time at this hospital he encountered children with PKU and took an interest in the biochemical abnormalities of the disease [21]. In 1951, Woolf and Vulliamy reported a similar idea as Penrose about the potential of "restricting the phenylalanine intake in the diet to the basic minimum early in life," for the treatment of PKU [22]. With all of his training in nutrition and isolating various components of milk, Woolf was able to develop a source of dietary protein that was free of Phe by performing acid hydrolysis of casein followed by treatment with activated charcoal to remove phenylalanine, referred to as Woolf's formula. Unfortunately, the physicians at his institution, the Great Ormand Street Hospital, refused to test his formula on PKU patients. Two years later, Horst Bickel wrote to Woolf requesting the Phe-free hydrolysate recipe, who along with collaborators John Gerrard and Evelyn Hickmans, implemented Woolf's formula

and recorded its effects on 8mm film in some troubling studies performed on a 2-year old phenylketonuric child named Sheila at the Birmingham Children's Hospital [23-25]. In their studies, the child was placed on a Phe-restricted diet for nine months, in which her mental state dramatically improved. Then, without the consent of the mother, the group placed the child on 4 mg of phenylalanine a day (essentially regular milk) as morning outpatient procedures with the goal of illustrating the effectiveness of the diet. Within a few days the child deteriorated quickly and reverted back to her prior catatonic state, which again, was captured on film. When the Phe-restricted diet was reimplemented, the child's catatonic-like state was alleviated, leading to the incontrovertible evidence of the effectiveness of a Phe-restricted diet for the treatment of PKU.

With the advent of an effective treatment, the next hurdle became how to treat patients before irreversible neurological damage occurred. Willard Centerwall, inspired by the loss of his second son to birth defects and severe mental impairment, was determined to design a method for early detection. He was a physician at the College of Medical Evangelists and played a central role in implementing the PKU diaper test, which was an adaptation of the urine ferric chloride test that led Asbjørn Følling to the discovery of PKU.

Centerwall describes the test in a correspondence to the editor of the Journal of the American Medical Association (JAMA):

"The test consists of placing a drop of 10% solution of ferric chloride on a freshly wet diaper. A positive reaction is the almost immediate appearance of a dark blue-green color. The test is positive in affected infants from about 4 weeks of age on," as Centerwall describes in 1957 after positively identifying two PKU children at 6-7weeks of age in the greater Los Angeles area. He goes on to say that, *"We believe, and hope that it will be proved, that this simple and extremely inexpensive test should be a routine well-baby examination in the early months of life [26]."*

By the late 1950s, the PKU diaper test was implemented throughout the United States, for newborns as well as mentally disabled people. Around this time, a famous author, Pearl S. Buck, published a book titled, "The Child Who Never Grew," about her mentally impaired child. In the book, her daughter was undiagnosed and eventually institutionalized for severe mental impairment. It was not until her daughter was an adult that she was tested and received a positive result from one of these PKU tests. Unfortunately, due to her daughter's advanced age, irreversible neurological damage had already occurred, and she required lifelong institutionalization. When Willard Centerwall visited Pearl Buck in 1960, she reiterated the words from her book written years earlier:

"What has been, need not forever continue to be so. It is too late for some of our children, but if their plight can make people realize how unnecessary much of the tragedy is, their lives, thwarted as they are, will not have been meaningless."

Between the development of an effective treatment and early detection with the diaper test, the prognoses for children identified with PKU in the first few months of life improved dramatically. However, it was found that by the time the phenylketones were high enough to detect with the diaper test, around 6-8 weeks, the infants were already showing signs of mental impairment. This is due to the toxic levels of phenylalanine disrupting proper brain development and function. While babies are born with most of their 85 billion neurons already generated, laying down the foundation of a functioning brain, the connections between neurons, also referred to as the connectome, is naïve. After birth, a phenomenon known as the “synaptic big bang” occurs, in which the number of neural connections explode for the first two years of life and then tapers off [27]. However brain development, including the fine-tuning of the connectome and myelination continues to occur throughout early adulthood. Unfortunately, high levels of Phe impair many of these processes, including of proper myelin and neurotransmitter production and neuronal maturation, which can collectively lead to gross abnormalities in the white and grey matter of the brain [28-30]. The next challenge became how to treat infants just after birth and before the irreversible brain damage ensued.

c. Newborn Screening

Robert Guthrie came from humble beginnings as he was raised during the thick of the Great Depression, an experience that taught him to persevere and overcome obstacles. Although he did not have the marks to attend university after high school, he was determined to continue his education and studied hard at the local college. Soon, he proceeded to medical and graduate school, where he earned six degrees in six years [31]. His career took him many directions, but the most noteworthy were his efforts for newborn screening for PKU and other IEMs. The motivation behind his work was personal. Guthrie and his wife, Margaret, had six children together, one of whom, John, was mentally disabled with a congenital undiagnosed illness. His niece, Margaret Doll, was diagnosed with PKU at 15 months of age and placed on a Phe-restricted diet, but unfortunately, irreversible neurological damage had already occurred. Inspired by his son and his niece, Guthrie sought to develop a test to detect PKU in newborn infants, as early treatment intervention was critical to prevent major neurological damage.

In order to implement a test, Guthrie knew it had to be feasible at a large scale, including factors such as time, resources, and overall benefit. He turned to affordable basic molecular biology techniques using the bacterium, *Bacillus subtilis*, in a simple bacterial inhibition assay. In this assay, an inhibitor, B2-thienyl-alanine, was added to the media to block bacterial growth in the absence of phenylalanine. Using small discs of filter paper with dried blood from PKU

patients, he found the inhibition could be overcome. The degree to which the bacteria grew outward from the disc indicated the level of phenylalanine in the sample (Figure 1-1). This simple, affordable bacterial inhibition assay became known as the Guthrie test [32, 33].

To assess the accuracy of his test, Guthrie implemented a trial run at a New York mental institution in which he was blind to the patient's medical records. His test accurately identified all patients known to have PKU and identified four more patients that had yet to be diagnosed. After this successful trial, Guthrie sought to start testing newborn infants. From 1961-1963, Guthrie tested 400,000 newborns, which resulted in the identification of 39 infants with PKU, and became the first-ever newborn screening method [33]. Soon thereafter, Carl Ashley, Chief of Maternal and Child Health for the state of Oregon, invited Guthrie to speak to the state public health laboratory. By 1963, Oregon (debatably) became the first state to implement and mandate newborn screening for PKU in all newborns (though Massachusetts claims to have also done so on the same exact day). The ease and benefits of this test were quickly appreciated as it expanded across the country and world. Over the next few decades metabolic tests were formed for other disorders, which were piloted in Oregon. Neil Buist, newborn screening advocate and director of the Pediatric Metabolic Laboratory at Oregon Health & Science University (OHSU), describes in an interview with The Oregonian newspaper:

"*Over the decades, as screening tests were developed for various disorders, Oregon was among the first states to add them. We became a testing ground, long before some other places in the country were even screening for PKU [34].*"

In the late 1990s, with the advent and ease of tandem mass spectrometry (MS/MS) to detect a multitude of disorders with dried blood spots, medically advanced countries, including the United States (U.S.), adopted this method to test for PKU and a wide array of other disorders for newborn screening [35]. On the horizon are efforts to implement massively highly paralleled next generation sequencing (NGS) from DNA isolated from dried blood spots. It has been suggested that this could replace MS/MS, though cost, false negatives, and the correlation of variants to biochemical phenotype remain a challenge [36, 37].

Figure 1-1: The Guthrie Bacterial Inhibition Assay

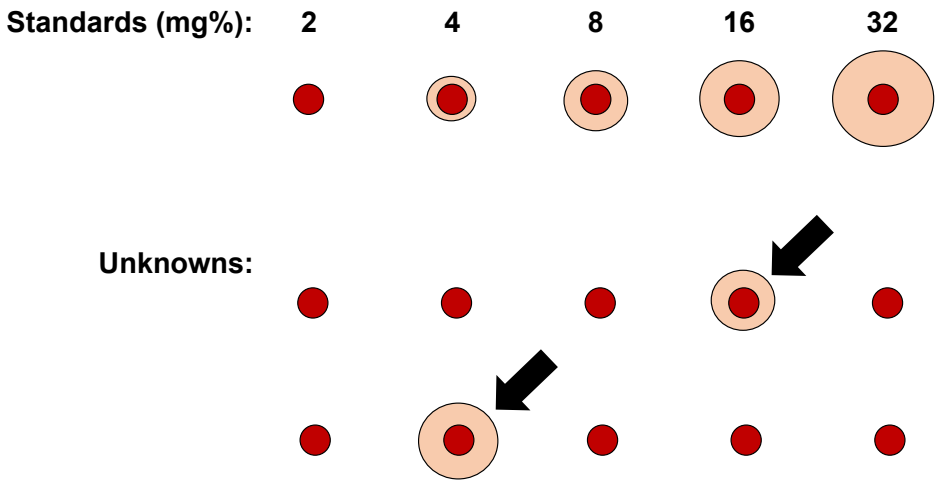

Figure 1-1: The Guthrie Bacterial Inhibition Assay.

The Guthrie test takes advantage of auxotrophic *Bacillus subtilis* bacteria that require phenylalanine for growth in the presence of B2-thienyl-alanine. In this test, the bacteria are spread on media containing the B2-thienyl-alanine growth inhibitor. A standard series of blood spots are made containing known amounts of Phe, ranging from 2 to 32 mg%, that allow growth of bacteria in diameters corresponding to the amount of Phe provided (top row). In unknown samples, like blood spots from newborn infants, the diameter of bacterial growth around a sample can be calculated for Phe concentration based on the standards, where larger diameters of growth indicate increasing elevations of blood Phe, and thus a positive newborn screening test for PKU (black arrows).

d. Maternal PKU Syndrome

While Phe-mediated damage is devastating to PKU individuals after birth, the effects are more pronounced if they occur during fetal development, even to healthy, non-PKU progeny, particularly if exposure occurs throughout the first trimester. The excess Phe exposure occurs when a mother with PKU has poor metabolic control, allowing for her high levels of phenylalanine to exert their teratogenic effects on the developing fetus, an unfortunate syndrome called maternal PKU. The chronic exposure of elevated Phe from maternal blood impairs fetal neurogenesis, brain and heart development, as well as placental transport of other essential amino acids required for proper fetal growth throughout all trimesters of gestation [38]. The pronounced effects of elevated maternal Phe during the first trimester on non-PKU fetuses are thought to be due, in part, to the fact that embryological development of the fetal liver has not yet occurred (not until 10 weeks), so the fetus has no protection from the insults of high Phe prior to that time.

Interestingly, Jervis was the first to point out this unusual observation of neonatal sequelae in PKU pregnancies from his studies back in 1937 [39], but it was not until two decades later that Charles Dent presented maternal PKU as a bonafide syndrome caused by high phenylalanine exposure during pregnancy at the Ross Pediatric Conference on the causative factors of mental retardation [40]. He concluded this from observations of Richards' studies at St. Lawrence Hospital, a mental asylum in Caterham, Surrey in England, describing a mentally impaired

PKU mother that had three children of unknown paternity with severe mental disability despite not having PKU [41]. The teratogenic effects of Phe were found to have striking similarity to those observed in fetal alcohol syndrome, including severe brain damage resulting in microcephaly and profound neurological impairments, as well as dysmorphic facial features and congenital heart defects [42].

This knowledge of maternal PKU inspired Neil Buist of OHSU to add a simple blood Phe test to the battery of tests for prenatal screening in the state of Oregon in 1975. Of 260,000 women screened, 9 were identified to have undiagnosed hyperphenylalaninemia, and despite intervention with a modest protein restricted diet in the first trimester, many of the children developed maternal PKU [43]. From 1984 to 2002, the international Maternal PKU Collaborative Study collected data regarding the impacts of maternal Phe on offspring, which indicated optimal outcomes as long as maternal Phe levels were between 120-360 µM by 8 to 10 weeks of gestation and throughout pregnancy [44]. However, the Charles Dent Metabolic Unit in London performed a similar study on maternal PKU cases in their care from 1977 to 2005 and concluded their strong recommendation for the prevention of maternal PKU syndrome to include maternal dietary restriction of Phe (below 300 µM) prior to contraception and throughout pregnancy [45].

e. Metabolism & Biochemistry

PKU is characterized by the inability to metabolize the essential amino acid phenylalanine [46] (Figure 1-2). The major enzyme involved with the metabolism of phenylalanine is the aromatic amino acid hydroxylase (AAAH) enzyme, phenylalanine 4-monooxygenase (Enzyme Commission [EC] 1.14.16.1), more commonly known as phenylalanine hydroxylase (PAH) [47]. Functional PAH is primarily found in the liver and secondarily in the kidney and gall bladder (Human Protein Atlas) [48], though other transcripts for PAH have been identified in the pancreas and brain [49]. PAH is translated as a monomer and requires co-chaperones DNA J domain containing protein member C12, (DNAJC12), a member of the heat shock protein 40 (HSP40) family, as well as Heat Shock Protein 70 (HSP70) for proper assembly into a homo-tetrameric holoenzyme complex in the cytoplasm [50]. Interestingly, biallelic mutations that disrupt DNAJC12 expression cause PKU-like syndrome called DNAJC12 deficiency (OMIM # 606060) that includes a wide range of similar symptoms including attention deficit hyperactivity disorder (ADHD), hyperphenylalaninemia (HPA), dystonia, and intellectual disability [51]. Conversely, overexpression of DNAJC12 has been linked with aggressive cancer types with poor prognoses [52, 53]. Like all AAAH enzymes, PAH also requires a catalytic non-heme ferrous iron, the co-factor tetrahydrobiopterin (BH_4), and molecular oxygen as an additional substrate for proper function [54]. Other enzymes that require BH_4 include alkylglycerol monooxygenase (AGMO), and nitric oxide synthase (NOS) [51]. Each region of the PAH enzyme plays a specific role; the N-terminal region contains the

regulatory domain (residues1-110), the central region contains the catalytic domain (residues 111-410), and the C-terminal region contains the oligomerization domain (residues 411-452) (Figure 1-3). The oligomerization domain assists in the assembly and structural integrity of the holoenzyme PAH complex, which is a combination of two dimer configurations to create a homo-tetramer. Ubiquitination is a negative mark of regulation, as it leads to protein degradation. Phosphorylation at amino acid residue serine (Ser)-16 by glucagon stimulated cyclic adenosine monophosphate (cAMP)-dependent Protein Kinase (PK) elicits an interaction of Ser16 with residues arginine (Arg)-13 and lysine (Lys)-14 that opens the active site, allowing for increased access of the substrate Phe [55]. Interestingly, Phe also acts as a positive regulator of PAH activity through allosteric interactions and activates PAH to metabolize excess Phe by the para-hydroxylation of L-Phe into L- tyrosine (Tyr) [47].

PKU is a unique biochemical disorder that affects the central nervous system, yet the site of defective metabolism is in the periphery- primarily the liver and secondarily in the kidney and gall bladder. In PKU, these peripheral tissues lack functional PAH and therefore the ability to metabolize excess Phe in the body. Phe accumulates in the blood and brain, causing devastating symptoms in the neurological system. There are no pathological consequences to the liver, kidney, or gall bladder. Within the brain, excess Phe causes notable hypomyelination, gliosis, neurotransmitter deficits, and gross abnormalities of grey and white matter tissue [28, 30] (Figure 1-4).

Without proper PAH function, a multitude of metabolic dysfunctions ensue, particularly that of the aromatic amino acids phenylalanine, tyrosine, and tryptophan (Trp), as their metabolism is intertwined. The most prominent abnormal metabolite results from transamination of phenylalanine to phenylpyruvate which is excreted in excess in urine, the original product isolated by Asbjørn Følling in 1934. While phenylpyruvate is readily excreted in the urine, at high levels it has the potential to accumulate in the brain and has been demonstrated to inhibit a plethora of brain enzymes that are critical for proper metabolism, including pyruvate kinase and hexokinase [56]. Other abnormal metabolites in the urine of individuals with PKU include p-hydroxyphenyllactate and p-hydroxyphenylacetate from further metabolism of phenylpyruvate [57, 58] and indolelactate, indolacetate, and indican from disruptions in tryptophan metabolism [59, 60]. The levels of tyrosine are generally low in PKU due to the lack of hydroxylation of Phe into Tyr. Tyr plays important roles in the body, including neurotransmitter production and melanin synthesis. In PKU, there is a lack of Tyr available for melanin synthesis due to the lack of PAH activity. Additionally, Phe inhibits tyrosinase activity, the rate limiting step of melanin production. Together, these lead to the characteristic hypopigmentation of skin, nails, and hair of people with PKU [61]. If left untreated, PKU causes severe neurological symptoms, including abnormal brain development, intellectual disability, psychiatric disorders, seizures, eczema, impaired melanogenesis, and a musty odor [46].

The exact molecular underpinnings of the pathology of PKU have been difficult to elucidate and remain unclear. Large Neutral Amino Acids (LNAA), including phenylalanine, tyrosine, tryptophan, isoleucine, leucine, methionine, threonine, and histidine, enter the brain through facilitated diffusion across the blood brain barrier (BBB) by the LNAA transporter 1 (LAT1) down their concentration gradient. Up until recently, it was widely accepted that in PKU, the high levels of Phe in the periphery saturate LAT1, resulting in an over-import of Phe and reduced import of other LNAA like Tyr and Trp, the precursors for the neurotransmitters dopamine and serotonin, respectively. It was long thought that this oversaturation of Phe on LAT1 was the cause of abnormal brain aromatic amino acid homeostasis, leading to the pathological disturbances in neurotransmitter production and hypomyelination [47]. However, there is a problem with this theory, as it assumes Phe only enters the brain through LAT1. It is known that LAT1 is saturated at normal physiologic LNAA plasma levels, yet in PKU, brain Phe never becomes fully saturated within the brain, as it continues to elevate as blood Phe elevates without an upper limit. It was recently shown that Phe-mediated disruption of LAT1 transport was not the source of pathology in PKU, as brain aromatic amino acid levels for Tyr and Trp were not different between PKU and wild type (WT) mice [28]. Rather it was found that Phe inhibition of tyrosine hydroxylase (TH) and tryptophan hydroxylase (TPH), the enzymes responsible for converting Tyr and Trp into dopamine and serotonin precursors levodopa (L-dopa) and 5-hydroxytryptophan (5-HTP), respectively, was the driving cause of neurological and behavioral deficits in PKU mice [28].

While further studies are warranted to validate competitive inhibition of Phe on TH and TPH, it is clear that HPA in the brain is associated with deficiencies in neurotransmitters, aberrant neuronal arborization and pruning during development, and abnormal white and gray brain matter in humans, even those that have metabolic control of their PKU with the Phe-restricted diet [62, 63].

All of these findings taken together lead to the unique and important observations regarding PKU biology that 1) a lack of Phe metabolism in the periphery (liver, kidney, and gall bladder) causes an accumulation of blood Phe and a lack of Tyr production; 2) Phe is the primary pathological molecule in PKU; and 3) the pathologic effects of Phe occur primarily in the brain, including hypomyelination and competitive inhibition of critical enzymes that produce neurotransmitters. The only effective mechanism to prevent the symptoms of PKU, and maternal PKU for that matter, are to simply lower phenylalanine levels in the body, which can be largely accomplished through diet.

Figure 1-2: Phenylalanine Metabolism in PKU

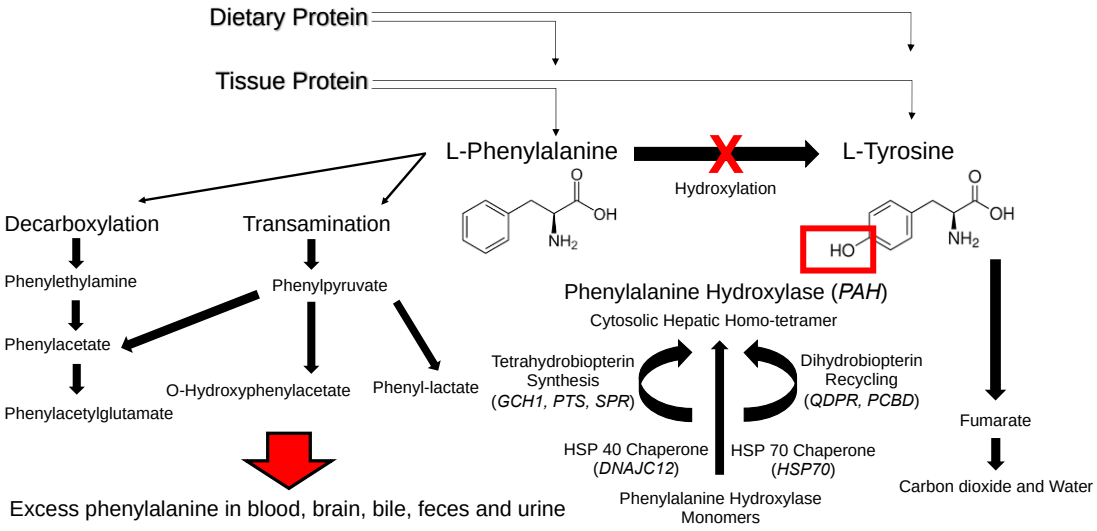

Figure 1-2: Phenylalanine Metabolism in PKU

Dietary and tissue protein contribute to the amino acid pools of phenylalanine and tyrosine within the body (indicated by arrows at top). PAH acts primarily in liver hepatocytes as PAH monomers come together into a cytosolic homo-tetramer, requiring the assistance from HSP70 and DNAJC12 for proper folding as well as the maintenance of the required co-factor tetrahydrobiopterin (BH_4) through synthesis (GCH1, PTS, SPR) and dihydrobiopterin recycling (QDPR, PCBD). PAH metabolizes excess phenylalanine by conversion to tyrosine through para-hydroxylation, which can then be further metabolized into Kreb's cycle intermediate fumarate until its full oxidation into the final products of carbon dioxide and water. When PAH function is disrupted, as in homozygous recessive or compound heterozygous inheritance of *PAH*, *DNAJC12*, or co-factor synthesis or recycling gene mutations, excess phenylalanine in the body accumulates. Excess Phe is either decarboxylated into phenylethylamine or undergoes transamination into phenylpyruvate. These metabolic products are further metabolized into other phenylketone bodies that are excreted at high levels in the urine, but also exist in high levels in the blood, brain, bile, and gastrointestinal tract.

Figure 1-3: PAH Structure

PAH Polypeptide Structure

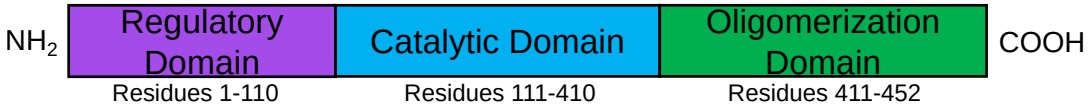

PAH Holoenzyme Structure & Regulation

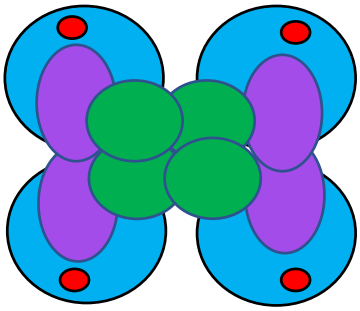

Negative regulation:

- Ubiquitination (protein degradation)
- Low Phe levels
- BH_4 (stabilizes low activity state)

Positive regulation:

- Phosphorylation at Ser16
- High Phe levels (allosteric activator)

Figure 1-3: PAH Structure

The PAH polypeptide contains three domains: the N-terminal regulatory domain (RD) that contains residues 1-110 (purple), the central catalytic domain (CD) that contains residues 111-410 (blue), and the C-terminal oligomerization domain that contains residues 411-452 (green). The tetrameric form illustrated is color coded according to domain, with an additional red dot to represent the iron molecule within the catalytic domain. Negative regulators of PAH activity include ubiquitination, low Phe levels, and BH_4 binding. Positive regulators include high phenylalanine levels and phosphorylation at residue Ser 16.

Figure 1-4: Pathology of PKU: Disruptions in Amino Acid Homeostasis

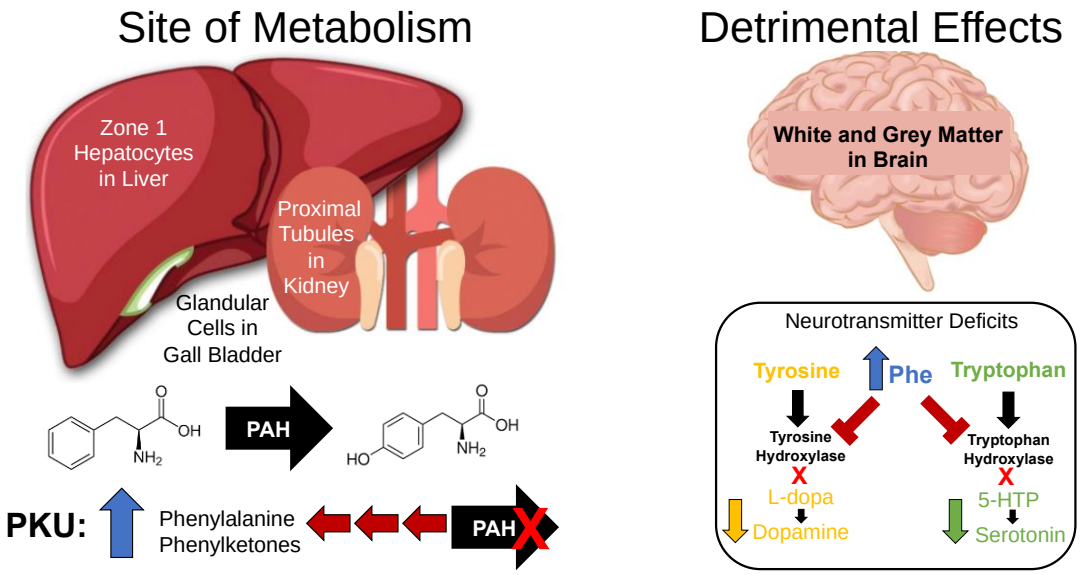

Figure 1-4: Pathophysiology of PKU

Phenylalanine is metabolized in zone 1 hepatocytes of the liver, proximal tubule cells in the kidney, and glandular cells in the gall bladder. PAH converts L-Phe into L-Tyr through para-hydroxylation. In PKU, PAH does not function properly (red X) which results in the accumulation (reverse red arrows) of Phe (upwards blue arrow) and various phenylketones like phenylpyruvate. The only organ that is adversely affected by this disruption in amino acid metabolism is the brain. LNAAs like phenylalanine, tyrosine, and tryptophan cross the BBB at the LAT1 receptor through facilitated diffusion. Brain amino acid pools are able to maintain homeostasis for LNAAs like Tyr and Trp, but not for Phe (upwards blue arrow). Phe inhibits (red stopper) tyrosine hydroxylase (TH) and (red stopper) tryptophan hydroxylase (TPH) that results in impaired ability (red Xs) to convert Tyr and Trp to levodopa (L-dopa) and 5-hydroxytryptophan (5-HTP) into dopamine and serotonin, respectively. With the impaired production of L-dopa and 5-HTP, dopamine (down green arrow) and serotonin (down yellow arrow) levels are reduced in the phenylketonuric brain.

f. Treatments

The Phe-restricted diet, which was first suggested by Lionel Penrose, generated by Louis Woolf, and successfully implemented by Horst Bickel and colleagues in the 1950s, was the first treatment for PKU. This low-Phe diet restricts most, though not all, natural sources of protein leaving primarily fruits and vegetables for safe consumption. It provides all amino acids except phenylalanine (though Woolf's formula was also low in tyrosine and tryptophan) and is notorious for being unpalatable and expensive, even today. While the Phe-restricted diet was originally thought to only be necessary from birth to around 6-10 years of age [64-67], the National Institutes of Health (NIH) announced the PKU Consensus Statement in 2000 for the standard of care for PKU to include adherence to this medical diet for life [68].

While the implementation of a Phe-free diet for the treatment of PKU has remained largely unchanged since the 1950s, there have been significant improvements to the diet itself. The PKU formula has been modified to address differing nutritional requirements throughout human development with specific formulas dedicated for neonatal, adolescent, and adult PKU, as well as modifications tailored for optimal vitamin and mineral supplementation and palatability. Most recently, the addition of casein glycomacropeptides (cGMP), a short peptide milk derivative formed during the process of making cheese, were included in PKU formula to improve palatability and satiety, as it contains little to no phenylalanine but provides more complex forms of polypeptides for the body

to digest than the synthesized mono amino acids in previous generations of the formula [69]. Medical foods void of Phe, like bread, pasta, and cheese, have been developed to expand and diversify the diet as well. Although there are many formula options today, with many flavors and even pill form, as well as the addition of low Phe medical foods, adherence to this demanding, complex, and arduous diet remains a challenge.

In the U.S., the reasons for impaired access to the medical diet and formula are complex, ranging from the shortage of specialized physicians, the lack of transportation to PKU clinics, and probably most notably, the cost, as the medical diet is expensive and third-party coverage is limiting [70]. This is in part due to the Food and Drug Administration (FDA) not having jurisdiction of medical foods, and therefore insurance companies do not deem this lifesaving diet a medical necessity. Each state has their own legislation regarding insurance coverage of medical foods resulting in disparate and complex issues for American families and adults with PKU. Since the early 2000s, the PKU community has been lobbying for the Medical Nutrition Equity Act (MNEA) (115th Congress S.1194/H.R.2587; 116th Congress H.R. 2501), a federal bill that would require insurance to cover the medical diet for PKU, other IEMs, and certain gastrointestinal (GI) disorders, and these efforts continue tirelessly today.

While the Phe-restricted diet has come a long way, efforts to pursue other therapeutic options for PKU has been long sought after. In the 1970s, with the

discovery of atypical PKU not caused by PAH deficiency [71-73], alternative therapies were attempted, including L-dopa, 5-HTP, and BH_4 administration [74, 75]. At that time, the cause of "PKU with no deficiency in phenylalanine hydroxylase" was unknown. One group, Bartholomé and Byrd, postulated that these individuals lacked the ability to turn brain tyrosine and tryptophan into their metabolic intermediates L-dopa and 5-HTP for the production of dopamine and serotonin, respectively [74]. Unfortunately, there were minimal, if any effects of these therapies in individuals with this atypical form of PKU. At the same time, another group, Danks, Cotton, and Schlesinger, postulated that it was due to a pterin-deficiency, and administered various forms of biopterin, orally and intravenously, to individuals with atypical PKU. Interestingly, the intravenous injection containing 5, 6, 7, 8,-tetrahydrobiopterin revealed marked reduction, down to normal, in the patient's serum Phe levels, and was the first clear indication that BH_4 functioned as a co-factor for PAH [76]. It is now known that atypical PKU is caused by deficiencies in the synthesis and recycling of BH_4, which is also referred to as BH_4-responsive PKU. While BH_4 supplementation showed great promise for individuals BH_4-responsive PKU, it would be another three decades before its debut into the clinic. In 2007, BH_4 therapy received orphan drug status and fast track designation for clinical trials for the orally active synthetic form of (6R)-L-erythro-5,6,7,8-tetrahydrobiopterin, also called sapropterin dihydrocholoride [77, 78]. In 2008 BioMarin, Inc. received FDA approval for the drug sapropterin dihydrochloride, trademarked Kuvan™, which has since shown efficacy in approximately 10% of the PKU community [79],

allowing for a completely unrestricted diet for some and more liberating diet in others.

While Kuvan™ greatly improved the quality of life for some patients with PKU, the latest and debatably the most exciting FDA approved therapy for PKU is an enzyme substitution therapy developed by BioMarin called Palynziq™. In this approach, a bacterial enzyme that metabolizes Phe, called phenylalanine lyase (PAL), converts Phe into cinnamic acid and ammonia, which is readily excreted by the body. In order to mask this foreign protein form immune-mediated degradation, it was modified to include polyethylene glycol (PEG) residues on the outer layer and referred to as PEG-PAL. PEG-PAL entered clinical trials the same year that Kuvan™ was approved and underwent several phases over the next decade before it was recently approved by the FDA in May 2018 and marketed as Palynziq™ [80]. In contrast with Kuvan™, Palynziq™ has the potential to be efficacious for all patients with PKU. The most common side effect is immune-mediated hypersensitivity responses to the foreign protein, despite PEGylation, including injection site inflammation, arthralgia, arthritis, and even anaphylaxis. Though still early in its dissemination, Palynziq™ has already made transformative impacts to patients all over the U.S., allowing many to go off dietary therapy completely. Some of the impacts include self-reported improvements in mental status, cognitive function, and darkening of skin and hair. Unfortunately for others though, the self-administered daily injections and immune reactions remain a barrier to therapeutic application and maintenance.

Despite the tremendous success of these novel therapies for some individuals, the majority of the PKU population remain reliant on the restrictive diet. While the diet is 'good enough' at alleviating the major neurological consequences of PKU, its highly restrictive nature is isolating and all-consuming, shackling patients from being able to live a free life to bond, celebrate, and enjoy day-to-day living with other people through the simple pleasures of food [81]. Nor does the diet fully prevent neurological sequelae including impaired executive functioning, emotional regulation, lower intellectual quotient (IQ), and abnormal brain white and gray matter, even when initiated early and continuously [29, 82, 83]. The PKU community wants and deserves better, and over 85% of the PKU community has voiced their desire for the development of a gene therapy treatment to cure PKU once and for all [81, 84].

g. Genetics

The genetics behind PKU research began in 1982 when Savio Woo and colleagues at the Baylor College of Medicine in Houston, Texas were able to successfully clone the human *PAH* gene [85] and subsequently sequence it in 1992 [86]. Charles Scriver of the DeBelle Laboratory for Biochemical Genetics at the McGill University-Montreal Children's Hospital spearheaded a database called PAH database (PAHdb), which curated the *PAH* variants submitted until the early 2000s [87, 88]. This wealth of information led to the better understanding of the molecular underpinnings of PKU, which turned out to be much more complex than originally anticipated.

The primary cause of PKU is homozygous or compound heterozygous mutations in the *PAH* gene, which is located on the long q-arm of chromosome 12 at position 23.2 (12q23.2) and contains 13 exons in *Homo sapiens*. To date, there are over 950 known pathogenic variants of *PAH*, most of which are missense, and most people with PKU, approximately 87%, are compound heterozygotes [46, 89]. The global incidence of PKU is 1 in 23,930 newborns, with the highest prevalence in European countries and lowest in Asian countries, as illustrated by the incidence of 1 in 4,000 in Italy and 1 in 227,273 in Thailand [90]. In the USA, the prevalence of PKU is 1 in 25,000 live births and in Canada it is 1 in 15,000 [90]. Mutations have been identified across the entirety of the *PAH* gene and have varying effects on residual PAH activity, with more BH_4-responsive phenotypes located in the oligomerization domain. While there is a rich diversity

of mutational burdens in the *PAH* locus, there are specific geographical regions and unmixed populations that are enriched for specific alleles. The most common allele, colloquially referred to as “R408W,” contains the mutation c.1222C>T (p.Arg408Trp) in the PAH catalytic domain and confers severe, classical PKU that accounts for approximately 50% of PKU alleles in Eastern Europe [46].

However, the complex PAH system can be affected by other genes as well. Those involved in the synthesis and recycling of BH_4, the required cofactor for PAH, as well as the newly discovered *DNAJC12* [54], a required co-chaperone for proper PAH folding, can also cause PKU. Which genes are affected and to what degree results in a wide spectrum of HPA ranging from mild HPA (blood Phe: 120-600 micromolar [μM]), mild PKU (blood Phe: 600-1200 μM) and the most severe, classical PKU (cPKU) (blood Phe: >1200 μM).

h. Animal Models

PKU research, particularly that of gene and cell therapeutic development, has taken place predominantly in mouse models of PKU. The *Pah* gene is located at chromosome 10 NC_000076.6 (87521795..87584137) in *Mus musculus*, containing 13 exons and 1.5 kilobases (kb) of coding DNA (cDNA). Three animal models of PAH deficiency, *Pah*$^{enu1/enu1}$, *Pah*$^{enu2/enu2}$, and *Pah*$^{enu3/enu3}$, were developed at the University of Wisconsin-Madison by Drs. David McDonald and Alexandra Shedlovsky in the laboratory of Prof. William Dove at the McArdle Cancer Institute through random N-ethyl-N-nitrosourea (ENU)-mediated mutagenesis screens on Black and Tan Brachyury T+ *Itpr3tf*/J (BTBR) mouse strains in the early 1990s [91].

Pah^{enu1} contains a missense mutation in exon 3 (p.Val106Ala) in the oligomerization domain that causes mild HPA and is BH_4 responsive. *Pah*^{enu2} allele contains a c.835T>C missense mutation (p.Phe263Ser) in exon 7 within the catalytic domain, which causes classical PKU and is not BH_4 responsive. The *Pah*^{enu3} allele is unfortunately no longer available due to breeding difficulties but contained a frameshift mutation that resulted in complete absence of liver PAH and recapitulated cPKU [92]. An additional model of PKU combines the *Pah*^{enu1} and *Pah*^{enu2} alleles as a heteroallelic *Pah*$^{enu1/enu2}$ model that recapitulates the compound heterozygosity of *PAH* mutations in humans, which occurs in approximately 87% of individuals with PKU [93, 94]. This model displays mild

HPA that is slightly more severe than *Pah*$^{enu1/enu1}$ and is significantly less BH_4-responsive, approximately 50% reduced [95].

Interestingly, other animal models of PKU do exist. Prior to the ENU-mediated generation of genetic PAH-deficient mice, scientists administered increased dietary Phe or injected bolus Phe, with or without the addition of chemical inhibitors of AAAH enzymes like p-chlorophenylalanine, to induce acute hyperphenylalaninemia to generate non-genetic rat and pig models of PKU [96, 97]. There are two independent groups attempting to develop porcine models of PKU: the Mayo Clinic is using TALENS to create a humanized model of the common cPKU allele p.Arg408Trp [98], and the Children's Hospital of Pittsburg is using the CRISPR system to generate a PAH knockout [99]. The latter group was able to successfully generate a knockout pig model that exhibited all of the human manifestations of cPKU including hyperphenylalaninemia, hypopigmentation, and abnormal grey matter of the brain, which will undoubtedly be an invaluable tool for the future development of novel therapies for PKU moving forward [100].

Excitingly, through some collaborative efforts with Dr. Betsy Ferguson at the OHSU Oregon National Primate Research Center, we were able to identify heterozygous carriers of PKU in the Oregon macaque colony. This effort started with Dr. Ferguson's Molecular & Medical Genetics Grand Rounds presentation of the Macaque Genotype and Phenotype (mGAP) resource, the purpose of which,

she explained, was to identify existing disease-causing alleles within the macaque colony in order to generate more non-human primate (NHP) models for scientific research. The mGAP project includes a database of whole genome sequencing of individual monkeys within the colony that is available to researchers, with lab approval. Scientists then have the unique opportunity to search all of their favorite disease-causing genes for the presence of pathogenic alleles in the colony that may not be otherwise apparent at the phenotypic level. This is due to the fact that carrier monkeys, in line with carriers of any recessive disorder, do not exhibit any manifestation of the disease, and are therefore indistinguishable from other monkeys in the colony. Out of pure curiosity, I searched the database for alleles carrying mutations in the *PAH* gene. I stumbled upon a suspicious variant and requested further evaluation with the Ferguson lab. Variant analysis confirmed the presence of an allele containing a known pathogenic human mutation p.Pro175Ser (c.523C>T) with a Combined Annotation Depletion Dependent (CADD) score of 32, indicating it is likely deleterious. While this was rather exhilarating, we wanted to confirm these findings at the molecular level. In addition to the whole genome sequencing, the mGAP project stores tissue samples from post-mortem animals that have undergone sequencing, so they were able to provide us blind samples of liver tissue from carrier animals and wildtype (WT) animals. I was able to perform a PAH enzyme activity assay on all of the samples and determine, with high accuracy, all of the carriers from WT animals by the marked reduction of PAH

enzyme activity in the p.Pro175Ser carriers (Figure 1-5), further confirming the pathogenicity of this allele.

The discovery of a non-human primate model of PKU has the potential to transform the world of PKU research, not only for the purposes of therapeutic development, but also to better our understanding of the pathophysiology of PKU. In terms of drug development, up to this point, all of the preclinical research for PKU has been produced in mice. While mice are useful for research purposes, from their high attrition rate, generally applicable biological mechanisms, and ease of care, they are limited in translatability. Phylogenetically, mice are 85% similar to humans, whereas NHP models, like the macaque, have 93% genetic similarity with humans [101]. At an organismal level, macaques have more anatomical, physiological, and pathophysiological similarities to humans than do mice. A NHP of PKU would provide an opportunity to better understand the molecular underpinnings of this disease, and in terms of pharmaceutical development, would have a higher predictability of clinical efficacy than rodent models [102].

Of all the existing animal models of PKU, the *Pah*$^{enu2/enu2}$ mouse model has been the most widely utilized for PKU research. It recapitulates classical PKU with toxic hyperphenylalaninemia that causes neurological damage, and due to this classical PKU phenotype, is the most ideal for testing novel therapeutics. If left untreated, brain Phe impairs cognitive and behavioral abilities, as well as proper

monoamine neurotransmitter production [28]. It is minimally Kuvan-responsive (restricted to brain monoamine neurotransmitter turnover restoration [103]) so it is less ideal for biopterin studies. Conveniently, the pigmentation of its fur coat is a indicator of internal Phe and Tyr levels that becomes hypopigmented under chronic hyperphenylalaninemic conditions, and conversely, dark under normal or chronic hypertyrosinemic conditions. Unfortunately, this model contains abundant levels of stable, nonfunctional PAH protein. This complicates the efficacy and molecular analyses of gene therapy studies because the mutant PAH binds with and lowers overall activity of the gene therapy derived WT PAH, a phenomenon known as the dominant negative effect, which results in an overall lower therapeutic efficacy. Additionally, the mutant PAH is readily detected by polyclonal anti-human PAH antibodies that are produced against the PAH residues 371 – 420, making post-gene therapy WT PAH quantification and localization analyses an impossible feat [91]. While this model of classical PKU has been the most popular for gene and cell therapeutic development due to the cPKU phenotype, challenges in gene therapy efficacy and post-therapy analyses remain a challenge.

Figure 1-5: Identification of a PKU Allele with Reduced Enzymatic Activity in the Oregon Macaque Colony

Mutation Data

DNA	**c.523C>T**
Protein	**p.Pro175Ser**
CADD score	**32**

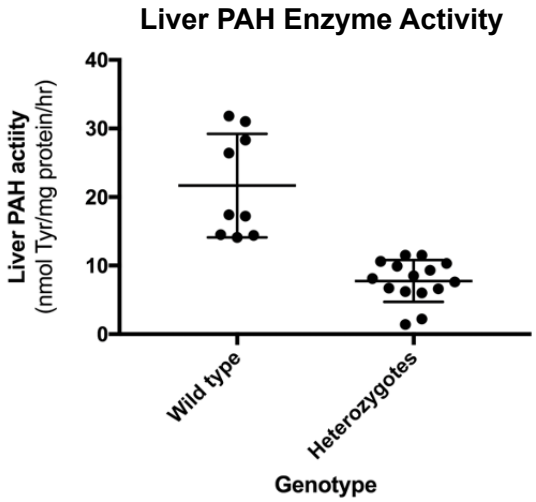

Figure 1-5: Identification of a PKU Allele with Reduced Enzymatic Activity in the Oregon Macaque Colony

Within the mGAP database, a p.Pro175Ser mutation was identified in the macaque colony that contained a c.523C>T point mutation in the *PAH* gene, with a CADD score of 32, indicating its highly likely pathogenicity. This was confirmed with liver PAH enzyme activity that revealed a significant reduction of Phe metabolism in heterozygous carriers (mean 7.76 nmol Tyr/mg protein/hour ± SEM 0.7853) compared to WT animals (mean 21.68 nmol Tyr/mg protein/hour ± SEM 2.516) in a one-tailed t-test ($p > 0.0001$).

Gene Therapy

a. Background

The field of gene therapy began before the identification of DNA as heritable information with the, at the time, perplexing phenomenon of the transforming principle described in Griffith's experiment in 1928. In these experiments, Dr. Frederick Griffith injected mice with a mixture of heat-killed virulent strains of bacterial pneumonia (smooth) with live non-virulent strains (rough) which resulted in death, indicating some sort of transfer between heat-killed virulent strains and live non-virulent strains [104]. It took almost two decades, in 1944, before DNA was identified as the molecule responsible for these curious results through an elegant experiment by Avery, McCloud, and McCarty in which they showed that the virulent strain only became transforming-defective in the presence of DNase [105]. This elucidated DNA as the responsible molecule for heritable and transferable information, which then led to the idea of genetic transfer.

Within a few years, the first viral gene transfer experimentation in bacteria was performed in 1952 by Lederberg & Zinder who discovered bacteriophage mediated gene transfer in *Salmonella typhimurium* and coined the term "transduction" to describe genetic unilateral transfer [106]. This in turn led to the birth of mammalian gene therapy a decade later with the first mammalian heritable gene transfer performed by Szybalski who showed D-98S hypoxanthinephosphoribosyl transferase (HGPRT)-deficient cells combined with HGPRT+ cells through somatic fusion and subsequent hypoxanthine aminopterin

thymidine (HAT) selection for successfully transformed cells conferred stable survival in HAT medium that persisted with future daughter cells [107, 108]. Dr. Szybalski's intent, even in 1962, was to pave the path towards human gene therapy to cure genetic diseases [109].

In 1968, Rogers & Pfuderer performed the first virus-mediated gene transfer using tobacco mosaic virus (TMV) containing poly-adenine-nucleotide sequences which resulted in the translation of poly-lysine peptides in Turkish tobacco plants [110]. Over the next two decades gene therapy progressed until its first application in the clinic by Dr. Rosenberg in 1989, who used *ex vivo* gene modified tumor infiltrating lymphocytes (TILs) as a cancer therapeutic for malignant melanoma [111-113].

The concept of gene therapy is quite elegant and simple: it is the use of nucleic acids as a drug. The U.S. FDA defines human gene therapy as "the modification or manipulation of the expression of a gene to alter the biological properties of living cells for therapeutic use" [114]. There are several types of gene therapy: gene addition therapy (add functional gene), gene editing (permanent modifications to the genome), RNA interference (RNAi) (inhibit gene expression), oncogenic viruses (cancer), Chimeric Antigen Receptor (CAR)-T cell therapy (cancer immunotherapy), and vaccines (dendritic cell manipulations), to name a few [115]. While gene therapy approaches are ample and in theory, capable of

treating any human disease of nucleic acid origin, implementing it to achieve therapeutic efficacy, let alone cure genetic diseases, is challenging.

One major hurdle to gene therapy is delivery. There are many ways to deliver genetic material to patient's cells: it can take place *in vivo*, within the patient's body, typically by way of a viral vector; or *ex vivo*, outside the patient's body. In the latter approach, gene modified cells are transferred into the patient. To determine which method is optimal for a specific disease, one must take into consideration the biological mechanisms and pathophysiology of the disease. For example, in PKU the organ that primarily metabolizes Phe and contains all of the co-factors for proper PAH function is located in hepatocytes of the liver, so it would be wise to use a delivery method that targets the liver. Additionally, there are many vectors available for gene therapy, including a multitude of viruses that have fundamentally different biological characteristics including DNA-based, RNA-based, integrating, non-integrating, tissue tropism profiles (typically organism-specific), production methods, and so on [116]. There are also non-viral vectors, like nanoparticles or even naked DNA or RNA, and chemical or physical methods to induce gene transfer *ex vivo,* like lipofectamine or electroporation, respectively. Which method of gene transfer to use must take into consideration not only biology, but safety.

Throughout the 1990s gene therapy research exploded and virus-mediated gene therapy for the treatment of genetic diseases made its debut [117]. In 1993 Dr. Blaese led the first clinical trial for a rare disorder using *ex vivo* gene therapy with the integrating Moloney murine leukemia virus (MMLV) to insert a functional adenosine deaminase (ADA) in T-cells to treat ADA-deficiency associated severe combined immunodeficiency (SCID) [118, 119]. Unfortunately, this clinical trial, as well as parallel trials in Europe, led to the discovery of genotoxicity caused by insertional mutagenesis. The MMLV virus was shown to have a proclivity to integrate into a specific region in chromosome 11 activating pro-oncogene LIM domain only 2 (*LMO2*), which is a driver of T-cell acute lymphoblastic leukemia (T-ALL). Importantly, through these trials they found that discontinuation of the patient's enzyme replacement therapy (ERT) during gene therapy conferred a selective advantage to cells containing the functional ADA enzyme, a concept that continues to be meaningful in gene therapy development [120]. In retrospect, it is debatable whether the field was too quick to rush into human trials with viral vectors, but alas, it would take another alarming incident for the field to step back and critically examine the goal of their efforts.

The field of human gene therapy was abruptly halted in 1999 in a clinical trial for ornithine transcarbamylase (OTC) deficiency led by Dr. James Wilson of the University of Pennsylvania which used adenovirus to deliver the *OTC* gene to liver cells. In this study subject 019, Mr. Jesse Gelsinger, who just turned 18-years-old three months prior, suffered severe whole-body toxicity after the

infusion of the viral drug, which caused an enormous, uncontrolled cytokine storm that resulted in multi-organ failure and eventual death 99 hours later. Jesse's death, which was abruptly reported, was investigated thoroughly by several government entities. Wilson and associates were sued for several matters by Jesse's family and the U.S. government, including not disclosing preclinical research that resulted in the death of animals that received the gene therapy, inadequate consent, improper protocol implementation, and financial conflicts of interest, to name a few. The cases were settled and a decade after the incident Wilson published an article of the lessons he learned from the experience as a condition to his settlement with the federal government if he wished to continue human gene therapy [121]. One aspect he highlighted that was a positive outcome from this experience was the implementation of better governmental oversight in gene therapy clinical trials in the U.S.

After this event, the field took a step back and re-evaluated the goal of gene therapy, which is not only to be efficacious, but even more importantly, it must be *safe*. One of the safest vectors for virus-mediated gene therapy is AAV. It was discovered by accident in a preparation of simian adenovirus and declared a defective virus that was termed "adeno-associated virus" since it was only able to be produced in the presence of adenovirus [122]. AAV is small but mighty. It is a 26 nm diameter single-stranded DNA *Dependoparvovirus* with a packaging capacity of approximately 5 kb (Figure 1-6). It does not induce a strong immune response like adenovirus, and was once classified as non-pathogenic until it was

identified to cause hepatocellular carcinoma in mice [123] and humans [124-126] due to insertional mutagenesis of the WT virus. It is unclear whether this will hold true for vectorized AAV used for gene therapy purposes, since most of the AAV genome is replaced with a therapeutic transgene. Regardless, AAV is primarily non-integrating, expressing the transgene from episomal concatemers that contain tens-to-hundreds of copies of the transgene and thus is less of a threat for insertional mutagenesis as seen with MMLV, though it remains a primary safety concern for AAV gene therapy. In terms of the immune response to AAV, the greatest concern is the potential presence of pre-existing neutralizing antibodies, which are prevalent in the human population [127], and act to neutralize AAV upon administration and lead to ineffectiveness of its genetic therapeutic application [128]. AAV research has expanded to find ways to modulate the immune system and develop stealth vectors so future gene therapies may be applied to all people for which it could be beneficial, regardless of pre-existing AAV antibodies [129]. While AAV has been well-tolerated in a multitude of AAV gene therapy clinical trials in humans to date, it was recently found to be responsible for the demise of two boys with X-linked myotubular myopathy following an enormous dose ($3x10^{14}$ vg/kg) of AAV8-based AT132 drug, leading to sepsis and death, in the ASPIRO trial by Audentes Therapeutics, Inc. [130].

Despite these safety-related concerns, AAV is advantageous in the gene therapy toolbox as it comes in many variations: from the 13 naturally occurring serotypes

to the thousands of recombinant, mutant vectors created by scientists, each with slightly different capsid structures. The subtle changes in capsid amino acid residues of WT vectors affect tropism and packaging capacity and can be altered to induce unique functional characteristics like, for instance, the ability to cross the blood brain barrier after systemic administration; cross the basal lamina of the retina after vitreous administration; evade existing neutralizing antibodies; or even increase packaging capacity.

The AAV genome consists of two genes, *Rep* and *Cap*, flanked by 5' and 3' inverted terminal repeats (ITR) on either end [131, 132] (Figure 1-6). *Rep* produces replication regulatory proteins Rep78, Rep68, Rep52, and Rep40 while *Cap* translates into viral proteins for the capsid, termed VP1, VP2, and VP3, that are produced in a ratio of 1:1:10. Interestingly, a new protein product in the *Cap* gene was discovered recently, assembly activating protein (AAP), which assists in the assembly of the viral proteins into a functional icosahedral structure [133] though it is not required for AAV4, AAV5, and AAV11 [134]. In terms of harnessing this virus for gene therapy purposes, the only component of the viral genome that must be maintained are the 5' and 3' ITRs. These regions are critical for transgene packaging into viral capsids and post-transduction processing within target cells. Since these regions are quite small, about 130 base pairs (bp) in length, that leaves about 4.8 kb to incorporate a therapeutic transgene [131]. There are three main therapeutic approaches of AAV mediated gene therapy: gene addition, targeted integration, and gene editing (Table 1-1).

In gene addition, the virus delivers a transgene containing a tissue specific promoter driving the cDNA of the defective gene. In AAV-mediated targeted integration, the transgene contains a therapeutic cassette flanked by homology arms targeted to a specific region of the genome. This approach was elucidated by David Russell and colleagues at University of Washington, revealing that AAV delivered single-stranded DNA is effective at inducing targeted homologous recombination within the cell [135]. In gene editing, the AAV contains a targeted double-stranded DNA break (DSB)-inducing nuclease in conjunction with a repair template that corrects any defects in the genomic DNA sequence. In this approach the nuclease induces a targeted DSB, and the endogenous cellular machinery incorporates the repair template through homology directed repair (HDR). All three approaches have their own unique limitations and barriers to achieve efficacy, including episomal loss of the transgene, low frequency of integration events, and low frequency of HDR, respectively.

Classically, gene therapy has pursued a gene addition approach, in which a promoter that is specific to the target cells is used to drive the coding DNA of the gene of interest and packaged into an AAV that has a high tropism for the target tissue (Table 1-1). To date, there have been three AAV gene therapies that have utilized this approach that have been approved for clinical use for the treatment of rare disorders: Glybera™, or alipogene tiparvovec, was approved in the European Union (EU) in 2010 for lipoprotein lipase deficiency (LPLD) [136], (though it was intentionally not renewed in 2017 due to a lack of profit despite

being the most expensive drug in the world at $1.6 million a dose); Luxturna™, or voretigene neparvovec, was approved in the U.S. in 2018 for Leber's congenital amaurosis [137]; and Zolgensma™, or onasemnogene abeparvovec, was approved in the United States in 2019 for spinal muscular atrophy [138]. Up next to seek FDA approval are AAV-mediated liver-directed gene addition therapies for hemophilia A and hemophilia B, an effort that has been pursued by several companies in clinical trials since 2014 [139].

Excitingly, as of today, two independent companies, Homology Medicines, Inc. and BioMarin, Inc., have entered clinical trials performing AAV-mediated liver-directed PKU gene addition therapy in humans. Homology will be using a clade F vector isolated from human hematopoietic stem cells, coined AAVHSC that is similar to AAV9, while BioMarin will be using AAV5, but both are harnessing a similar approach to the original preclinical PKU gene addition therapy reported by the Harding Lab in 2006 [140]. As of today, 6 PKU patients have been dosed with AAVHSC based drug, HMI-102 in the Homology Medicines, Inc. pheNIX trial, with either low (N=2), medium (N=2), or high (N=2) doses. While all doses were well tolerated, the low dose cohort showed no efficacy. Patients in both the medium and high dose cohorts showed markedly reduced Phe, and two patients, one from medium and one from high dose cohorts with baselines of blood Phe around 1,0000 µM, had blood Phe >360 µM or >600 µM at multiple time points throughout 48 and 13 weeks, respectively [141]. Recently, BioMarin dosed their first patient with BMN 307 in their PHEARLESS Phase I/II clinical trial as well,

though no efficacy data has yet to be reported [142]. While it may seem exciting that the field of clinical gene therapy now includes PKU, concerns for achieving lasting-effects in AAV-based gene addition approaches remain.

Figure 1-6: Adeno-associated virus gene therapy

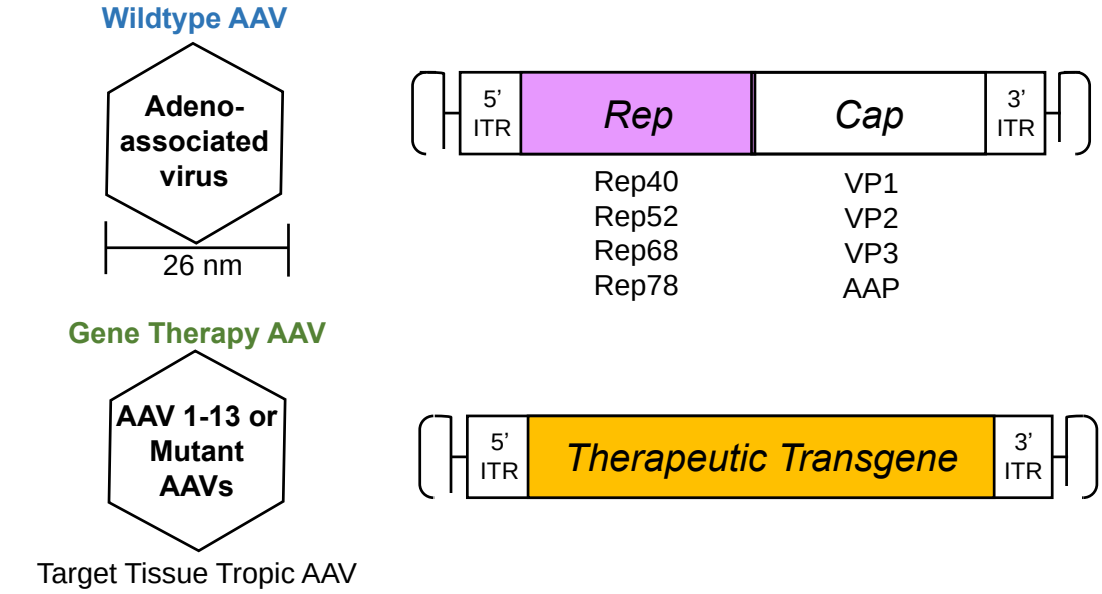

Figure 1-6: Adeno-associated virus gene therapy

Wildtype AAV is 26 nm diameter icosahedral virus containing an approximate 5 kb genome with two genes, *Rep* and *Cap*. *Rep* produces replication regulatory proteins Rep42, Rep52, Rep68, and Rep48. *Cap* produces viral capsid proteins VP1, VP2, and VP3. Optimizing AAV-mediated gene therapy includes selecting a proper target tissue tropic AAV from the 13 natural occurring or multitude of mutant AAVs developed with unique characteristics. The AAV genome is gutted of *Rep* and *Cap* genes and replaced with a therapeutic transgene, which can be designed to accomplish gene addition, targeted integration, or gene editing approaches.

Table 1-1: AAV Gene Therapy Approaches

Gene Therapy Approach	Therapeutic Transgene	Limitations
Gene Addition	1. Tissue specific promoter driving cDNA of YFP*	Episomal Loss
Targeted Integration	1. Homology arm– cDNA of YFP–Homology Arm	Low Integration Frequency
Gene Correction	1. Tissue specific promoter driving Cas9 2. Homology repair template–sgRNA	Low HDR Off-targets

*YFP = Your Favorite Protein

b. Preclinical PKU Gene Therapy

The liver is an organ underappreciated for the near five-hundred vital functions it provides for the body, including metabolism, blood homeostasis, immune roles, and detoxifying processes [143]. It has been described as a "blob" that is bathed in blood to provide optimal exchange of nutrients and waste and is the primary location of dietary metabolism within the body, including amino acid oxidation and ketogenesis [144]. It highly regenerative and has "superunique" properties, as Dr. Markus Grompe of OHSU describes in an interview with the New York Times, including the ploidy-conveyor system, in which the hepatocyte pool transitions from diploid (2n), tetraploid (4n), up to 128n and back as a part of its plasticity to respond to the ever-changing demands placed on it throughout everyday life. At the molecular level, liver structure consists of hexagonal hepatic lobules full of leaky hepatic capillary sinusoids with a central vein (CV) and peripheral portal triads, each containing a portal venule (PV), hepatic arteriole (HA), and bile duct (BD). The regions of hepatocytes that extend from the CV out to the portal triads are termed zones 3, 2, and 1 and have been found to have subtle but different metabolic priorities. Hepatocytes located in zone 1, nearest the portal venules, are the primary location of amino acid metabolism (Figure 1-7).

In designing a PKU gene therapy, one must first consider the biology of PKU. While the brain is the major organ affected by this disease, the liver is the primary site of metabolism of phenylalanine, and thus where all of the

chaperones and co-factors are already present. The most logical target site for gene delivery is therefore the liver, and more specifically, zone 1 hepatocytes, although PAH is expressed in all three zones to some degree. For an *in vivo* approach, a vector that has a high tropism for liver tissue would be ideal, and the transgene for a gene addition approach should include an extra level of safety by using a liver-specific promoter so the transgene is not expressed in off-target tissues. The most ideal administration route for transduction efficiency would be directly into the liver through the portal vein, which is sufficiently leaky with slower flow rates allowing for ideal perfusion of zone 1 periportal hepatocytes, but due to the invasive nature of that route, and poor clinical applicability, a systemic route is most often utilized [145]. In the systemic route, virus travels through the higher pressure, less leaky hepatic artery for liver perfusion, which tends to result in greater transduction of zone 3 pericentral hepatocytes, perhaps due to the increased velocity through sinusoidal crossing of the liver parenchyma towards the central vein as compared to hepatic lobule portal blood flow. In performing PKU gene addition therapy studies in our lab using a recombinant murine liver-tropic AAV8 packaged with AAV2 genome containing a liver specific promoter driving murine PAH expression, PV administration revealed higher efficacy at lower doses in comparison to systemic administration in mice. However, whether administered through PV or systemically, an observation made in our lab that has yet to be fully explained is the temporary effect of this gene addition therapy despite optimization [146], which is likely due to the episomal therapeutic AAV transgenes being lost as hepatocytes divide. Interestingly, some metabolic

disorders in which treated hepatocytes allow for improved health of the cell, there is a selective advantage. Metabolic disorders such as hereditary tyrosinemia, methylmalonic acidemia, alpha1-antitrypsin deficiency, and progressive familial intrahepatic cholestasis, all have a selective advantage for liver cells in which the enzyme function has been restored and no longer produce toxic metabolic products affecting cellular function. Although AAV is considered to be a non-integrating virus, it does integrate into the genome at low levels, around 1 in 1,000 vector genomes. For hepatocytes that have integrated AAV in the genome, the selective advantage of the newly acquired therapeutic transgene allows for clonal expansion of that cell resulting in nodules of liver tissue containing restored enzyme function and long-term efficacy. However, if there is no benefit from restored enzyme function in the liver, as in PKU, there is no selective advantage, and long-term efficacy is uncertain in AAV-based gene addition therapy approaches.

Preclinical studies performing PKU gene addition therapy with AAV in adult *Pah*$^{enu2/enu2}$ PKU mice have shown robust and long-term effectiveness [140, 147], over a year. These curative effects wain over time despite testing various AAV serotypes and doses [146], and was supported by attempts to cure *Pah*$^{enu2/enu2}$ breeders for studies in this dissertation (unpublished data). The loss of efficacy is attributed to both the lack of selective advantage for PAH-positive hepatocytes and the episomal loss of AAV-transgenes as liver cells divide due to normal liver tissue maintenance. An additional challenge for PKU is that it has a therapeutic

threshold of approximately 10% [148], which may seem low, but with the challenges gene therapy has faced to achieve efficacy in hemophilia disorders, which only require 1% expression to achieve therapeutic benefit, it poses yet an additional barrier. One approach to address the limitation of temporary efficacy would be to incorporate a form of selection into the transgene that would allow for a selective advantage for cells in which the vector has integrated. For PKU, this would be best suited using a targeted approach in a locus that contained a strong endogenous liver-specific promoter to drive expression and is in fact the premise for GeneRide™ [149]. The novel GeneRide™ technology, developed by the Kay lab of Stanford, is a liver-targeted AAV integrating system in which the transgene contains homologous regions to the last intron of the albumin locus. In this approach the integrating vector is promoterless and instead uses the endogenous albumin promoter for expression. It accomplishes this by containing a self-cleaving peptide sequence prior to the therapeutic gene which allows for fused transcription but production of two independent proteins. The limitation in this approach is the low level of recombination events, less than 1%. It can be ameliorated by incorporation of a means for selection, like the universal hepatocyte selection technology developed by the Grompe laboratory, which in combination was successfully performed in hemophiliac mice [150].

The universal hepatocyte selection technology harnesses the powerful selective advantage of hereditary tyrosinemia type 1 (HT1). HT1 is characterized by fumarylacetoacetate hydrolase (FAH) deficiency, allowing the accumulation of

toxic upstream metabolites, most notably succinylacetone (SA), that causes severe cell-autonomous hepatic injury. The universal hepatocyte selection method provides protection from these toxic insults by expressing an inhibitory miRNA against an upstream enzyme in the pathway called 4-hydroxyphenylpyruvate hydrolase (HPPD). In cells that express the HPPD miRNA, the tyrosine metabolic pathway is halted at the level of the HPPD enzyme, preventing the production of SA. This method can be combined with GeneRide™ to allow for clonal expansion of the integrated construct containing the therapeutic transgene, but only in the presence of tyrosinemia like conditions, which can be generated genetically or chemically. While this combinatorial approach reveals great promise in ameliorating the temporary nature of PKU gene addition therapy, another alternative to address the anticipated episomal loss of episomal AAV transgenes is to perform gene editing to correct the mutation that causes the disease in the first place.

Figure 1-7:
Hepatic Lobule

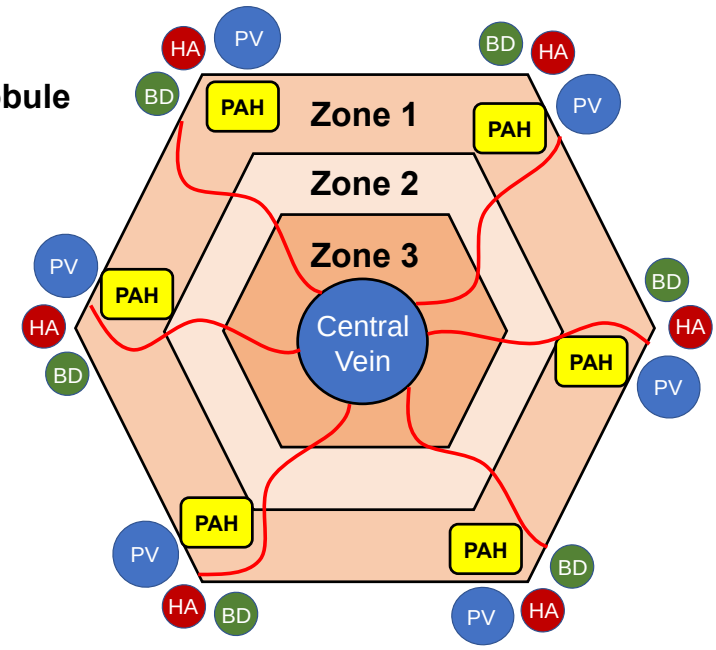

Figure 1-7: Hepatic Lobule

The liver is arranged macro-histologically in organized hexagonal structures called hepatic lobules. At the periphery of each point of the hexagon are portal triads, each containing a portal venule (PV), hepatic arteriole (HA), and bile duct (BD). Leaky sinusoidal capillaries (red wavy lines) extend from these structures and drain centrally into the central vein located at the center of the hepatic lobule. Hepatocytes are organized into three zones that carry out metabolically distinct functions, with zone 1 containing peri-portal hepatocytes, zone 3 containing peri-central hepatocytes, and zone 2 containing hepatocytes between those two regions. Zone 1, the peri-portal region, is where PAH is primarily expressed to metabolize dietary Phe, among other dietary acquired nutrients from the intestine coming to the liver through the portal vein. The zone 1 peri-portal region is therefore the target for PKU gene therapy, as all of the required co-factors and chaperones for PAH are optimally regulated in this region.

Gene Editing

a. History of Gene Editing

The past seventy years have laid the foundation for better understanding the genetic basis of human disease: the discovery of DNA as heritable information by Avery, Macleod and McCarty in 1944 [105]; the structure of the double helix by James Watson, Francis Crick and Rosalind Franklin in 1953 [151, 152]; the ability to sequence DNA by the dideoxy (Sanger) method discovered by Frederick Sanger in the 1977 [153]; the targeted amplification of specific DNA regions by polymerase chain reaction (PCR) discovered by Kary Mullis in 1986 [154]; the sequencing of the entire human genome by the International Human Genome Sequencing Consortium in 2001 [155]; and finally, and probably most singularly, the development of massively parallel deep sequencing of DNA called NGS developed by Nick McCooke and his team at Solexa [156], which has laid the foundation for precision medicine today. Each one of these groundbreaking advancements has impacted the ease of otherwise daunting molecular research, enhanced the understanding of human genetics and genomics, and provided a platform to streamline the diagnosis, treatment, and prevention of human disease in medicine. Along with these technologies came a vast new knowledge of how genetic mutations cause disease, as well as the desire to repair mutations to cure human disease.

Gene editing has been sought after since natural studies of DNA repair in prokaryotes and eukaryotes revealed endogenous cellular machinery capable of repairing DSB with or without homologous recombination (HR) [157-160]. The repair pathway without homologous recombination, referred to as non-homologous end joining (NHEJ), is more commonly used to repair DSBs. It is flexible in nature, consisting of proteins that recognize, resect, polymerize and ligate the DNA lesion in any DNA-end configuration, but has a proclivity to result in imperfect repair, known as alternative end-joining (Alt-EJ). While Alt-EJ results in insertions or deletions (indels) in the DNA, it has the potential to knock-out deleterious gain of function mutations to correct human disease. The second major pathway to repair DSBs is called homology directed repair (HDR), which is much less common and utilizes an exogenous or endogenous repair template to precisely repair the DNA lesion. This pathway is desired for the correction of genetic mutations that cause disease.

Since the early 1990s, scientists have been pursuing DSB-mediated genetic manipulations. It started by fusing chemical DNA recognition agents, such as oligonucleotides, peptide nucleic acids (PNA), or polyamides to DNA-cleavage or interlinking chemicals, such as bleomycin and psoralen, which resulted in minimal site-directed repair [161]. More robust methods were developed by fusing the sequence-independent endonuclease FokI domain to sequence-specific peptide systems, called zinc-finger nucleases (ZFNs) [162] and transcription-activator-like-effector nucleases (TALENs) [163]. While these

methods have the potential to be highly site-specific and effective at inducing targeted DSBs, design and execution remains arduous, expensive, and challenging. This all changed with the discovery of the CRISPR/Cas9 system.

The revolutionary gene manipulating CRISPR/Cas9 system was discovered over several decades by various research groups across the world. The initial observation of clustered direct-repeat sequences occurred in an alkaline phosphatase metabolism study in *E. coli* by the Nakata research group at Osaka University, Japan [164]. Throughout the 1990s and early 2000s, Francisco Mojica of the University of Alicante, Spain dedicated his research to this prokaryotic DNA repeat phenomenon, which was found to be present in other bacteria and archaea, and led to the discovery of CRISPR and its function [165]. The term CRISPR was coined to describe these repetitive sequences, which stands for Clustered Regularly Interspaced Short Palindromic Repeats. Mojica's discovery was driven by the observation that the spacer sequences were of pathogen origin, primarily that of viruses, and he hypothesized, correctly, that these functioned as a form of adaptive immunity in prokaryotes [166]. In 2005, Alexander Bolotin of the French National Institute for Agricultural Research identified novel Cas (CRISPR-associated) gene encoding one large protein containing helicase and endonuclease function, and additionally identified a common shared sequence at one end of the CRISPR regions, which he coined as protospacer adjacent motifs (PAM) [165].

Up until this point, Cas genes were thought to be a novel DNA repair system specific to prokaryotes. They were found to come in two main types: Type I, which contains multiple proteins that work in concert as a holoenzyme complex, and Type II, which contains a single enzyme [167]. It was not until 2006 that Eugene Koonin of the U.S. National Center for Biotechnology Information at the NIH proposed the CRISPR/Cas9 system as a model of bacterial adaptive immunity [168], which was experimentally demonstrated in 2007 by Philippe Horvath of Danisco France [169]. Dr. Hovarth showed that after phage infection, the CRISPR locus contained newly incorporated segments specific to the phage, and along with the association of a single Cas protein (in Type II Cas systems), developed the ability to inactivate subsequent infections.

The details of how this system worked came about piece by piece over the next five years. First, John van der Oost of the University of Wageningen, Netherlands discovered the spacer sequences were transcribed into guide RNAs, which he termed CRISPR-RNAs (crRNAs), that guide the Cas proteins to the target DNA [170]. Next, Luciano Marraffini and Erik Sontheimer of the Northwestern University, Illinois showed that the CRISPR/Cas system acted on DNA, not RNA as predicted [171]. Finally, Sylvain Moineau of the University of Laval in Canada showed that the Cas protein cleaved target DNA precisely three nucleotides upstream of the PAM [172]. One puzzling aspect of this system was how the Cas protein was able to link with a wide variety of uniquely different sequences. The answer came through the work of Emmanuelle Charpentier of Umea University,

Sweden and University of Vienna, Austria in which she found a separate RNA, which she coined trans-activating CRISPR RNA (tracrRNA), that formed a duplex with the transcribed spacer sequences which was then bound to the Cas protein and assisted in directing it to the target DNA [173]. In 2011, Virginijus Siksnys of Vilnius University, Lithuania demonstrated Type II Cas functions in heterologous species void of Type II Cas, verifying all components of the Type II Cas system had been identified [174]. In 2012, Dr. Siksnys group performed biochemical characterization of the Cas9-mediated DNA cleavage. They identified that the RuvC domain cleaves the non-complementary strand while the HNH domain cleaves the complementary site, resulting in a DSB of the target DNA [175]. Additionally, they found that the crRNA only required 20 nucleotides to function as a guide and that it could be manipulated to target specific regions of DNA. At the same time, Emmanuelle Charpentier and Jennifer Doudna of the University of California (UC), Berkeley reported similar findings, and additionally found that the crRNA and tracRNA could be fused together, further simplifying the system [176]. In 2013, Feng Zhang of the Broad Institute of the Massachusetts Institute of Technology (MIT) and Harvard was the first to publish targeted genome cleavage in human and mouse cells using two Type II Cas systems, *Streptococcus thermophiles* and *Streptococcus pyogenes*, and demonstrated its ability to be programmed to target multiple loci and direct HDR [177]. While it was debated who should be recognized for harnessing the CRISPR/Cas9 system as a facile genome editing tool, Emmanuelle Charpentier and Jennifer Doudna or Feng Zhang, all three have their own companies working on different aspects of

genome editing technologies in medicine, agriculture, and science. The legal battle regarding patents on this intellectual property was finalized in 2018, in which the United States Patent and Trademark Office (USPTO) decided to uphold patents from each group: UC Berkley has the patent on using the CRISPR system on loose DNA in test tubes and MIT and Harvard have the patent on using CRISPR/Cas9 genome editing in eukaryotic cells.

Excitingly, the 2020 Nobel Prize selection committee announced Dr. Doudna and Dr. Charpentier alone as laureates in chemistry for the discovery of the CRISPR/Cas gene modifying system, recognizing their pioneering efforts and inspirational roles as two female scientists [178]. Their work is being recognized as basic microbiology enzyme research in which they were able to identify profound application implications that eventually led to clinical trials aiming to cure human genetic diseases, among a plethora of other research uses to better understand physiology and disease. Their awards make the past 120 years of Nobel laureates to now include seven women (3%).

b. Application and Considerations of a Facile Genetic Tool

Since the identification of the simple, easy, and inexpensive CRISPR/Cas9-mediated genome editing in complex cells, scientists over the world have harnessed this technology for *in vitro* and *in vivo* genetic manipulations to explore novel cellular mechanisms, understand pathophysiology of disease, create a plethora of new animal models, and even alter human genetics [179].

Application is remarkably simple (Figure 1-8). The Type II Cas9 system requires two components to mediate a targeted double strand break: a single guide RNA adjacent to a PAM sequence in the desired region of modification and the Cas9 enzyme itself. After the targeted DSB, the job of the Cas9 enzyme is complete. The cellular repair machinery is responsible for the subsequent DNA modifications. There are two main pathways the cell utilizes for the repair of DSBs: NHEJ and HDR. NHEJ may result in no net effect but has a propensity to induce indels through Alt-EJ, while HDR uses a template with homologous sequences to rewrite the code [180]. The proclivity of the cell to use one pathway or the other has profound impacts on the outcome and therefore must be considered during experimental design regarding the purpose of the genetic intervention. The possible uses for Cas9-mediated genomic alterations are numerous but most notably include that of gene knockout and gene correction, which rely on NHEJ or HDR, respectively, in order to be successful [181]. Factors that impact which pathway the cell uses include stage of development, cell cycle,

and the presence of inhibitors or enhancers of DNA repair pathways, which can be modified for experimental purposes [182, 183].

While the revolutionary CRISPR/Cas9 gene editing technology has the potential to cure human disease, its powerful yet facile nature also warrants ethical discussions regarding human application. According to the National Academies of Sciences, gene and cell therapy technologies, including CRISPR/Cas9 gene editing, should only be used to treat human disease in somatic cells, and avoid germline cells that will pass genetic information down to progeny, with the following recommendations:

> *"Heritable genome editing needs more research before it might be ready to be tried; also public input and engagement are needed. When tried, heritable genome editing must be approached cautiously: used only for treating or preventing severe diseases (no enhancement), and according to strict criteria with stringent oversight [184]."*

Despite this, highly controversial CRISPR/Cas9 gene editing research has been performed on human embryos and in 2018, resulted in the birth of twin baby girls in China, Lulu and Nana, that presumably have enhanced protection from human immunodeficiency virus (HIV) infection through knockout of C-C chemokine receptor type 5 (*CCR5)*, the primary receptor for HIV-entry on white blood cells

[185]. However, the true motivations are debated as *CCR5* knockout mice are shown to have enhanced memory and cognition [186]. While this rogue scientist was denounced by the field, it has opened the frightening door to human embryo gene modification for human enhancement.

This powerful technology must be used responsibly, and the work within this dissertation aligns with the recommendations of the National Academy of Sciences for the development of gene and cell therapies for humans to be limited to somatic cells for the treatment of genetic diseases. While this work did use this powerful technology to create a novel mammalian model for PKU, its purpose was purely for the development of a superior animal model with which to test novel therapeutics for PKU.

Figure 1-8: CRISPR/Cas9 Gene Manipulation

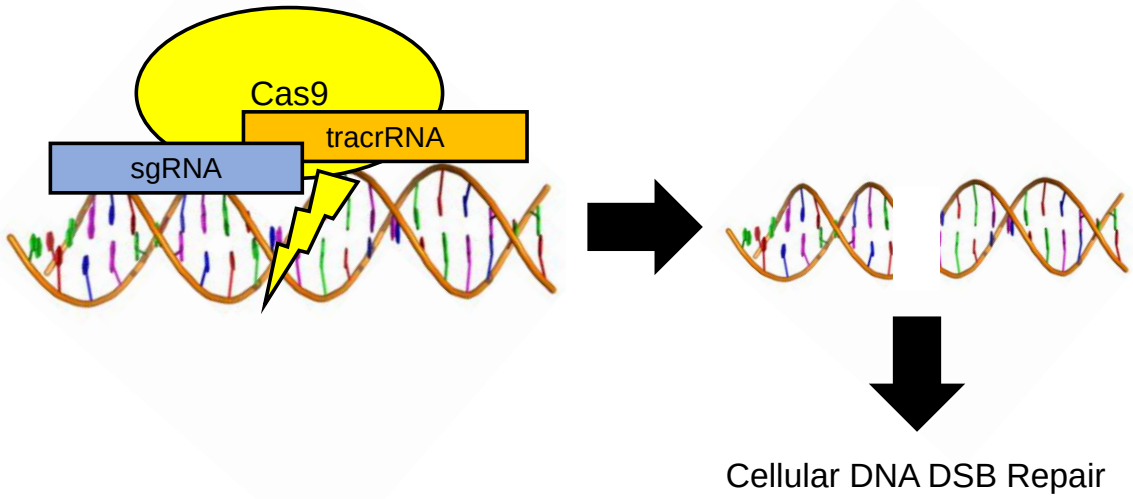

Figure 1-8: CRISPR/Cas9 Gene Manipulation

The CRISPR/Cas9 enzyme (in yellow) binds with the tracrRNA (orange) that can be fused with the sgRNA (blue) through complementary RNA binding to create the holoenzyme targeted Cas9 ribonucleoprotein complex. This complex scans the genome for the target region (represented by the double helix). The high binding affinity of the sgRNA and target DNA induces a confirmational change in the Cas9 enzyme (lightning bolt) that causes a DSB in the target DNA region (represented by two halves of the double helix). At this point the CRISPR/Cas9 modification to the genome is complete, and the remaining DSB repair is performed by the endogenous cellular machinery.

Dissertation Aims

Preclinical PKU gene therapy has shown great promise using liver directed AAV-mediated gene addition therapy in adult *Pah*$^{enu2/enu2}$ animals, with robust and long-term outcomes, yet these effects are ultimately temporary and cannot be achieved from birth. This is attributed to the episomal delivery of the therapeutic AAV transgenes to hepatic target cells, which are lost as cells divide due to normal tissue maintenance and development. This dissertation work attempts two potentially permanent gene therapy approaches in neonatal *Pah*$^{enu2/enu2}$ animals to address the temporary nature of the existing preclinical PKU gene addition therapy. One approach harnesses the powerful CRISPR/Cas9-mediated gene correction in chapter two and the second uses a combinatorial GeneRide™ and universal hepatocyte selection for targeted gene integration and selection in chapter three. These studies will be, to our knowledge, the first neonatal genome editing approaches attempted in PKU gene therapy preclinical research.

While the *Pah*$^{enu2/enu2}$ mouse model has been the longstanding and most utilized model for classical PKU research, it contains inherent limitations for gene therapy development in terms of achieving efficacy and post-gene therapy molecular analyses. The *Pah*^{enu2} allele produces abundant albeit inactive mutant PAH protein that is thought to interact with and lower overall WT PAH activity, a long-proposed phenomenon known as the dominant negative effect, though it has yet to be clearly demonstrated in *in vivo* studies. This provides yet an additional

barrier to preclinical gene therapy that aims to supply WT PAH to hepatic cells, as achieving and maintaining expression of gene therapy delivered DNA has remained a challenge across the field of gene therapy research. Additionally, the mutant PAH is readily detected by anti-PAH antibody, making antibody-based analyses of gene therapy experiments to quantify and localize transgene expression impossible. This work therefore sought out to create a novel mouse model that would be completely void of Pah protein expression by attempting to knock out exon 1 of the *Pah* gene in murine zygotes with the CRISPR/Cas9 technology.

Taken together, this dissertation work attempts to advance the field of PKU gene therapy by testing novel gene editing approaches in the pursuit of a permanent and effective treatment for PKU and generating a novel mouse model that will facilitate the ease of post-gene therapy analyses with fewer confounding variables.

CHAPTER 2:

AAV-Mediated CRISPR/Cas9 Gene Editing in Murine Phenylketonuria

This work has been published in the journal of

Molecular Therapy: Methods & Clinical Development [187].

Title Page

AAV-Mediated CRISPR/Cas9 Gene Editing in Murine Phenylketonuria

Daelyn Y. Richards[1], Shelley R. Winn[1], Sandra Dudley[1], Sean Nygaard[1], Taylor L. Mighell[1], Markus Grompe[1], and Cary O. Harding[1,2]

Department of [1]Molecular and Medical Genetics and [2]Pediatrics

Oregon Health & Science University

Correspondence should be addressed to C.O.H. (hardingc@ohsu.edu)

Portland, Oregon, United States of America

Corresponding Author Contact Information:

Address: 3181 SW Sam Jackson Park Road, Mail Code L103, Portland, Oregon 97239

Tel: 503 494-7608

Fax: 503 494-6886

Email: hardingc@ohsu.edu

Short title of 60 characters or less:

CRISPR/Cas9 Gene Editing in Murine Phenylketonuria

Abstract

Phenylketonuria (PKU) due to recessively inherited phenylalanine hydroxylase (PAH) deficiency results in hyperphenylalaninemia, which is toxic to the central nervous system. Restriction of dietary phenylalanine intake remains the standard of PKU care and prevents the major neurologic manifestations of the disease, yet shortcomings of dietary therapy remain, including poor adherence to a difficult and unpalatable diet, an increased incidence of neuropsychiatric illness, and imperfect neurocognitive outcomes. Gene therapy for PKU is a promising novel approach to promote lifelong neurological protection while allowing unrestricted dietary phenylalanine intake. In this study, liver-tropic recombinant AAV2/8 vectors were used to deliver CRISPR/Cas9 machinery and facilitate correction of the *Pah*^{enu2} allele by homologous recombination. Additionally, a non-homologous end joining (NHEJ) inhibitor, vanillin, was co-administered with the viral drug to promote homology-directed repair (HDR) with the AAV-provided repair template. This combinatorial drug administration allowed for lifelong, permanent correction of the *Pah*^{enu2} allele in a portion of treated hepatocytes of mice with PKU, yielding partial restoration of liver PAH activity, substantial reduction of blood phenylalanine, and prevention of maternal PKU effects during breeding. This work reveals that CRISPR/Cas9 gene editing is a promising tool for permanent PKU gene editing.

Keywords: Phenylketonuria, Phenylalanine, Gene Therapy, Gene Editing, Gene Correction, CRISPR/Cas9, Phenylalanine Hydroxylase, Homology Directed Repair

Introduction

Phenylketonuria (PKU), caused by recessively-inherited phenylalanine hydroxylase (PAH) deficiency (OMIM # 261600), is one of the most common inborn errors of metabolism (IEM), and results in hyperphenylalaninemia and neurotoxic effects of phenylalanine upon brain [46]. PAH is a cytosolic hepatic homo-tetramer that metabolizes L-phenylalanine (Phe) into L-tyrosine [47]. Without PAH function, chronic untreated hyperphenylalaninemia causes severe neurological damage leading to intellectual disability, psychological disorders, and seizures [46, 188]. It is important to note that human clinical PKU phenotypes form a disease continuum, ranging from mild hyperphenylalaninemia (blood Phe = 120–600 μM) to mild PKU (blood Phe = 600–1200 μM), to the most severe, classical PKU (cPKU) (blood Phe > 1200 μM), depending upon the amount of residual liver PAH activity in the patient. Due to the severity of largely preventable neurological symptoms, all infants born in medically advanced countries undergo newborn screening for hyperphenylalaninemia and are placed on dietary treatment early in life [89].

The current standard of care for PKU is lifelong dietary restriction of Phe intake, which requires supplementation with medical foods lacking Phe but containing critical nutrients including amino acids other than Phe, along with vitamins and minerals, that individuals with PKU are unable to retrieve from the severely restricted diet [189-193]. Impaired access to specialized medical foods is prevalent in the United States due to inconsistent insurance coverage,

particularly for adults. Inconsistent access to medical foods is associated with chronic hyperphenylalaninemia, cognitive and behavioral symptoms, and functional disability [84]. Federal legislative efforts to guarantee uniform insurance coverage of medical foods across state boundaries are ongoing through the proposed Medical Nutrition Equity Act. Though the diet is successful at preventing the major manifestations of this disease, cognitive and behavioral abnormalities remain prevalent in the treated PKU population and may occur even in individuals who successfully maintain blood Phe concentrations between 120-360 μM, the currently recommended treatment range [192]. These abnormalities can include lower IQ, executive functioning deficits, and psychiatric disorders (anxiety and depression) with the incidence of deficits increasing with increased blood Phe concentration [62, 194, 195].

A recent FDA approved enzyme substitution therapy (pegvaliase) for adults with uncontrolled hyperphenylalaninemia on diet has revealed dramatic improvements in blood Phe management [80, 196-198], but is associated with a significant incidence of immune-mediated hypersensitivity reactions against this foreign protein. Additionally, pegvaliase is not approved for use in individuals under 18 years of age. Pegvaliase therapy requires daily injections, while gene therapy has the potential to correct the disease in a single treatment. In a survey performed by the National PKU Alliance (NPKUA), a national non-profit organization committed to unite, inform, and support people with PKU, over 85% of the community were interested in gene therapy administered as a one-time

infusion that would alleviate the lifelong limitations, burdens, and consequences of PKU [84]. Preclinical studies using adeno-associated virus (AAV) mediated gene addition therapy in the *Pah*$^{enu2/enu2}$ mouse have shown robust efficacy, but the effectiveness is limiting in neonatal mice [140, 147]. This loss of therapeutic efficacy is multifactorial, including the loss of AAV episomes as liver cells divide, the lack of selective advantage for PAH+ liver cells, and the high therapeutic threshold of PKU (~10% hepatocyte correction to lower blood Phe) [148, 199, 200]. In pursuit of a more permanent gene therapy approach, this study aimed to correct the mutation causing PKU in *Pah*$^{enu2/enu2}$ mice using a targeted integrating AAV approach. We utilized the CRISPR/Cas9 nuclease system [201, 202] to induce a double-strand break (DSB) near the *Pah*^{enu2} mutation and to enhance the opportunity for homologous recombination with the provided repair template harboring the wild-type (WT) sequence.

This correction is expected to be permanent even if the targeted hepatocyte divides and its genome is replicated. The barrier impeding efficacy with this approach is the ability to achieve a sufficient number of correctly gene edited hepatocytes to produce a physiologically relevant improvement in Phe clearance in the absence of any selective growth advantage for PAH+ cells. To address this challenge, a non-homologous end joining (NHEJ) inhibitor shown to facilitate homology-directed repair (HDR) was evaluated as a means of increasing the frequency of successful gene repair in our system [203].

The *Pah*$^{enu2/enu2}$ mouse model of cPKU is ideal for this proof of principle study, as it contains a single missense mutation in the *Pah* gene associated with hyperphenylalaninemia. The pathologic c.835T>C missense mutation alters amino acid position 263 from a phenylalanine into a serine, disrupting proper function of the catalytic domain of PAH. *Pah*$^{enu2/enu2}$ homozygotes exhibit all of the symptoms of classical untreated human PKU, including blood phenylalanine concentration >2,000 μM while consuming normal mouse chow, hypopigmentation, and associated neuropathology resulting in cognitive and behavioral deficits [91, 204].

Results

Experimental Design

Gene repair occurs through homologous recombination and is greatly enhanced by DSBs, which can be mediated by the *Streptococcus pyogenes* CRISPR/Cas9 system. In order to correct the *Pah*^{enu2} mutation in this fashion, three components must be delivered to hepatocytes by the liver-tropic AAV serotype 8 (AAV8): the Cas9 enzyme, a single-guide RNA (sgRNA) near the target mutation, and a repair template containing homology to the target allele except for a thymine at position c.835, the WT sequence [201] (Figure 1). Due to the limiting packaging capacity of AAV, this system must be manipulated into two AAV vectors in a dual AAV approach [202]. Here, one recombinant AAV genome contained the *S. pyogenes* Cas9 coding sequence with expression driven by a liver-specific promoter (LSP) designated P3 (minimal transthyretin promoter, TTRmin, coupled to a *de novo* designed hepatocyte-specific cis-regulatory module 8, HS-CRM8 [205, 206]), and a second vector expressed a validated guide RNA 46 bp downstream of the c.835 mutation site under the expression control of the human U6 RNA polymerase III (pol III) promoter. This second vector also contained a 2-kb fragment of the WT mouse *Pah* genomic sequence (GRCm38:87569274-87571296) flanking the *Pah*^{enu2} mutation site in exon 7, with purposefully introduced synonymous and intronic mutations that alter the PAM and guide sequence, thereby preventing re-cutting by Cas9 as well as facilitating downstream sequence analyses (Figure 2-1A). Expression of Cas9 and the guide RNA was expected to result in DNA double strand breaks (DSB) 46 bp

downstream of the *Pah*^{enu2} mutation. Innate cellular DNA repair mechanisms could alternately repair the DSB by NHEJ, yielding either perfectly repaired *Pah*^{enu2} sequence or the introduction of small insertions or deletions (indels), or by HDR using the *Pah* genomic DNA fragment from the second AAV vector as a repair template (Figure 2-1B). The latter, desired outcome would restore the nucleotide at cDNA position 835 to a thymine and lead to the functional correction of PAH activity in the edited hepatocyte. In an effort to maximize the frequency of HDR in preference over NHEJ, vanillin, a potent NHEJ-inhibitor previously shown to increase HDR in a gene-targeting AAV system [203], was co-administered with the viral vectors. Animals were re-dosed with drug as adolescents due to volume restraints in neonates and to provide an opportunity for additional correction.

Three animal cohorts were tested in this study. In two cohorts (labeled dAAV+Van and dAAV; dAAV = dual AAV), all animals received both AAV vectors, and the former also received vanillin injections. In a third cohort, rtAAV+Van (rtAAV = repair template AAV), animals received the repair template vector only, without the Cas9 expressing vector, but did receive vanillin (Figure 2-1C). All animals were screened for and tested positive for presence of appropriate viral DNA according to treatment group in liver tissue via PCR post-harvest.

Therapeutic Efficacy

Single male and female mice from each treatment cohort were reserved for breeding experiments (Figure 2-2A) and allowed to survive out to 65 weeks age. The remaining animals were euthanized at 16-24 weeks of age for characterization and tissue harvest. At the time of euthanasia, the coat color on all dAAV+Van treated animals was indistinguishable from that of heterozygous or WT animals, while animals in the dAAV and rtAAV+Van groups had minimal, if any, coat color darkening, suggesting that substantial reduction of blood phenylalanine concentration had occurred in dAAV+Van animals only (Figure 2-2D).

Mean serum phenylalanine concentration at euthanasia was individually variable but approximately two-fold lower on average in dAAV+Van treated mice (685.2 μM ± 81.79, mean ± SEM, range 252-1168 μM) in comparison to either dAAV (1518 μM ± 72.04; range 1231-1863 μM) or rtAAV+Van treated animals (1314 μM ± 119.2; range 827-1850 μM). Statistical analysis by one-way ANOVA revealed an overall significant difference in mean serum Phe among the three treatment groups ($F(2, 27) = 24.11$, $p < 0.0001$) (Figure 2-2B). A post hoc intergroup comparison revealed significant differences between dAAV+Van and the other two groups but no differences between dAAV and rtAAV+Van. There appeared to be no significant additional effects from the second AAV administration in any treatment group. The decrease in serum Phe was sustained

through 65 weeks in the two animals in dAAV+Van cohort that were allowed to survive to that age (Figure 2-4A).

Mean liver phenylalanine hydroxylase activity at euthanasia was, again, individually variable and approximately ten-fold higher in dAAV+Van-treated mice (mean percent WT PAH activity ± SEM: 9.6% ± 1.9%; range = 3.3%–24.8%) in comparison to either dAAV-treated animals (1.2% ± 0.5%; range = 0%–5.7%) or rtAAV+Van-treated animals (0.5% ± 0.3; range = 0%–2.3%). One-way ANOVA revealed an overall significant difference in mean PAH enzyme activity among the three treatment groups ($F(2, 27) = 16.02$, $p < 0.0001$) (Figure 2-2B). A post hoc intergroup comparison revealed significant differences between dAAV+Van and the other two groups but no differences between dAAV and rtAAV+Van.

On-Target Genetic Analysis

PCR-based next-generation sequencing (NGS) was applied to on- and off-target genomic regions of treated mice (Figure 2-3A). In order to avoid amplifying and sequencing residual episomal or non-targeted integrations of AAV genomes containing the repair template, we used a nested PCR approach on genomic DNA isolated from treated mouse liver to amplify the on-target genomic region. To produce our first amplicon, a 1.3-kb fragment spanning *Pah* exon 7, we used a forward primer that was homologous to sequences in *Pah* intron 6 but outside the 5′ end of the repair template; this fragment was subjected to a second amplification using nested primers containing convenient indexing adapters to

yield a 350-bp product. The products of these PCR reactions were indexed with unique barcodes and submitted for NGS on the Illumina MiSeq platform.

We define NHEJ as DNA repair of a DSB that results in perfect restoration of the original sequence without correction of the *Pah*^{enu2} mutation, an event that cannot be detected experimentally. Repair that results in a deletion of 1 bp or greater in size but retains the c.835C *Pah*^{enu2} mutation is defined as Alt-EJ, and on-target HDR was defined as detecting exonic and intronic genomic sequences that were consistent with 98% identity to the repair template having been appropriately incorporated into the amplicon in the expected orientation. The percentages of NGS reads with Alt-EJ (indels) or properly targeted HDR are displayed in Figure 2-3B. A two-way ANOVA revealed a significant difference between treatment groups, $F(2, 54) = 12.87$, $p < 0.0001$; and DNA repair, $F(1, 54) = 13.11$, $p = 0.0006$. The percentage of reads with indels in dAAV+Van-treated animals (mean ± SEM: 21.27% ± 2.63%; range = 12.25%–39.29%) was approximately 2- to 3-fold higher than that in either the dAAV group (12.92% ± 3.64%; range = 2.21–39.54) or the rtAAV+Van group (6.59% ± 1.81%; range = 2.52–19.34). There was no statistical difference in the percentage of indels between dAAV+Van and dAAV or between dAAV and rtAAV+Van, but there was between dAAV+Van and rtAAV+Van, with a p value of 0.0007. The percentage of reads with properly targeted HDR in dAAV+Van-treated animals (mean percentage ± SEM: 13.06% ± 11.54%; range = 4.13–36.78) was significantly higher than that in either the dAAV group (0.96% ± 1.23%; range = 0–3.90) or the

rtAAV+Van group (3.51% ± 4.32%; range = 0.01–12.57). There was no statistical difference in HDR between dAAV- and rtAAV+Van-treated animals.

NGS data were further analyzed for functional cDNA, in which NGS reads were trimmed to contain only the exon 7 sequence and evaluated for the ability to encode a functional enzyme (Figure 2-3C), again, revealing a similar significant difference among treatment groups, $F(2, 27) = 5.805$, $p = 0.008$ by one-way ANOVA. NGS analysis of dAAV+Van-treated animals, again, revealed an approximately 4-fold increase in the percentage of functional *Pah* cDNA in the dAAV+Van-treated group (mean ± SEM: 7.54% ± 2.33%; range = 1.94%–24.00%) in comparison to the dAAV group (0.70% ± 0.25%; range = 0.07%–2.54%) or the rtAAV+Van group (2.07% ± 0.73%; range = 0.08%–5.58%).

Correction of the c.835T > C mutation back to thymine by Sanger sequencing in a small portion of genomic liver DNA from treated animals could only be detected in dAAV+Van-treated animals (Figure 2-3D).

Off-Target Genetic Analysis

Possible sites of off-target Cas9-mediated genotoxicity were selected for NGS analysis using the *in silico* COSMID tool, which used the guide 1 sequence to determine the top 45 off-target cutting sites in the mouse genome, scored for likelihood of cutting where 0 = highest confidence cutting and 40.7 = lowest confidence cutting (Supplementary Figure 2-2). The top three sites selected for

further investigation were chromosome chr 10:116187078, chr12:60323904, and chrX:140587182, with scores of 0.17, 1.33, and 2.93, respectively (Figure 3A). PCR-based NGS of liver genomic DNA from treated animals revealed minimal off-target *Sp*Cas9 cutting in all three chromosomal regions, with none accumulating to more than 2% of reads (Figure 3E). Surprisingly, a one-way ANOVA of each chromosomal region between treatment groups revealed a significant difference in only the chr 12 region, $F(2, 27) = 5.71$, $p = 0.0086$; with an approximately 2-fold higher percentage of indels in the rtAAV+Van-treated group (mean percentage of indels ± SEM: 0.89% ± 0.19%; range = 0.19%–1.66%) than either treatment group containing the *Sp*Cas9 enzyme, dAAV+Van (0.33% ± 0.09%; range = 0%–0.91%) or dAAV (0.38% ± 0.09%; range = 0%–0.80%). Despite this significant increase in indels on chr 12 in the rtAAV+Van treatment group—which cannot be easily explained, as this cohort did not receive any Cas9 enzyme—these data show minimal off-target cutting by *Sp*Cas9 at the three locations investigated in these animals. While this was not an exhaustive investigation of all off-target indels in the whole genome, this therapy seems safe for genomic integrity in the three highest predicted off-target cutting sites.

Correlations between Functional Pah Genomes, Liver PAH Activity, and Mean Serum Phe Concentrations

The amount of PAH activity measured in liver homogenates from dAAV+Van mice is linearly related to the percentage of functional PAH reads restored by CRISPR/Cas9-mediated exon 7-directed DSB and successful HDR (Figure 4C).

The relationships between serum Phe and the percentage of functional PAH reads (Figure 4D) or between serum Phe and liver PAH activity (Figure 4E) fit best to a one-phase exponential decay model, which is consistent with the known first-order Michaelis-Menten kinetics of the PAH reaction.

Adverse effects

No adverse effects of treatment were seen in any cohort. The overall health and development of the animals in the dAAV and rtAAV+Van treatment groups were consistent with that expected for untreated *Pah*$^{enu2/enu2}$ mice, including hypopigmentation and impaired growth. The animals in the dAAV+Van treatment group showed improved health in comparison to the expected *Pah*$^{enu2/enu2}$ development with dark coat pigmentation and improved growth (Figure 4B). Mice were euthanized at ages ranging from 16 to 65 weeks of age; the gross macroscopic appearance of all internal organs was normal at necropsy in all mice. There was no gross evidence of liver neoplasia in any animal, though molecular markers of hepatocellular carcinoma were not evaluated for low-grade carcinogenic transformation in this study.

Successful breeding of gene corrected *Pah*^{enu2} mice

One pair (a single male and a single female) of gene-corrected *Pah*$^{enu2/enu2}$ mice from the dAAV+Van treatment group were allowed to survive past 24 weeks to test both the duration of response and evaluate the breeding potential of gene-corrected mice. Although hyperphenylalaninemic mice are fertile,

female *Pah*$^{enu2/enu2}$ mice cannibalize all their offspring soon after birth due to a powerful maternal PKU effect, as well as congenital defects in the pups [207]. Typically, the *Pah*^{enu2} colony is maintained through *Pah*$^{enu2/enu2}$ male × *Pah*$^{enu2/+}$ female crosses to avoid the maternal PKU effect. The efficacy of dAAV+Van upon serum Phe in both the male and female *Pah*$^{enu2/enu2}$ mice was durable through 65 weeks of life (Figure 4A). This breeding pair utilized provided nesting materials to build well-constructed nests, a behavior not typically seen in hyperphenylalaninemic *Pah*$^{enu2/enu2}$ mice (Supplementary Figure 2-3) [28]. Furthermore, and impressively, this breeding pair yielded four liveborn litters with a total of 26 progeny (12 males and 14 females), which the dam successfully delivered and nursed through weaning without any losses. All of the progeny were hypopigmented, hyperphenylalaninemic, and genotyped with toe-tissue-extracted DNA to be consistent with homozygosity of the *Pah*^{enu2} mutation. While germline cells of breeders were not directly tested, these results support that there was no germline transmission of the CRISPR/Cas9-mediated gene correction from dAAV+Van-treated mice to their offspring.

In contrast, the breeding pairs from the dAAV and rtAAV+Van treatment groups that were allowed to survive past 24 weeks to evaluate the breeding potential in control treatment groups were both unsuccessful. All animals, two males and two females, were hypopigmented and hyperphenylalaninemic. Each pair, one dAAV and one rtAAV+Van, gestated to term, but neonates were instantly cannibalized

upon birth. Neither of these breeding pairs utilized nesting materials to build nests and remained hypopigmented and hyperphenylalaninemic until harvest at 28 weeks.

Figures

Figure 2-1: Design of *in vivo* CRISPR/Cas9 gene editing strategy in *Pah*^{enu2} mice

A. Dual AAV Constructs

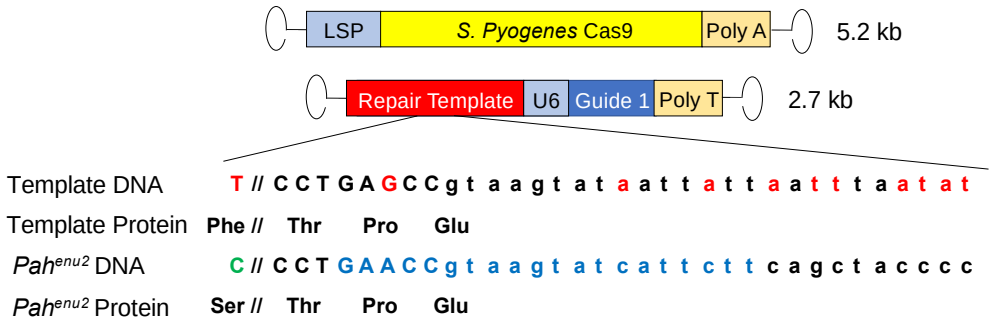

B. Diagram of expected Cas9-mediated DNA cutting and cellular repair.

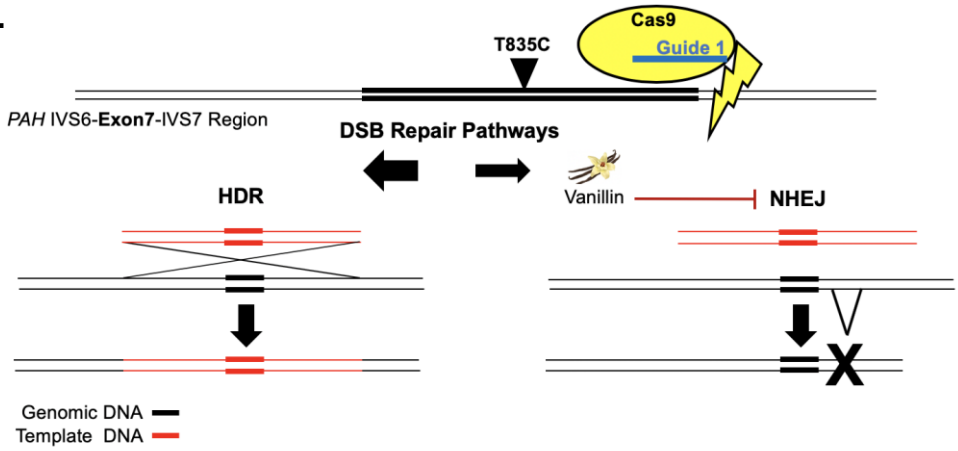

C. Table of experimental animal cohorts.

Cohort ID	Treatment	Male (N)	Female (N)	Total (N)
dAAV+Van	Dual AAV and Vanillin	5	6	11
dAAV	Dual AAV	4	6	10
rtAAV+Van	Repair Template AAV and Vanillin	2	7	9

Figure 2-1: Design of *In Vivo* CRISPR/Cas9 Gene-Editing Strategy in *Pah*^{enu2} Mice

A. Dual AAV constructs. The Cas9-expressing rAAV2/8 vector genome was 5.2 kb in length and contained the *S. pyogenes* Cas9 gene driven by a transthyretin-based liver-specific promoter (LSP). The second rAAV2/8 vector genome was 2.7 kb in length and contained a 2-kb repair template flanking 1 kb in either direction of the *enu2* missense mutation, as well as guide 1 driven by a human U6 promoter. The repair template sequence pictured below the vector genomes contained the wild-type *Pah* exon 7 sequence with correction of the *Pah*^{enu2} mutation, as well as purposefully introduced synonymous and intronic mutations (denoted in red) to hinder Cas9 cutting of corrected alleles. Uppercase denotes exonic *Pah* sequence, and lowercase indicates intronic sequence. The wild-type protein sequence of the repair template demonstrates correction of the Ser263Phe and a synonymous mutation at Pro279. The *Pah*^{enu2} allele below reveals the c.835T > C mutation in green and the guide targeted sequence in blue. The symbol "//" indicates 46-bp DNA and 15-aa separation. **B. Diagram of expected Cas9-mediated DNA cutting and cellular repair.** Guide 1, indicated in blue, directs Cas9 (yellow oval) to induce a double-strand break (DSB) (indicated by the lightning bolt) 46 bp downstream of the c.835T > C mutation (black arrow) in the *Pah*^{enu2} allele; double lines indicate double-stranded DNA (dsDNA), where thick lines are exons and thin lines are introns. Potential DSB intracellular pathways that the cell may utilize to repair the Cas9 DSB are depicted below. The repair template, indicated in red, may be incorporated into

the genome by homology-directed repair (HDR), pictured on the left. Alternatively, non-homologous end joining (NHEJ) restores the mutant allele (not shown); or alternate end joining (Alt-EJ), pictured at the right, results in a small insertion or deletion (indel, indicated by the bold X). Either NHEJ or Alt-EJ fails to incorporate the repair template. Vanillin is a potent NHEJ inhibitor (indicated by the smaller arrow at the right) that directs DSB repair toward HDR (indicated by the larger arrow at the left). **C. Table of experimental animal cohorts.** Three experimental animal cohorts were tested in this study. The cohort with dual AAV plus vanillin (dAAV+Van) received both viral vectors plus vanillin, with a total of 11 animals treated: 5 males and 6 females. The dual-AAV (dAAV) cohort received both viruses but no vanillin, with a total of 10 animals treated: 4 males and 6 females. The cohort with repair template vector plus vanillin (rtAAV+Van) received only the repair template virus with vanillin, with a total of 9 animals treated: 2 males and 7 females.

Figure 2-2: Efficacy of *in vivo* CRISPR/Cas9 gene editing in *Pah*^{enu2} mice

A. Experimental Timeline

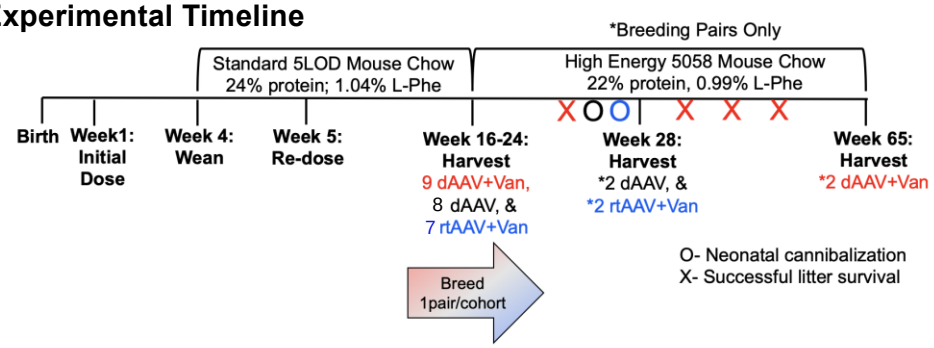

B. Serum Phenylalanine

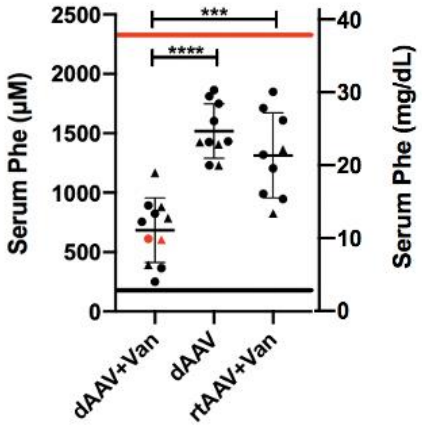

C. PAH Enzyme Activity

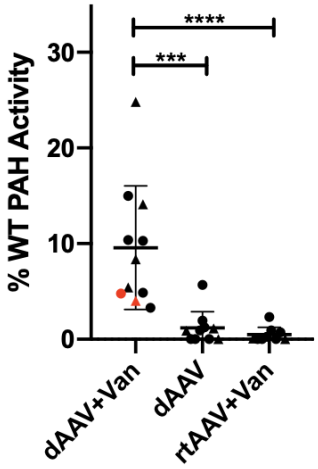

D. Coat Color at Euthanasia

Wildtype ***Pah***^{enu2} ***Pah***^{enu2} **dAAV+Van** ***Pah***^{enu2} **rtAAV+Van** ***Pah***^{enu2} **dAAV**

Figure 2-2: Efficacy of *In Vivo* CRISPR/Cas9 Gene Editing in *Pah*^{enu2} Mice

A. Experimental timeline. *Pah*$^{enu2/enu2}$ mice were born, administered the initial dose of drug in the first week of life, weaned at 4 weeks, and placed on standard mouse chow. At week 5, mice were re-dosed with drug. Between 16 and 24 weeks, mice from each cohort were harvested, and one breeding pair per treatment group was placed on high-energy mouse chow and allowed to breed. By 28 weeks, one successful litter was produced by the dAAV+Van pair, while the dAAV and rtAAV+Van pairs did not successfully breed. At this point, the dAAV and rtAAV+Van breeding pairs were euthanized for tissue collection. The dAAV+Van breeder pair produced three more successful litters and were euthanized at 65 weeks. **B. Serum phenylalanine.** The graph shows serum phenylalanine levels of dAAV+Van, dAAV, and rtAAV+Van animals at time of euthanasia. The left y axis indicates serum Phe in micromol/l, while the right y axis indicates serum Phe in micrograms per deciliter. The red line indicates the mean serum phenylalanine concentration of an unrelated cohort of untreated male and female *Pah*$^{enu2/enu2}$ animals combined consuming standard mouse chow [28]. The black line indicates the upper limit of serum Phe levels in wild-type mice (180 µM or 3 mg/dL). The x axis is separated by treatment group, in the order of dAAV+Van, dAAV, and rtAAV+Van from left to right, whisker plots depict mean serum phenylalanine ± 2 SD, and each dot on the graph indicates an individual animal. Males are depicted with triangles and females with circles. Red indicates 65-week-old animals, and black indicates 16- to 24-week-old animals. The average Phe levels were 685 µM, 1,518 µM, and 1,314 µM,

respectively; and ranges were 252–1,168 μM, 1,231–1,863 μM, and 827–1,850 μM, respectively. Intergroup comparisons (depicted as brackets above the treatment groups) revealed significant differences between dAAV+Van and dAAV ($p < 0.0001$, ****) and between dAAV+Van and rtAAV+Van ($p = 0.0001$, ***). **C. PAH enzyme activity.** The graph shows the PAH enzyme activity levels of dAAV+Van, dAAV, and rtAAV+Van animals at time of euthanasia. The y axis indicates percent wild-type PAH activity; the x axis is separated by treatment group in the order of dAAV+Van, dAAV, and rtAAV+Van from left to right, whisker plots depict mean liver PAH activity ± 2 SD, and each dot on the graph indicates an individual animal. Males are depicted with triangles, and females are depicted with circles. Red indicates 65-week-old animals, and black indicates 16- to 24-week-old animals. The average activity was 9.5%, 1.2%, and 0.5%, respectively, and ranges were 3.3%–25%, 0%–5.7%, and 0%–2.3%, respectively. Intergroup comparison reveals a significant difference between dAAV+Van and dAAV ($p = 0.0002$, ***) and between dAAV+Van and rtAAV+Van ($p < 0.0001$, ****). **D. Coat color at euthanasia.** Photograph of coat colors of mice from each treatment group at 16–24 weeks of age in comparison to wild-type or untreated *Pah*$^{enu2/enu2}$ mice. Mice are lined up from left to right as wild-type, untreated *Pah*$^{enu2/enu2}$, dAAV+Van, rtAAV+Van, and dAAV.

Figure 2-3: On- and Off-Target CRISPR/Cas9 DNA Analyses

A. Table of top four cutting sites for *Sp*Cas9+Guide 1 in the mouse genome

Genomic Location	Chr. Region	Gene Name	Gene Region	Target Sequence PAM	Score
Chr10:87570336	10qC	*PAH*	Exon7-Intron7	AAGAATGATACT TACGGTTCAGG	0.00
Chr10:116187078	10qD2	*PTPRR*	Intron5	AAGAAAGATGCTT ACGGTTCTGG	0.71
Chr12:60323904	12qC1	N/A	N/A	AAACATGATCTT ACGGTTCAGG	1.33
ChrX:140587182	XqF1	Tcs22d3	Intron 3	ATGAATGATTCT TACTGTTCAGG	2.93

B. On-Target Repair

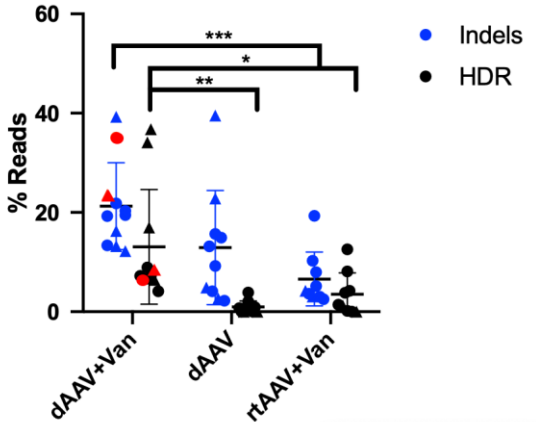

C. Functional Reads

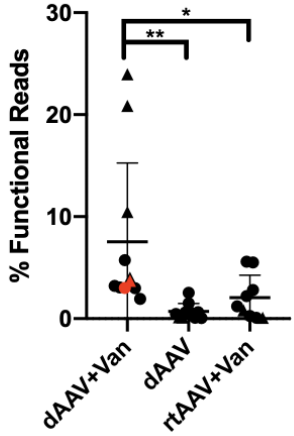

D. Sanger sequencing of dAAV+Van *enu2* correction

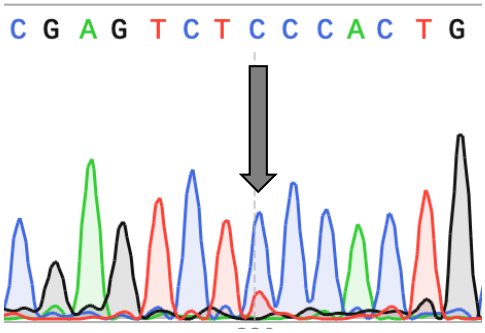

E. Percent Off Target Indels

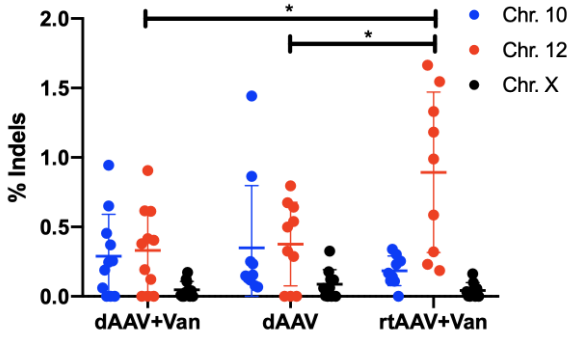

Figure 2-3: On- and Off-Target CRISPR/Cas9 DNA Analyses

A. Table of Top Four Cutting Sites for *Sp*Cas9+Guide 1 in the Mouse Genome. Two *in silico* tools, Cas-OFFinder and COSMID, were used to identify the top four *Sp*Cas9-Guide1 cutting sites in the mouse genome. Locations of cutting sites are described in the first four columns, followed by target sequence (black) and PAM (red) in the next column. The last column indicates the COSMID score, in which the lowest, 0, indicated the highest probability of cutting (the target site) and ranged to over 40, with the lowest probability of cutting. The top three off-target sites located on chr 10, chr 12, and chr X were scored as 0.17, 1.33, and 2.93, respectively, as indicated in the last column. **B. On-target repair.** The graph shows percent reads of indels (blue) or "full" HDR (including exonic and intronic sequences) (black) in dAAV+Van, dAAV, and rtAAV+Van animals at time of euthanasia. The y axis indicates percent reads of overall NGS reads; the x axis is separated by treatment group in order of dAAV+Van, dAAV, and rtAAV+Van from left to right, whisker plots depict the mean percent reads ± 2 SD, and each dot on the graph indicates an individual animal. Males are depicted with triangles, and females are depicted with circles. Red indicates animals at 65 weeks, and black indicates animals at 16–24 weeks. The average percentages of indel reads were 21.27%, 12.92%, and 6.58%, respectively, with ranges of 12.25%–39.29%, 2.2%–39.54%, and 2.52%–19.34%, respectively. The average percentages of HDR reads were 13.06%, 0.96%, and 3.51%, respectively, and ranges were 4.13%–36.78%, 0%– 3.90%, and 0%–12.57%, respectively. Two-way ANOVA revealed a significant difference between

treatment groups, $F(2, 54) = 12.87$, $p < 0.0001$; and DNA repair, $F(1, 54) = 13.11$, $p = 0.0006$. Brackets above the treatment groups depict post hoc intergroup statistical comparisons. * - $p < 0.05$; ** - $p < 0.01$, *** - $p < 0.001$, **** - $p < 0.0001$

C. Functional reads. The graph indicates functional reads of exonic-only NGS reads in dAAV+Van, dAAV, and rtAAV+Van animals at time of euthanasia. The y axis indicates the percentages of functional *Pah*-exon7 NGS reads. The x axis is separated by treatment group in order of dAAV+Van, dAAV, and rtAAV+Van from left to right, whisker plots depict the mean percent functional reads ± 2 SD, and each dot on the graph indicates an individual animal. Males are depicted with triangles, and females are depicted with circles. Red indicates 65-week-old animals, and black indicates 16- to 24-week-old animals. The averages of functional reads were 7.54%, 0.70%, and 2.06%, respectively; and ranges were 1.94%–23.97%, 0.11%–2.54%, and 0.08%–5.58%, respectively. One-way ANOVA revealed significant difference of treatment groups, $F(2, 27) = 5.805$, $p = 0.0080$; with a p value of 0.0093 between dAAV+Van and dAAV and a p value of 0.048 between dAAV+Van and rtAAV+Van. Brackets above the treatment groups depict post hoc intergroup statistical comparisons. * - $p < 0.05$; ** - $p < 0.01$. **D. Sanger sequencing of dAAV+Van *enu2* allele correction.** The Sanger sequencing chromatogram shows low levels of correction in liver genomic DNA, as indicated with the large arrow pointing to the *Pah*^{enu2} c.835T > C (indicated with "C" in blue) site that contains a small peak of corrected (indicated with "T" in red) DNA. **E. Percent off-target indels.** The graph shows the percentage of overall NGS reads containing indels in the top three off-target regions identified

in Figure 3A. The y axis shows the percentage of indels; the x axis is separated by treatment groups in the order of dAAV+Van, dAAV, and rtAAV+Van from left to right, with further nested separation of each chromosomal region in order of highest likelihood of cutting to lowest; chr 10, chr 12, and chr X, for each treatment group. Each animal is represented by a blue, a red, and a black dot, indicating chr 10, chr 12, and chr X, respectively. Whisker plots depict the mean percent off target indels ± 2 SD. The average percentages of indels for chr 10 were 0.29%, 0.35%, and 0.18%, respectively; for chr 12, they were 0.33%, 0.38%, and 0.89%, respectively; and for chr X, they were 0.05%, 0.09%, and 0.04%, respectively. The ranges of percent indels for chr 10 were 0%–0.94%, 0.07%–1.44%, and 0%–0.34%, respectively; for chr 12, they were 0%–0.91%, 0%–0.80%, and 0.19%–1.66%, respectively; and for chr X, they were 0%–0.17%, 0%–0.33%, and 0%–0.16%, respectively. One-way ANOVA of each chromosomal region between treatment groups revealed significant difference in only the chr 12 region, $F(2, 27) = 5.709$, $p = 0.0086$; with a p value of 0.012 between rtAAV+Van and dAAV+Van and a p value of 0.0248 between rtAAV+Van and dAAV. Brackets above the treatment groups depict post hoc intergroup statistical comparisons. * - $p < 0.05$.

Figure 2-4: On- and Off-Target CRISPR/Cas9 DNA Analyses

A. Longitudinal Phe in dAAV+Van Animals

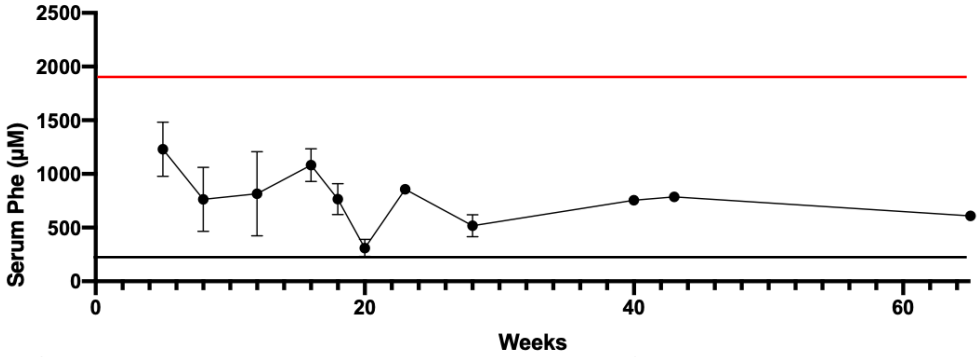

B. Growth in Untreated vs. dAAV+Van treated PKU Mice

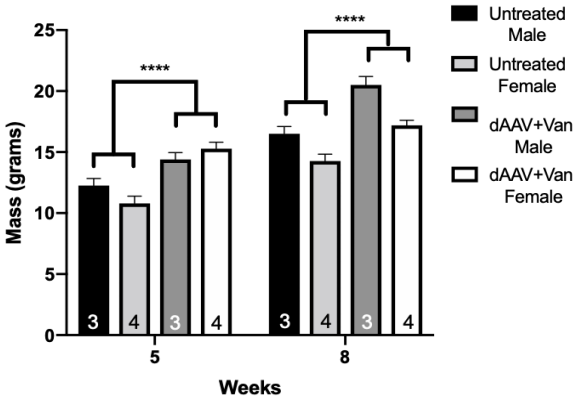

C. PAH Activity by Functional Reads

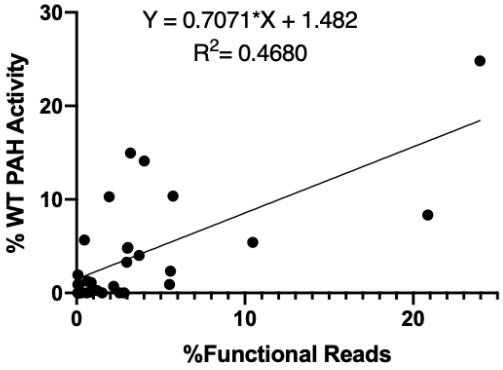

D. Serum Phe by Functional Reads

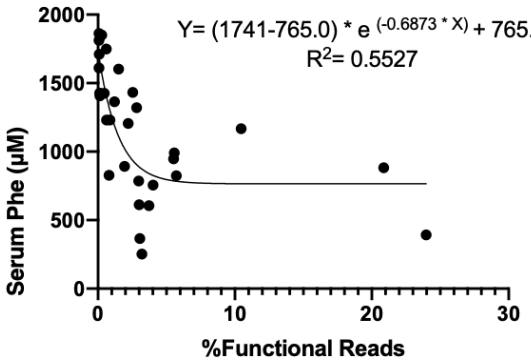

E. Serum Phe by PAH Activity

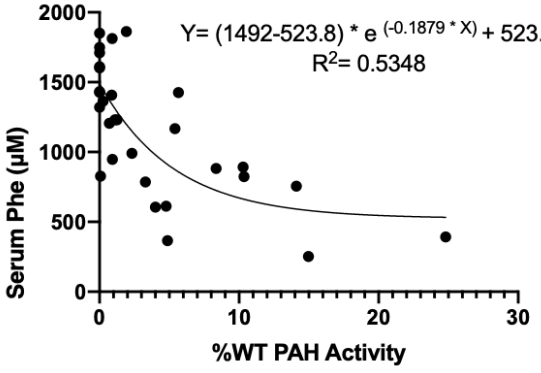

Figure 4. Efficacy of *In Vivo* CRISPR/Cas9 Gene Editing in dAAV+Van-Treated Animals

A. Longitudinal Phe in dAAV+Van animals. Plot of long-term (up to 65 weeks) serum phenylalanine concentration in the dAAV+Van cohort mice. The red line denotes the mean serum phenylalanine concentration of an unrelated cohort of untreated male and female combined *Pah*$^{enu2/enu2}$ animals consuming standard mouse chow [28]. The black line indicates the upper limit of serum Phe concentration in wild-type C57BL/6 mice (180 μM). For the time points for which Phe measurements in multiple mice were available, the data are presented as mean ± SEM. Data at 40–65 weeks are means of the two dAAV+Van animals, one male and one female, that remained a breeding pair until euthanasia. **B. Improved growth in dAAV+Van-treated animals.** Three untreated age-matched males and three untreated age matched females were compared to dAAV+Van-treated animals. A three-way ANOVA comparing age, treatment group (control versus treated), and sex showed statistically significant differences between these animals, albeit low sample sizes, $F(1, 10) = 10.44$, $p = 0.0090$. Post hoc intergroup comparisons revealed consistent significant differences between each treated and untreated group of either sex ($p < 0.0001$) as depicted by the brackets with asterisks (****). **C. Correlation between liver PAH activity and functional *Pah* exon 7 reads in dAAV+Van-treated mice.** Plot of percent wild-type liver PAH enzyme activity on y axis versus the percent functional *Pah* exon 7 reads on the x axis with linear regression analysis. Each point is a single dAAV+Van mouse at euthanasia. Graph shows percent

functional *Pah* exon 7 reads on the x axis and percent wild-type PAH enzyme activity on the y axis. Each point represents a dAAV+Van animal at time of euthanasia. (D) Correlation between serum Phe and percent functional *Pah* exon 7 reads in dAAV+Van-treated animals. Plot of serum Phe on the y axis versus percent functional *Pah* exon 7 reads on the x axis. Each point represents a dAAV+Van animal at time of euthanasia. The data were fit with a non-weighted, non-linear exponential one-phase decay using least-squares regression. **E. Correlation between serum Phe and liver PAH enzyme activity in dAAV+Van-treated animals.** Plot of serum Phe on the y axis versus percent wild-type liver PAH enzyme activity on the x axis. Each point represents a dAAV+Van animal at time of euthanasia. The data were fit with a non-weighted, non-linear exponential one-phase decay using least-squares regression.

Supplementary Figure 2-1: Guide 1 Validation

A. Surveyor Assay

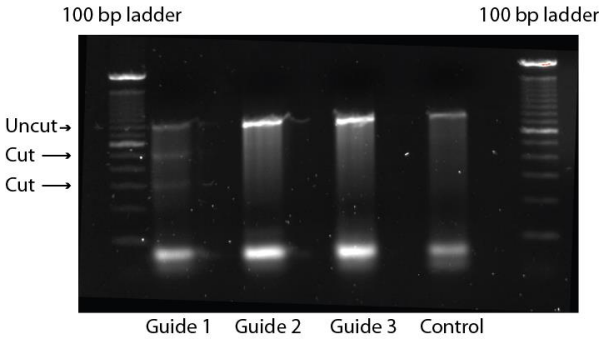

B. Takara Guide-It Assay

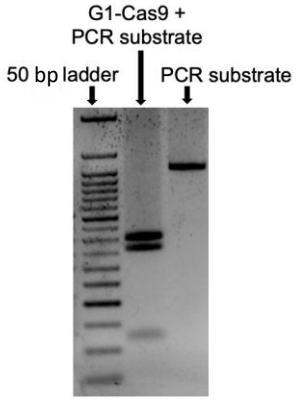

Supplementary Figure 2-1: Guide 1 Validation

A. Surveyor Assay. Gel electrophoresis of Surveyor Assay performed with Guide 1, 2, and 3, as indicated, with control uncut 800bp PCR target and flanking 100bp ladder. Guide 1 was the only guide showing any visible cutting of the target, as indicated. **B. Takara Guide-It Assay.** Gel electrophoresis of in vitro Guide-It Takara Assay performed with Guide 1, with 50bp ladder on the left and uncut 800bp substrate on the right. Again, RNP-Guide1 showed visible cutting of the target PCR substrate.

Supplementary Figure 2-2: NGS Selection and Validation

A. COSMID Output: *Sp*Cas9-Guide1 Target Sites

Chr Position	Strand	Cut site	Score
Chr10:87570336-87570358	-	87570342	0
Chr3:62532887-62532909	+	62532903	5.42
ChrX:140587182-14058720	-	140587188	2.93
Chr17:78827214-78827236	+	78827230	22.45
ChrX:52428425-52428447	+	52428441	11.19
Chr10:116187078-1161871	+	116187094	0.71
Chr11:107380762-1073807	-	107380768	9.27
Chr1:193399721-19339974	-	193399727	6.6
Chr10:87570336-87570357	-	87570342	0.63
Chr10:116187079-1161871	+	116187094	1.34
Chr3:62532888-62532909	+	62532903	5.93
Chr10:87570336-87570357	-	87570342	0.79
Chr10:87570336-87570357	-	87570342	0.96
Chr7:71689783-71689804	+	71689798	23.04
Chr16:26312076-26312097	+	26312091	8.78
Chr18:59943710-59943731	+	59943725	23.86
Chr12:60323904-60323925	+	60323919	1.33
Chr4:69351258-69351279	+	69351273	7.11
Chr13:48943433-48943454	-	48943439	5.6
Chr18:52791504-52791525	-	52791510	7.11
Chr12:99734046-99734067	-	99734052	11.41
Chr19:32989811-32989832	+	32989826	5.93
Chr10:11174367-11174388	-	11174373	6.16
Chr11:81943011-81943032	+	81943026	7.08
Chr5:93684753-93684774	+	93684768	10.01
Chr5:93948467-93948488	-	93948473	10.01
Chr5:94140055-94140076	-	94140061	10.01
Chr5:94457664-94457685	-	94457670	10.01
Chr5:95614290-95614311	-	95614296	10.01
Chr5:95755669-95755690	-	95755675	10.01
Chr10:87570337-87570358	-	87570343	30.51
Chr10:87570337-87570358	-	87570343	26.51
Chr10:87570337-87570358	-	87570343	40.51
Chr10:87570337-87570358	-	87570343	20.51
Chr10:116187078-1161870	+	116187093	21.22
Chr10:87570336-87570359	-	87570342	0.95
Chr10:87570336-87570359	-	87570342	0.97
Chr10:87570336-87570359	-	87570342	1.14
Chr13:37361079-37361102	+	37361096	3.89
Chr12:57512651-57512674	-	57512657	3.67
Chr7:5484550-5484573	-	5484556	7.23
Chr14:72236511-72236534	+	72236528	7.72
Chr10:87570335-87570358	-	87570341	32.7
Chr17:78827214-78827237	+	78827231	23.15
Chr10:87570335-87570358	-	87570341	40.7
Chr10:87570335-87570358	-	87570341	40.7

B. NGS Read Uniformity

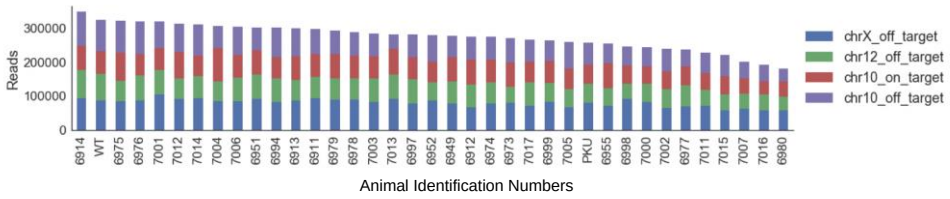

Supplementary Figure 2-2: NGS Selection and Validation

A. SpCas9-Guide1 Target Sites. Table of all COSMID produced SpCas9-Guide1 potential cutting sites. Yellow is on-target site, orange is off-target sites selected for further investigation. **B. NGS Read Uniformity.** Display of NGS read depth at every location investigated in every animal, indicating all samples were represented and no samples were dropped.

Supplementary Figure 2-3: dAAV+Van Breeders

A. dAAV+Van Breeder Nesting

B. *Pah*^{enu2}/+ Breeder Nesting

C. Female Breeder at 65 Weeks

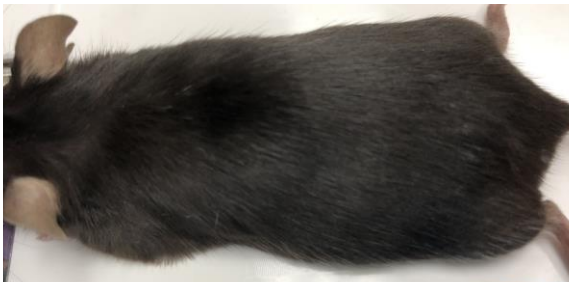

D. Male Breeder at 65 Weeks

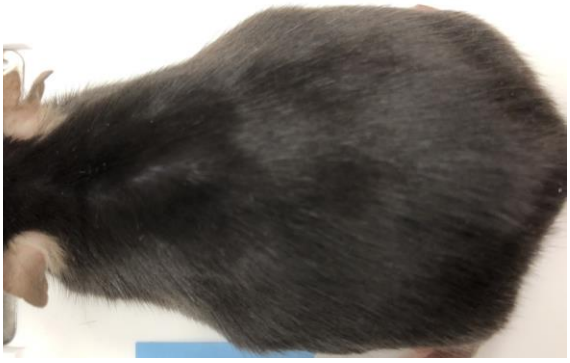

Supplementary Figure 2-3: dAAV+Van Breeders

A. dAAV+Van Breeder Nesting. Photograph of dAAV+Van breeder pair nesting. **B. Pah^{enu2}/+ Breeder Nesting.** *Pah$^{enu2/+}$* Breeder Nesting Photograph of heterozygous breeder pair nesting. **C. Female dAAV+Van Breeder.** Female dAAV+Van breeder animal at 65 weeks, with a dark fur coat and healthy mass of 29.2 grams. **D. Male dAAV+Van Breeder.** Male dAAV+Van breeder animal at 65 weeks, with a dark fur coat and obese mass of 40.7 grams.

Discussion

This study reveals promise for the utilization of the CRISPR/Cas9 system followed by HDR of the AAV-supplied donor DNA to achieve *in vivo* liver-directed gene correction for PKU. The permanent nature of editing mutations within the genome removes the concern for temporary effectiveness as seen in traditional AAV-mediated gene addition therapy for PKU. Our prior attempts with AAV-mediated, liver-directed gene addition in neonatal mice resulted in the rapid clearance of AAV episomes and only brief periods of liver PAH expression (data not shown). This result has been reported by other investigators following administration of liver-directed AAV vectors to juvenile animals in the absence of any selective growth advantage for random AAV integration events [208, 209]. For the first time, we have achieved liver-directed gene therapy in neonatal mice that persisted beyond adolescence into adult mice that was associated with substantial, albeit partial, correction of hyperphenylalaninemia for up to at least 6 months of age (at the time when most animals were euthanized for tissue harvest) and impressively up to 65 weeks in the case of a single breeder pair. Importantly, all animals in the dAAV+Van treatment group were improved in classification from severe, classical PKU to either mild PKU or mild hyperphenylalaninemia. If this dAAV+Van regimen were applied to humans suffering from classical PKU, it would greatly improve the overall quality of life by allowing increased dietary phenylalanine intake, improved maternal PKU outcomes, and possibly improved behavior and cognition, even in the case with the lowest correction (4.1% HDR, 3.3% PAH enzyme activity, 1,168 μM blood

Phe on an unrestricted diet). This treatment approach was not associated with any notable acute toxicity or any long-term adverse effects. In fact, the treatment was associated with complete reversal of the abnormal phenotypes associated with chronic hyperphenylalaninemia in *Pah*$^{enu2/enu2}$ mice, including impaired growth and hypopigmentation, despite the fact that serum phenylalanine concentrations were not fully corrected to levels typical of WT mice. Although most animals did not achieve phenylalanine levels in the recommended therapeutic range of 120–360 μM, this is the first gene therapy approach for PKU that has demonstrated lifelong effectiveness from early infancy in a PKU mouse model.

Furthermore, AAV-delivered, CRISPR/Cas9-mediated, liver-directed gene correction was associated with the prevention of maternal PKU syndrome in *Pah*$^{enu2/enu2}$ mice. Elevated maternal blood phenylalanine in humans during pregnancy causes microcephaly, intrauterine growth retardation, congenital heart disease, and postnatal developmental disability, the so-called maternal PKU syndrome [210]. Hyperphenylalaninemic *Pah*$^{enu2/enu2}$ dams gestate to term but invariably cannibalize their progeny [207]. The single breeder pair from the dAAV+Van group successfully produced four litters (Figure 2A) without any observed pregnancy losses, an outcome that is unprecedented in our laboratory, although we and others have had prior limited success with breeding *Pah*$^{enu2/enu2}$ dams following treatment of hyperphenylalaninemia applied to adult mice [211].

CRISPR/Cas9-mediated genome editing is widely used to introduce DSBs in DNA and to facilitate the deletion of functional genes in cultured cells and in whole organisms, but correction of mutant genes following Cas9-mediated DSB is entirely dependent upon the innate DNA repair activity of the host cell [180]. NHEJ, in most cases, is the default repair mechanism used to repair the DSB; this blunt end joining can result in full restoration of the original sequence (an event that cannot be detected experimentally), leaving the mutant gene intact. Alternatively, some 3′ clipping of the free ends may occur prior to annealing of the break (so-called Alt-EJ) or healing of the break with incorporation of a repair template through HDR [180, 212]. The former, less well-understood repair mechanism, Alt-EJ, yields a small deletion at the site of the DSB. If NHEJ or Alt-EJ occurs following Cas9-mediated cleavage of a mutant gene target, a functional open reading frame will not be restored. Only HDR with the incorporation of a repair template harboring the normal functional sequence will yield a functional open reading frame, but under typical conditions, the desired HDR is a rare event. In our experiment, following administration of both AAV vectors carrying the repair template and expressing the Cas9 reagents (but without the NHEJ inhibitor vanillin), the mean percentage of functional *Pah* open reading frames recovered following HDR was fewer than 1%. This repair frequency is insufficient to cause any appreciable effect upon the PKU phenotype, although it may be sufficient for treatment for some disorders such as hemophilia, where secreted protein from even a small population of hepatocytes

can be therapeutic [213]. In diseases and model systems where corrected cells enjoy a selective growth advantage, a small number of gene-edited hepatocytes can expand under selective pressure to a therapeutically relevant population. Such results have been reported for the treatment of murine fumarylacetoacetate hydrolase deficiency, a model of human tyrosinemia type 1 [214]. Unfortunately, PAH expressing hepatocytes do not enjoy a selective growth advantage over PAH-negative cells [148]. Only when we treated the mice with vanillin, a potent NHEJ-inhibitor, did the frequency of HDR increase to a level that became physiologically relevant in this model.

Our results were somewhat less robust than those of the Wilson laboratory, who used a similar dAAV system in the murine ornithine transcarbamylase (OTC) model, *OTC spf*^{ash}, and achieved approximately 10% gene correction in a disease that does not enjoy a selective growth advantage for corrected cells without use of NHEJ inhibitors. These conflicting findings could be due to differences in either the initial efficiency of Cas9-mediated double-strand breakage or the efficiency of on-target HDR using the repair template. In our study, only 14% of *Pah* alleles in dAAV-treated mice demonstrated molecular evidence of genomic alterations (HDR or indels due to Alt-EJ combined) in comparison to 41% overall genomic alteration in the OTC study. This suggests that the efficiency of Cas9-mediated double-strand breakage was much lower in our experiment. This could be attributed to differences in the total dose of AAV vectors delivered or the ratio of Cas9-expressing to repair template vectors

administered between the two experiments, both of which could have affected the efficiency of Cas9-mediated DSB formation. Alternatively, it is also possible that perfect NHEJ following Cas9 administration resulted in the restoration of the original pathogenic sequence in a majority of cleaved alleles, a result that cannot be detected experimentally. When we added the NHEJ inhibitor vanillin to dAAV, the mean frequency of total genomic alteration increased to 34% (21% indels and 13% HDR). This result supports our hypothesis that the initial frequency of Cas9-mediated DSBs was likely similar to that of the previously published OTC experiment but that the majority of Cas9-mediated DSBs were perfectly repaired by NHEJ in dAAV-treated mice rather than by Alt-EJ or HDR. The precise reason for the difference in the efficiency of on-target HDR is yet unknown. Both the repair template in our experiment and the OTC template contained multiple mismatches in comparison to their genomic targets; these differences could impair HDR efficiency. It is possible that nuanced design differences between the two templates or innate differences in the genomic target regions could have contributed to increased heteroduplex rejection, D-loop instability during HDR, or mismatch-repair-mediated antirecombination in our study [215]. While the dAAV on-target HDR remained low, the addition of vanillin improved the on-target HDR efficiency to a level similar to that achieved in the OTC study.

The therapeutic effectiveness of this gene-editing approach was highly variable between individual mice. One source of variability could be the technically challenging facial vein injection. While we were able to measure correlations

between the percentage of functional open reading frames, liver PAH activity, and final blood Phe concentration, some mice still exhibited higher than expected final blood Phe concentrations for the percentage of functional open reading frames and corresponding liver PAH activity achieved in those animals. Typically, in mice treated with AAV-mediated gene addition, restoring liver PAH activity to greater than 10% of WT activity is sufficient to fully correct blood Phe levels to normal [140]. These discordant results could be attributed to the number of PAH-expressing cells, which is also a critical factor in total body Phe flux. PAH activity must be expressed in at least 10% of hepatocytes for complete normalization of blood Phe concentrations; restriction of PAH activity to a smaller population of hepatocytes (i.e., lower transduction frequency) significantly limits Phe clearance [216]. We hypothesize that, in this experiment, HDR occurred in a small population of evenly dispersed hepatocytes (likely fewer than 10% of hepatocytes). Given that hepatocytes are polyploid [217-219] (the genetic complement can range from diploid [2n] to octoploid [8n] and even higher [128n]), a small number of cells with many edited genomes per cell could be responsible for the relatively high number of functional genomic reads and PAH activity that we have measured. The therapeutic effect may be limited by total Phe transport capacity into the restricted cell population rather than functional enzyme availability. Alternatively, it is possible that gene correction occurred predominantly within peri-central venous hepatocytes, a zone within the hepatic acinus that is not typically responsible for substantial phenylalanine hydroxylation; this is a function normally accomplished by periportal hepatocytes

[220]. In this study, we performed systemic injections of AAV8 vectors, which, in adult mice, leads to primarily peri-central venous transduction but may lead to mixed periportal and peri-central venous transduction in newborn mice [221]. Unfortunately, we are unable to directly evaluate the percentage or location of gene-corrected hepatocytes in treated liver by immunohistology, because the *Pah*$^{enu2/enu2}$ model produces abundant, albeit inactive, PAH protein; no available antibody is able to distinguish between active and inactive PAH protein. Further studies using single-cell omics would be informative for understanding the effects of this therapy at the level of individual cells.

While the *Pah*$^{enu2/enu2}$ mouse recapitulates human PKU phenotypically, this isogenic model does not capture the wide range of almost 1,000 known pathogenic variants in the *PAH* gene [222]. One limitation of CRISPR/Cas9-mediated gene editing as we have used it here or as others have used a CRISPR/Cas9 base-editor fusion [223] is that a different guide RNA—and, therefore, one of the two AAV vectors—would have to be redesigned for each patient with a novel mutation, or at least there would need to be unique reagents for each exon of the *Pah* gene. Future development of CRISPR/Cas9 gene editing should be designed to be broadly applicable to all human PKU genotypes and should aim to drive Phe levels down to WT levels. While this study was a beginning for CRISPR/Cas9 gene editing for PKU, further studies are needed before *in vivo* gene-editing translation into human medicine.

Materials and Methods

Animal husbandry

Animal care and experimentation were performed in accordance with the guidelines of the Department of Comparative Medicine, Oregon Health & Science University, and the NIH Guide for the Care and Use of Laboratory Animals. C57BL/6-*Pah*$^{enu2/enu2}$ mice, which are homozygous for a missense c.835T > C (p.F263S) mutation in exon 7 of the murine *Pah* gene, are completely deficient in liver PAH activity; are, consequently, hyperphenylalaninemic on an unrestricted diet; and are a representative animal model of human PKU [224].

Neonatal *Pah*$^{enu2/enu2}$ mice for these experiments were generated through breeding of *Pah*$^{enu2/enu2}$ sires to *Pah*$^{enu2/+}$ dams. Genotyping for the presence of the *Pah*^{enu2} mutation was performed by a TaqMan qPCR assay. All mice were fed tap water and standard mouse chow (LabDiet Picolab Rodent Diet 5LOD, St. Louis, MO, USA) *ad libitum*, providing approximately 24% protein and 1.04% L-Phe by weight, except the breeders that received high-energy chow (LabDiet Rodent High Energy Diet 5058, St. Louis, MO, USA), providing approximately 22% protein and 0.99% L-Phe. Given that adult mice consume approximately 5 g chow per day, daily L-Phe intake was estimated to be approximately 50 mg/day. The animals were housed under a standard 12-h:12-h on-off light cycle. All surgical procedures were carried out with inhaled isoflurane general anesthesia to minimize pain and discomfort.

Guide Design and Validation

The sequence flanking c.835T > C was entered into the MIT Guide Design tool. Three guides were chosen for validation using the cell-culture-based Surveyor system and revalidated with the *in vitro* Takara Guide-It Kit (Supplementary Figure 2-1).

Viral Production

Plasmid AAV2 LSP-Cas9 was graciously supplied by the Grompe laboratory, and the AAV2 repair template with guide plasmid was synthesized by GeneScript. Plasmids were confirmed for overall integrity, and intact Inverted Terminal Repeats (ITRs) via RE screen using Taq1 and Ahd1, respectively. The OHSU Molecular Virology Core produced large-scale preparations of recombinant rAAV2/8 viruses, referenced as rAAV2/8_LSP_SpCas9 and AAV2/8_Ex7RepairTemp_U6G1, using standard triple plasmid transfection procedures into cultured HEK293 cells and purified by iodixanol gradient ultracentrifugation [225]. AAV titers were determined using ITR-based qPCR analysis.

Vector Administration and Vanillin Treatment

Post-natal day 3 *Pah*^{enu2} mice were injected through the facial vein with 2.1 × 10^{11} vg AAV2/8_LSP_SpCas9 and 3.3 × 10^{11} vg AAV2/8_Ex7RepairTemp_U6G1 in a single injection, with a total volume of 10 µL and administered daily intraperitoneal injections of 100 mg/kg vanillin for 7 days, according to treatment

designation. Mice were weaned at 4 weeks of age. Between 5 and 8 weeks of age, mice underwent a retro-orbital bleed to collect plasma using heparinized capillary tubes followed by a tail vein injection of 2.1×10^{12} vg AAV2/8_LSP_SpCas9 and 3.3×10^{12} vg AAV2/8_Ex7RepairTemp_U6G1 in a single injection, with a total volume of 100 µL and administered daily intraperitoneal injections of 100 mg/kg vanillin for 7 days, according to treatment designation.

Euthanasia and Tissue Harvest

Animals were sedated using inhaled isoflurane anesthesia. Whole blood was collected by cardiac puncture and allowed to clot in an Eppendorf tube, and serum was separated by centrifugation. The mice were then euthanized by exsanguination and perfused with 20 mL normal saline via the left cardiac ventricle to clear blood from the liver.

Serum Phenylalanine

Serum phenylalanine was determined using an established fluorometric protocol [226].

Liver PAH Enzyme Activity

PAH enzyme activity was determined using an established radioactive chromatography assay [227] with modifications [228].

Liver DNA Extraction

Separate liver biopsies, approximately of 7 mg each, were collected from four different lobes for each animal and collectively put through the Qiagen DNeasy Blood & Tissue Kit according to manufacturer's protocol.

Screening for Viral DNA

Liver DNA was screened for the presence of viral DNA by standard bench-top PCR using primers specific to each transgene. A portion of Cas9 sequence was amplified from the Cas9 vector (forward primer: 5′-CAGCCAGGAAGAGTTCTACAAG-3′; reverse primer: 5′-CATTCCCTCGGTCACGTATTT-3′), and the human U6 sequence was amplified from the repair template vector (forward primer: 5′-GAGGGCCTATTTCCCATGATT-3′; reverse primer: 5′-TGTTTCGTCCTTTCCACAAGATA-3′).

On-Target PCR Amplicon Preparation

The QIAGEN LongRange PCR Kit was used according to the manufacturer's protocol on genomic liver DNA using a forward primer targeting genomic DNA 58 bp upstream of the 5′ end of the repair template sequence, 5′-AGTTACTGTCGTTTGCAATGCCGC-3′, and a reverse primer, 5′-GCACAGTAGCCACTAATTCTCTCCTTAG-3′, located 426 bp downstream of the C836T mutation within the repair template region. A secondary nested PCR was performed using the 5′-GGGTTGTAGTCTCTCTGGATTTACCA-3′ forward primer

and 5′-GCACAGTAGCCACTAATTCTCTCCTTAG-3′ reverse primer with Invitrogen Platinum Taq DNA Polymerase according to the manufacturer's recommendations.

On- and Off-Target Next Generation Sequencing

Off-target sites were selected using two *in silico* tools: Cas-OFFinder and COSMID [229, 230]. Three guides present in both algorithms scored with the highest probability of off-target cutting were selected: Chr10:116187094 (COSMID score, 0.17), Chr12:60323919 (COSMID score, 1.33), and ChrX:140587188 (COSMID score, 2.93), as well as the target site Chr10: 87570342 (COSMID score, 0.00). COSMID-designed Illumina primers were ordered with adaptor sequences developed by the O'Roak lab. The four regions were PCR amplified for each animal with the Invitrogen Platinum Taq DNA Polymerase PCR Kit using genomic liver DNA according to the manufacturer's protocol. Products were run on a 1.2% agar gel and purified with the QIAGEN PCR Purification Kit according to the manufacturer's protocol. A secondary PCR was performed to index each animal with a unique barcode using primers developed by the O'Roak lab using the Invitrogen Platinum Taq DNA Polymerase PCR Kit for 6 cycles. Products were run on a 1.2% gel and purified with the QIAGEN QIAquick PCR Purification Kit. Samples were quantified using the Epoch Microplate Spectrophotometer and pooled in 1:1 ratios for each region. Pooled samples were then quantified with the Qubit 4 Fluorometer and diluted to 2-nM concentrations. Each region was then combined in a 1:1 ratio in 20 µL and

sent to the Molecular Technologies Core at Oregon Health and Science University. Samples were prepared with the V2 500 kit and run on the Illumina MiSeq instrument that downloaded raw data in FASTQ format to Illumina Base Space.

MiSeq Sequencing Data Analysis

FASTQ files generated by NGS with were split by index using Python, pair-end reads were merged with PEAR v0.9.6 [231], and common primer sequences were trimmed using Cutadapt v1.18 [232] as previously described [233]. Reads were split into each region for each animal by match to the first 25 bp in each amplicon. Data were analyzed in CRISPResso using the *Pah*^{enu2} allele as the reference sequence for the target region, and mouse reference for each off-target region; indels were called with >1-bp indel mismatch to the reference, and HDR was called with a 98% identity to the repair template sequence [234]. In addition, on-target data were run for percent match to the functional coding sequence of the PAH exon 7 region.

Sanger Sequencing

The purified on-target PCR product described earlier was quantified using the Epoch Microplate Spectrophotometer and sent for standard Sanger sequencing with the 5′-GGGTTGTAGTCTCTCTGGATTTACCA-3′ forward primer on an ABI 3130XL sequencer at the Vollum DNA Services Core at Oregon Health & Science University.

Acknowledgements

DYR and the experiments were funded by the National PKU Alliance. SRW, SD, COH were funded by NIH R01 NS080866.

We would like to acknowledge the O'Roak laboratory for supplying us with NGS expertise and reagents. We would also like to express our gratitude to the National PKU Alliance for supporting this research.

Author Contributions

D.Y.R. performed the experiments, analyzed data, and wrote the manuscript.

S.R.W. performed the surgical procedures and assisted with mouse breeding, molecular techniques, and experimental design.

S.D. assisted with mouse breeding and molecular techniques.

S.N. assisted with experimental design and reagents.

T.L.M. assisted with NGS preparation and bioinformatic analyses.

M.G. assisted with reagents, experimental design, analyses, data interpretation, manuscript editing, and oversaw D.R. as a dissertation advisory committee member.

C.O.H. assisted with funding, experimental design, analyses, data interpretation, manuscript editing, and was primary mentor to D.R. during graduate school.

CHAPTER 3:

Integrating & Selective Liver-Directed AAV Gene Therapy in Murine Phenylketonuria

This work was unpublished.

Abstract

Despite being the most common and well-studied inborn error of metabolism, the standard of care for phenylketonuria (PKU) has remained largely unchanged since the development of Phe-free sustenance in the 1950s. The lifelong adherence to a highly restrictive, expensive and unpalatable diet is onerous for all and unrealistic for most. Gene therapy has the potential to be a one-time treatment allowing an unrestricted diet for life, without the devastating neurological consequences of non-adherence to the current standard of care.

While adeno-associated virus (AAV) mediated gene addition therapy has shown promise of robust and long-lasting therapeutic effects in *Pah*$^{enu2/enu2}$ mice, a model of classical PKU, the effect is ultimately temporary due to loss of transgene expression. This is primarily due to the loss of episomal concatemers of the transgene after cell division, as well as the lack of selective advantage for PAH-positive hepatocytes. In an attempt to abrogate the loss of transgene expression, this study aimed to use GeneRide™, promoterless vector that integrates into the 3' region of the albumin locus, in combination with universal hepatocyte selection, a method of conferring selective advantage of properly integrated vector to allow for clonal expansion and repopulation of the liver under tyrosinemia conditions, in a singular gene therapy approach to treat murine PKU. The degree of clonal expansion can be determined indirectly through immunohistological visualization of the therapeutic protein. However this is

problematic in *Pah*$^{enu2/enu2}$ mice, which produce abundant mutant PAH that is readily detected by PAH antibodies.

In anticipation of this obstacle, the transgene derived PAH enzyme in this study was modified to contain an N-terminal hemagglutinin (HA) peptide tag. Preliminary studies in tyrosinemic mice showed promise for the selective advantage aspect of this construct, as high dose treated mice were able to tolerate removal of tyrosinemia protection for longer periods of time than low dose animals. Unfortunately, administration of this therapy in *Pah*$^{enu2/enu2}$ animals using chemically induced tyrosinemia led to unexpected toxicity that halted this study prematurely. Ultimately this study led to the identification of a peptide tag of the PAH enzyme that does not interfere with function and can be visualized *in vitro* and *in vivo* without denaturation.

Introduction

Despite being the most common and well-studied inborn error of metabolism, the standard of care for phenylketonuria (PKU) has remained largely unchanged since the development of Phe-free sustenance in the 1950s [24]. The lifelong adherence to a highly restrictive, expensive and unpalatable diet is onerous for all and unrealistic for most [84]. Gene therapy has the potential to be a one-time treatment allowing an unrestricted diet for life, without the devastating neurological consequences of non-adherence to the current standard of care [193].

While liver-directed adeno-associated virus (AAV) mediated gene addition therapy has a robust and long-lasting therapeutic effect in adult *Pah*$^{enu2/enu2}$ mice [140], a model of classical PKU [91], the effect is ultimately temporary [146] and attributed to loss of transgene expression. This observation is likely due to the nature of AAV DNA delivery to target cells, which results in extrachromosomal episomes, predominantly high molecular weight concatemers of the transgene, within the nucleus [135]. These extrachromosomal concatemers are readily lost during cellular division, whether induced naturally through tissue maintenance or unnaturally, through a partial hepatectomy, as there are no biological signals for episomal fate in the host cells to mark it for replication, mitosis, or distribution into daughter cells [235]. Rarely, approximately 0.1% of vg administered, will insert into the genome through non-homologous recombination [135]. For the few hepatocytes that undergo an insertion of the transgene into the host genome,

there are certain conditions that will allow for selection and clonal expansion of those cells. These include diseases that induce hepatic toxicity that is alleviated with correction, such as Wilson's disease, alpha-1 antitrypsin deficiency, familial intrahepatic cholestasis, and most notably, hereditary tyrosinemia type 1 (HT1) [150].

HT1 is characterized by fumarylacetoacetate hydrolase (FAH) deficiency, which results in the accumulation of hepatotoxic metabolites, fumarylacetoacetate and succinylacetone, in a cell-autonomous fashion. In the HT1 liver, FAH-positive hepatocytes confer strong selective advantage and result in clonal expansion of hepatocytes that no longer accumulate toxic metabolites. This phenomenon is nicely illustrated in AAV gene addition therapy in HT1 mice, which revealed a strong selective advantage for hepatocytes expressing functional FAH from chromosomally integrated transgenes that clonally expanded to repopulate the liver [236]. Unfortunately, correction of PKU does not confer selective advantage in hepatocytes, as the toxic metabolites produced in this disease, phenylketones, primarily effect the brain and nervous tissues.

In an attempt to abrogate the loss of transgene expression in PKU, this study aimed to perform targeted genome integration with a transgene that is able to harness the selective power of HT1 in a liver directed AAV gene therapy. The two technologies that can accomplish this are GeneRide™ (GR) and universal hepatocyte selection (UHS), respectively [149, 150]. GeneRide™, trademarked

by Logic Bio Therapeutics, Inc. in 2016, is a promoterless AAV liver gene therapy that integrates a therapeutic transgene into the albumin locus by harnessing the power of AAV-mediated targeted integration [237]. AAV accomplishes this by delivering single-stranded DNA (ssDNA) that contains a payload flanked by homologous sequences to chromosomal DNA, which can then align and become incorporated into the genome of target cells through homologous recombination (HR). The GeneRide™ construct accomplishes this with flanking regions of homology to the 3' end of the endogenous albumin locus surrounding the payload containing an amino-terminal self-cleaving peptide sequence preceding the therapeutic DNA. This system allows for high expression of both albumin and the "gene along for the ride" under the strong endogenous albumin promoter.

While this approach will allow for targeted integration of *Pah, "*the riding gene", into the host genome, it is not expected to achieve therapeutic levels, as integrations occur in approximately 1% of hepatocytes at highest dose administered [149, 150]. PKU requires a therapeutic threshold of 10% PAH enzyme activity to confer correction, ideally dispersed evenly throughout zone 1 peri-portal hepatocytes [148, 238]. The use of a combinatorial approach including universal hepatocyte selection would allow for the expansion of these integrated hepatocytes to reach this threshold. The universal hepatocyte selection component allows properly integrated hepatocytes to repopulate the liver under tyrosinemia conditions, which can be achieved genetically through

fumarylacetoacetate hydrolase (FAH) deficiency or chemically with a FAH inhibitor [239-241].

The selective advantage of properly integrated hepatocytes is achieved by inhibiting an upstream enzyme in the FAH pathway, hydroxyphenylpyruvate dioxygenase (HPPD), by way of an embedded miRNA within the albumin intron region of the vector transgene 3' homology arm. This allows integrated vectors the ability to provide cells with a cell-autonomous mechanism for HPPD inhibition, preventing the toxic accumulation of fumarylacetoacetate and succinylacetone produced in FAH deficiency [150]. This HPPD enzyme is in fact the target of the triketone therapeutic, 2-(2-nitro-4-trifluoromethylbenzoyl)-1,3-cyclohexanedione (NTBC), used to treat HT1 in humans and mouse models [241-243]. In order to recapitulate tyrosinemia in a PKU mouse model that does not have genetic HT1, a small molecule synthetic drug, 4-[(2-carboxyethyl)-hydroxyphosphinyl]-3-oxobutyrate (CEHPOBA) can be administered, which mimics HT1 by inhibiting FAH [239]. Disruption of FAH causes the buildup of the cell-autonomous hepatotoxic metabolites fumarylacetoacetate and succinylacetone, causing hepatorenal-toxicity and renal Fanconi syndrome and porphyria-like disruption of heme synthesis, respectively [243-245]. These toxic assaults to the liver disrupt proper cell growth, DNA replication, and cell division, allowing for selective growth advantage of cells that have protection from these toxic metabolites, as with NTBC treatment or universal hepatocyte selection using a miRNA against the upstream enzyme HPPD.

The aim of this study was to employ the GeneRide™ and universal hepatocyte selection combinatorial approach (GR+UHS) to allow for clonal expansion of properly integrated hepatocytes to ultimately correct the pathology of PKU in a robust and permanent manner in classical PKU mice.

Results

In order to visualize the clonal expansions of integrated hepatocytes in a model that produces abundant mutant PAH, the transgene derived PAH enzyme needed to be modified to contain a peptide tag that would not be cross reactive endogenous proteins, including PAH. Previous studies in our lab adding a FLAG™-tag, the hydrophilic DYKDDDDK peptide sequence, to either the C- or N- terminal ends of the PAH enzyme were found to be unsuccessful. While the FLAG tag on the C terminal tetramerization domain was detectable by denaturing Western blot using anti-FLAG antibody, it unfortunately could not be visualized in *in vivo* studies, suggesting that it was possibly buried in the tetramerization domain. In contrast, the FLAG peptide on the N-terminal regulatory domain was detectable in both denaturing and native conditions but unfortunately resulted in a non-functional enzyme. This study aimed to create a tagged PAH enzyme that was both detectable and functional in an *in vivo* setting to add to the AAV construct for the gene therapy experiments performed in this study.

AAV Construct Design

The AAV construct used in this study contained the necessary targeted GeneRide™ integration components of 1 kb flanking homology arms to the 3' endogenous murine albumin locus, which was sequenced in our *Pah*$^{enu2/enu2}$ colony and confirmed to have 100% identity to the mouse reference genome. The murine *Pah* cDNA (mPAH) was placed centrally with a preceding porcine teschovirus 2A (P2A) self-cleaving peptide sequence and followed by a miRNA

against HPPD embedded in the terminal intron of the murine *Alb* locus (Figure 3-1A). The albumin homology arms were used for targeted integration in the genome, and the HPPD miRNA acted to promote selective advantage of properly integrated hepatocytes under genetic or chemically induced tyrosinemia conditions by preventing buildup of toxic metabolites (Figure 3-1B).

In order to visualize the PAH protein in the *Pah*$^{enu2/enu2}$ model that produces abundant mutant PAH that is cross reactive with PAH antibodies, a neutral hemagglutinin (HA) tag was added to either the N or C terminal ends and cloned into plasmids that would allow it to be driven by a liver specific promoter (LSP). Plasmids were transfected into HEK293 cells and molecularly analyzed for protein expression by Western blot and immunofluorescence, and function by radioactive PAH enzyme activity assays (Figure 3-1C, 3-1D, 3-1E). The neutral HA tag on either N or C terminal ends of the PAH enzyme were effective at producing detectable and functional PAH enzyme. The N-terminal HA tag was selected for use in the GeneRide™ construct, as it was rationalized that it could not become buried in the tetramerization domain.

Proof of Concept Gene Therapy Study in *Fah-/-* HT1 Mice

A proof of concept preliminary study was performed in a mouse model of HT1, homozygous *Fah*$^{\Delta exon5/\Delta exon5}$, denoted as *Fah*$^{-/-}$, which was generated by Markus Grompe of OHSU using phage-mediated insertional mutagenesis by way of a neomycin-expression cassette into a unique *SphI* site in exon 5 of the *Fah* gene,

resulting in a frameshift and overall null allele [242]. These mice recapitulate human HT1, which is a fatal disease that causes accumulation of toxic metabolites that result in acute liver failure. This fatal phenotype can be rescued with constant NTBC administration through drinking water, which is conveniently transferred *in utero* and through breastmilk to developing progeny.

In this study, neonatal homozygous *Fah*$^{-/-}$ mice were injected with either low dose (5.2×10^8 vg), indicated as the low dose cohort (N = 2 males), or highest possible dose (10 µL volume- 2.66×10^9 vg), indicated as the high dose cohort (N=10, 6 females, 4 males), of rAAV2/8 PAH-GR+UHS through the facial vein on P1. Of note, AAV doses reported in this study were determined by titer from transgene-specific radiolabeled probe via dot blot analysis (2.66×10^{11} vg/mL), which varied greatly from the titer reported by the OHSU Molecular Viral Support Core (MVSC) using ITR-based titer analysis (1.3×10^{14} vg/mL). NTBC (8mg/L) was included in the drinking water of the dam throughout the period prior to weaning. After weaning, the mice underwent NTBC withdraw conditioning (a forty-day period of repetitively cycling on NTBC for 4 days and then off for 3 days) to allow for short, discrete time periods of selection pressure to allow for expansion of properly integrated cells with minimal toxicity (Figure 3-2A). Body mass of both low dose and high dose cohorts were maintained during the conditioning stage. At day 45, animals were then challenged with indefinite NTBC removal until reduction of 20% body weight. Low dose animals experienced rapid physical deterioration and lost 20% body mass within the first ten days. This is in contrast

with the high dose animals, whose mass was maintained and unchanged for the full month off NTBC.

Three animals in the high dose cohort were sacrificed for molecular analyses. Since HT1 animals are FAH deficient but PAH sufficient and therefore not hyperphenylalaninemic, serum Phe and PAH enzyme activity and were not readily assessed. Long range PCR of total liver genomic DNA detected the expected integration of the *Pah* transgene into the albumin gene in all three mice (Figure 3-2B). Liver immunohistochemistry of all three animals indicated faint areas of HA expression (data not shown). Taken together, along with the increased tolerance of NTBC removal in high dose animals, these molecular findings demonstrate the proper integration and selection of this construct in the presence of tyrosinemia conditions.

Gene Therapy in *Pah*$^{enu2/enu2}$ Mice

With the promising outcome of proof of concept rAAV2/8 PAH-GR+UHS therapy in HT1 mice, the next step was to test the efficacy of this therapy in PKU mice using chemically induced tyrosinemia with administration of small molecule FAH inhibitor, CEHPOBA. The progeny (5 male and 5 female) from rAAV2/8 LSP-mPAH gene addition therapy treated male *Pah*$^{enu2/enu2}$ and female *Pah*$^{enu2/enu2}$ mice were treated with high dose rAAV2/8 PAH-GR+UHS via facial vein injections on P3. Genotyping of toe clips were performed with the custom made proprietary TaqMan assay to confirm *Pah*$^{enu2/enu2}$ genotype in all progeny. This

was necessary as an additional confirmation that breeders were of the presumed *Pah*$^{enu2/enu2}$ genotype since they became indistinguishable from heterozygous and wild type animals after gene therapy treatment. After weaning, animals underwent CEHPOBA intraperitoneal (IP) injections of 1 µmol/g, initiated in waves of 2-4 animals at a time, and body mass recorded with each CEHPOBA administration (Figure 3-2C). Animals that were able to withstand CEHPOBA injections for one week were placed on high protein chow to increase dietary intake of tyrosine, thus increasing the HT1-like selective pressure.

All male animals developed priapism leading to erosion of the skin of the chronically exposed penis. All five male mice died or were compassionately euthanized after 1-2 weeks of CEHPOBA administration. Postmortem examination was possible in three mice, and all three exhibited severe distention of the urinary bladder, occasionally containing over 1000 µL of urine, suggesting urethral obstruction due to the priapism. Blood amino acid profiles of two ill-appearing males were acutely abnormal with overall elevation of amino acids and metabolites (Table 3-1).

Fortunately, females did not experience any fatal CEHPOBA toxicity. All female coat colors darkened with black spots (Figure 3-2E), indicating effectiveness of the CEHPOBA to increase tyrosine to sufficient levels to allow for proper melanogenesis. Unfortunately, there was no effect on serum Phe from this therapy (Figure 3-2C and Table 3-1). In the longest treated female, 71 days, liver

immunohistology for HA-tagged PAH revealed overall negative staining except for select areas of minimal staining of hepatocytes around vascular structures, approximated to be less than 0.5% (Figure 3-2F). Liver PAH enzyme activity was undetectable in all animals (data not shown).

The combination of the male mortality from the chemically induced tyrosinemia and lack of therapeutic efficacy from the CEHPOBA treated rAAV2/8 PAH-GR+UHS females led to the, perhaps premature, but ultimate cessation of this study.

Figures

Figure 3-1: Experimental Concept and PAH Tag

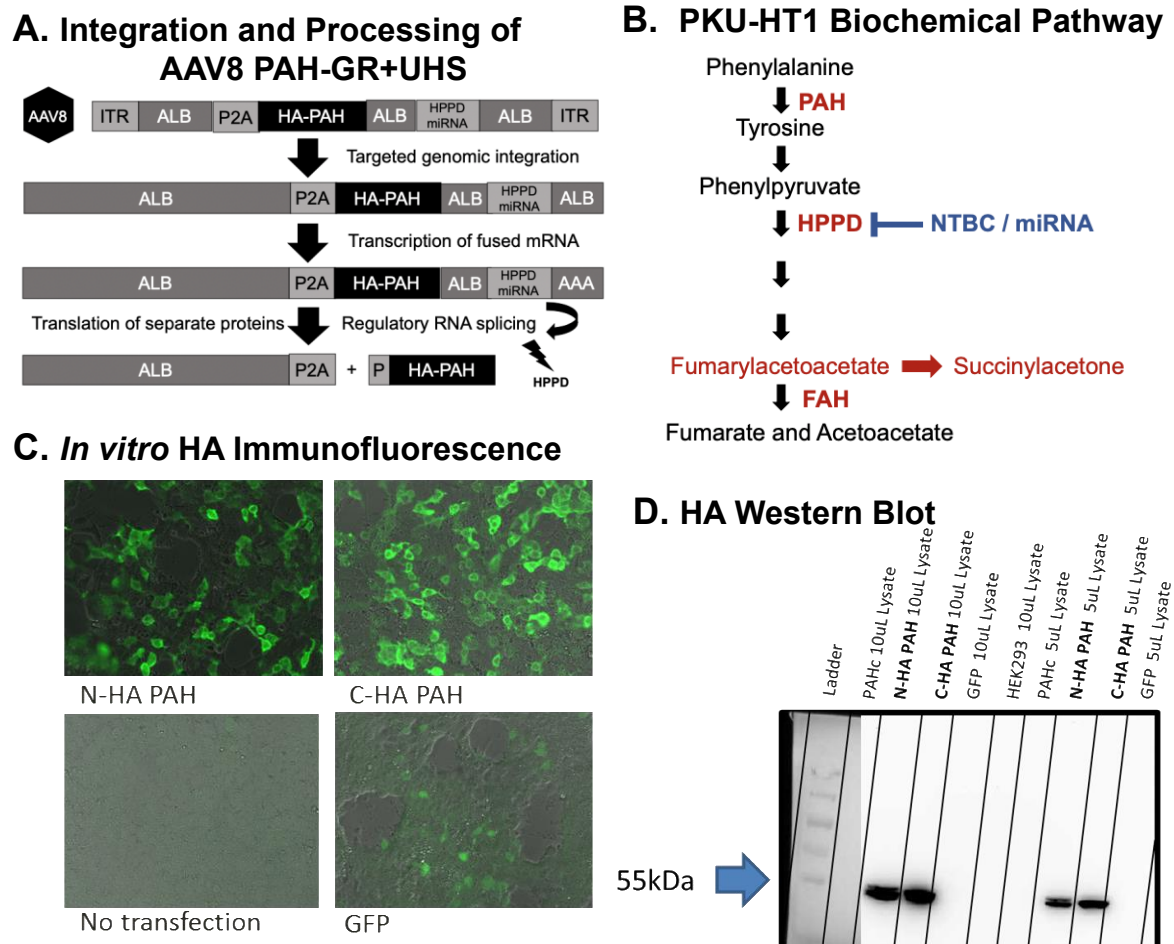

Figure 3-1: Experimental Concept and PAH Tag

A. Integration and Processing. The process of targeted genomic integration of this AAV construct relies on the GeneRide™ technology that uses homologous sequences in the transgene to the endogenous murine albumin locus, indicated as ALB, to drive homology directed events. The non-albumin sequences in the AAV transgene are passengers of these events that carried along in integration, and include a P2A self-cleaving sequence (P2A) to facilitate two distinct protein products after translation, the N-terminal HA tagged PAH cDNA (HA-PAH) to facilitate post-therapy analysis and therapeutic efficacy, and a microRNA targeted against the 4- hydroxyphenylpyruvate dioxygenase enzyme (HPPD miRNA) to facilitate selection of properly integrated transgenes. The AAV vector genome contains from left to right: 5' ITR, 3' albumin sequence, self-cleaving P2A sequence, N-terminal HA tagged PAH, HPPD miRNA embedded in albumin sequence, and 3' ITR. It is designed to integrate into murine genome at the 3' albumin locus. Transcription of the integrated albumin locus results in a fused transcript containing albumin cDNA with P2A preceding HA-PAH, as well as expression of the HPPD miRNA. Protein products include an albumin with 20 additional amino acids on the C-terminal region, and an HA-PAH with an additional proline amino acid on the N-terminal end. **B. PKU-HT1 Biochemical Pathway.** In liver and kidney cells, phenylalanine is hydroxylated to tyrosine by phenylalanine hydroxylase (PAH). The downstream metabolic product, phenylpyruvate, is subsequently process by 4- hydroxyphenylpyruvate dioxygenase (HPPD). Downstream metabolic product fumarylacetoacetate is

converted to fumarate and acetoacetate by fumarylacetoacetate hydrolase (FAH). In PKU, the PAH enzyme is deficient, resulting in toxic accumulation of phenylalanine and subsequent metabolic phenylketones. In hereditary tyrosinemia type 1, FAH is deficient, causing a toxic accumulation of fumarylacetoacetate and subsequent metabolic product succinylacetone, which is highly hepatorenal-toxic. Treatment for HT1 is targeted at inhibiting the upstream enzyme in tyrosine metabolism, HPPD, with small molecule inhibitor NTBC. HPPD can also be knocked down by targeted miRNA, as utilized is universal hepatocyte selection. **C. *In vitro* Immunofluorescence of HA-PAH in HEK293 Cells.** HEK293 cells were transfected with plasmids containing Liver Specific Promoter (LSP) driving expression of N-terminal HA tagged PAH (top left) or C-terminal HA tagged PAH (top right). Control wells were transfected with no plasmid (bottom left), or with plasmid containing cytomegalovirus (CMV) promoter driving green fluorescent protein (GFP) (bottom right). All wells except CMV-GFP were evaluated for HA expression by HA-immunofluorescence using rabbit IgG HA tag primary antibody and Alexa 488-conjugated goat anti-rabbit IgG secondary antibody. All wells were visualized under fluorescent microscopy. **D. HA Western Blot of HEK293 Cell Homogenates.** This is an image of a Western blot probing for HA protein expression from HEK293 cell lysates transfected with plasmids expressing Pah cDNA (PAHc), N-terminal HA tagged PAH (N-HA PAH), C-terminal HA tagged PAH (C-HA PAH), GFP, or no plasmid (indicated by HEK293). Western blot was loaded from left to right, ladder, 10 µL lysate of PAHc, N-HA PAH, C-HA PAH, GFP, HEK293, followed by 5 µL lysate

PAHc, N-HA PAH, C-HA PAH, and GFP. Blue arrow on the left indicates 55 kDa, the approximate size of PAH. Strong bands for HA protein expression appear at 55 kDa in 10 µL N-HA-PAH and C-HA PAH and less so in 5 µL N-HA-PAH and C-HA PAH. **E. PAH Enzyme Activity Assay.** Radioactive PAH enzyme activity assay was performed using C^{14} labeled Phe as an *in vitro* substrate for PAH derived from either liver samples or cell lysates and run on thin-layer chromatography (TLC) plates that were subsequently exposed to phosphor-imaging screens. The C^{14}-Phe metabolism into C^{14}-Tyr was captured via BioRad radioisotope imaging instrument (raw image displayed). In addition to radiolabeled Phe, reactions were controlled for addition of required PAH cofactor, tetrahydrobiopterin (BH_4) as an additional layer of control (labeled on top left of image). Reactions that were not provided BH_4 are indicated with a – and those that were provided BH_4 with a +. The samples run on the TLC plate from left to right are water without BH_4, water with BH_4, liver homogenates: wildtype mouse (positive control indicated as + CNTL) without BH_4, + CNTL with BH_4, *Pah*$^{enu2/enu2}$ mouse treated with AAV8-LSP-FLAG-PAH (indicated as FLAG-PAH) without BH_4, FLAG-PAH with BH_4, followed by HEK293 cell lysates transfected with LSP-N-HA PAH (indicated as N-HA-PAH) without BH_4, N-HA-PAH with BH_4, N-HA-PAH with BH_4, negative control HEK293 cell lysate without transfection (indicated as HEK293) with BH_4, CMV-GFP (indicated as GFP) with BH_4, LSP-C-HA-PAH (indicated as C-HA-PAH) with BH_4, and LSP-mPAH (indicated as PAHc) with BH_4. The lanes that display a visible amount of PAH metabolism of radiolabeled

Phe into Tyr are those provided BH_4 in +CNTL (strong), FLAG-PAH (faint), N-HA-PAH (moderate-faint), C-HA-PAH (moderate) and PAHc (moderate).

Figure 3-2: *In vivo* Outcome of rAAV2/8 PAH-GR+US Therapy

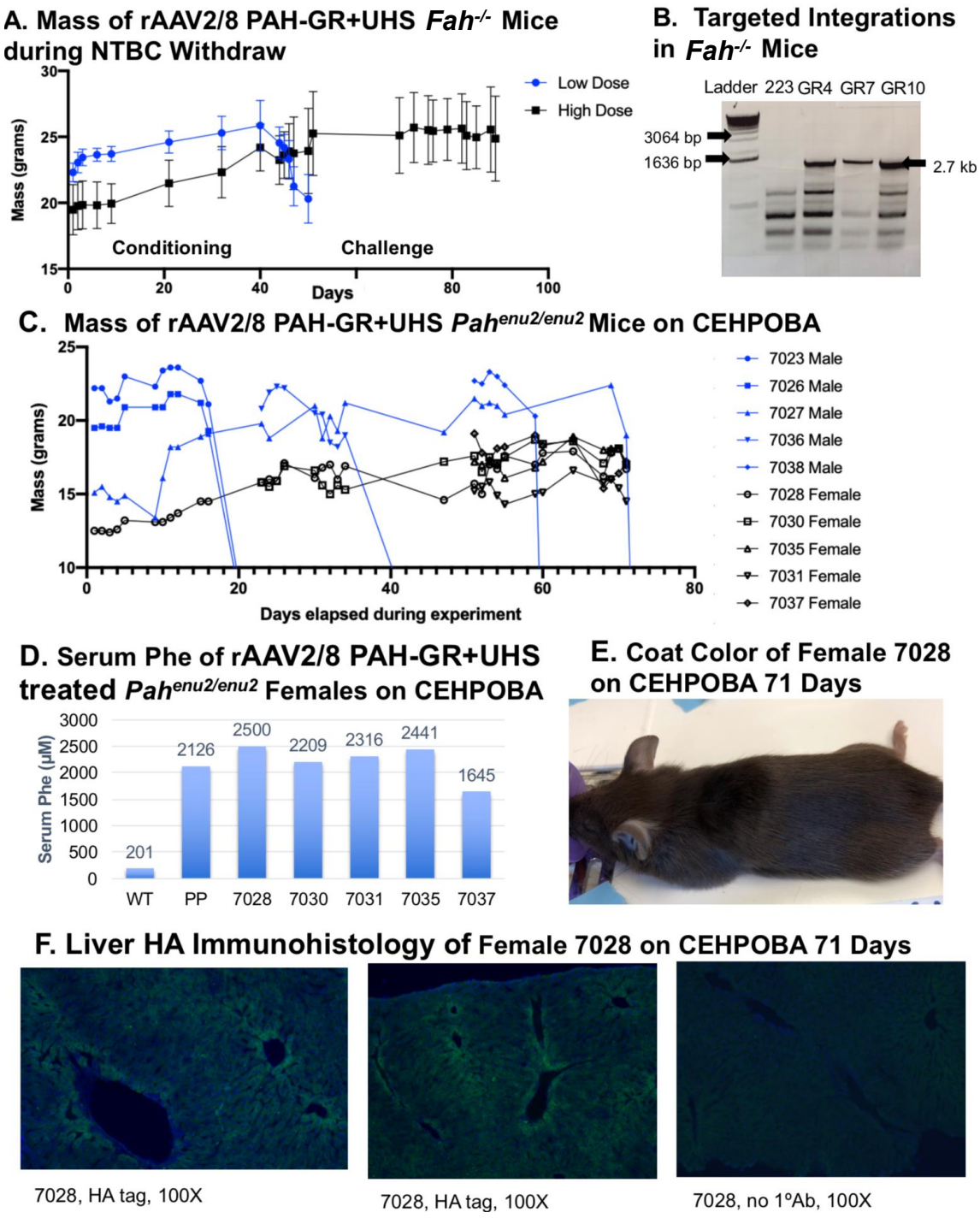

Figure 3-2: *In vivo* Outcome of rAAV2/8 PAH-GR+US Therapy

A. Mass of rAAV2/8 PAH-GR+US *Fah*$^{-/-}$ on NTBC Withdraw. The graph displays the longitudinal mass of gene therapy treated rAAV2/8 PAH-GR+US *Fah*$^{-/-}$ animals on NTBC withdraw conditioning (days 1-40) and challenge (days 45-90). The x-axis displays days elapsed where animals underwent a NTBC withdraw conditioning of 3 days off NTBC, 4 days on NTBC for days 1 through 40, followed by a NTBC withdraw challenge until reduction of 20% body mass. The y-axis indicates body mass in grams. The key indicates low dose rAAV2/8 PAH-GR+UHS treated *Fah*$^{-/-}$ animals in blue (N=2 males) and high dose rAAV2/8 PAH-GR+UHS treated *Fah*$^{-/-}$ animals in black (N=10, 6 females and 4 males). Each dot represents body mass of each cohort on a day weighed, with brackets to illustrate the standard error of the mean (SEM). **B. Targeted Integrations in *Fah*$^{-/-}$ Mice.** The image displays gel of long-range PCR reactions to detect targeted integrations of rAAV2/8 PAH-GR+UHS in high dose animals. The gel was loaded with 1kb DNA ladder in the first lane, and bands indicating 1636bp and 3056bp size are indicated with black arrows. The remaining lanes, from left to right, were loaded with long-range PCR products from a control untreated *Fah*$^{-/-}$ animal (indicated as 223), followed by three high dose treated *Fah*$^{-/-}$ animals (GR4, GR7, and GR10). DNA bands at 2.7kb, indicated with an arrow, indicated genomic integrations of rAAV2/8 PAH-GR+UHS. Smaller bands indicate non-specific PCR products. **C. Mass of rAAV2/8 PAH-GR+US treated *Pah*$^{enu2/enu2}$ Mice on CEHPOBA.** The graph displays the longitudinal mass of gene therapy treated rAAV2/8 PAH-GR+US *Pah*$^{enu2/enu2}$ animals on CEHPOBA.

The x-axis indicates days elapsed during the experiment (not total days of CEHPOBA treatment). The y-axis indicates body mass in grams. The key indicates animal identification number, sex, and representative shape-line on the graph, where males are in blue and females are in black. Each point indicates body mass of individual mice on a day that CEHPOBA was administered. Lines converging on the x-axis indicate animal death. Of note, female 7028 was the only animal on CEHPOBA treatment for the full 71 days, and all males died. **D. Serum Phe of rAAV2/8 PAH-GR+UHS treated *Pah*$^{enu2/enu2}$ Females after CEHPOBA.** The graph displays serum Phe of the *Pah*$^{enu2/enu2}$ rAAV2/8 PAH-GR+UHS treated animals that survived CEHPOBA treatment, which happen to be all females. The x-axis indicates individual animals, from left to right wildtype (indicated as WT), untreated *Pah*$^{enu2/enu2}$ (indicated as PP), followed by experimental animals via identification numbers. The y-axis indicates serum Phe in micromolar units. The numbers at the top of each bar indicate the exact value of Phe measured. **E. Coat Color of Female 7028.** Photograph demonstrating hyperpigmentation of fur coat of rAAV2/8 PAH-GR+UHS treated female 7028 on CEHPOBA 71 days. **F. Liver HA Immunohistology of Female 7028.** Images of liver HA-immunohistology of rAAV2/8 PAH-GR+UHS treated female 7028 on CEHPOBA 71 days. The first two images displays select areas of HA-positive hepatocytes, indicated with green fluorescence, of liver tissue exposed with primary anti-HA antibody and subsequently secondary green-fluorescent-conjugated antibody. The third image displays a control condition in which liver

tissue was only exposed to secondary green-fluorescent-conjugated antibody. Images are magnified at 100X.

Table 3-1: Serum amino acids profiles in gene therapy and CEHPOBA treated *Pah*$^{enu2/enu2}$ mice

Animal Sex and ID	Male 7036	Male 7038	Male 7027	Female 7028	Female 7030	Female 7031	Female 7035	Female 7037
Days on CEHPOBA	11 (ill-appearing)	9 (ill-appearing)	70 (on & off: 6 weight recoveries)	71	48	20	20	20
Phenylalanine (micromolar)	5455.13	3928.68	2620.58	3168.86	2818.1	3334.88	3183.47	1980.46
Tyrosine (micromolar)	1385.96	520.26	106.59	68.23	74.23	83.82	76.84	62.2
Methionine (micromolar)	686.05	419.84	88.42	34.54	46.14	89.66	71.52	78.56
Ornithine (micromolar)	1147.99	684.79	84.55	80.34	84.45	114.46	172.69	126.63
Isoleucine (micromolar)	1045.48	516.04	163.88	102.81	129.98	208.52	191.41	110.2
Arginine (micromolar)	3863.33	27.5	87.44	15.31	42.43	63.56	57.27	79.52
Citrulline (micromolar)	678.87	280.62	60.3	58.72	63.51	65.95	65.53	87.64
Tryptophan (micromolar)	143.01	145.64	64.19	55.8	77.55	81.21	81.05	79.06

Table 3-1: Serum amino acids profiles in gene therapy and CEHPOBA treated *Pah*$^{enu2/enu2}$ mice

This table displays serum amino acid profiles on gene therapy and CEHPOBA treated *Pah*$^{enu2/enu2}$ animals. The top row indicates animal sex and identification (ID). The next row displays the number of days animals were on CEHPOBA before blood was drawn for these samples. It is important to note the following: at time of blood draw males 7036 and 7038 were ill-appearing with scruffy fur, hunched posture, and minimal activity; male 7027 was calculated to be on "CEHPOBA treatment" for 70 days, however this includes 6 cycles of health and weight recovery, in part due to a malocclusion that needed frequent trimming. The subsequent rows display serum micromolar values of phenylalanine, tyrosine, methionine, ornithine, isoleucine, arginine, citrulline, and tryptophan, from top to bottom.

Discussion

This was an unfortunate end to a hopeful and promising experimental design to achieve robust and permanent PKU gene therapy. It remains unclear what exactly led to the failure of this therapy. It is noteworthy to mention that all HT1 animals allowed to survive to two years of age eventually developed massive hepatocellular carcinomas, a regular occurrence in this model due to the FAH deficiency related toxicity, indicating the protection of the miRNA in this construct was not sufficient to protect the liver from massive toxic damage and genomic insults during the selection process. The PKU mice were not maintained beyond the administration of CEHPOBA, so it is not possible to mention the potential long-term consequences from the CEHPOBA selection, however with the fatal consequences in male mice, it does not seem to be a promising approach for translation into human medicine. It is noteworthy that male mice did not exhibit significant weight reduction prior to their demise, so using body mass as an indicator of toxicity for prompt removal of selection pressure (in this case, CEHPOBA), was ineffective.

As for the lack of efficacy in PKU animals, it is possible the rAAV2/8 PAH-GR+UHS injected into neonates was largely degraded by neutralizing antibodies transferred from the mother through the placenta and breastmilk in response to the previously administered AAV8 LSP-mPAH gene addition therapy. The gene addition therapy was performed in the breeders in order to increase the number of *Pah*$^{enu2/enu2}$ offspring, as PKU animals were becoming difficult to produce in

sufficient numbers for the multiple ongoing studies in the laboratory. While neutralizing antibodies may have been transmitted from gene therapy treated mothers to progeny, the female mouse that received the full 71 days of CEHPOBA treatment showed *some* HA-positive hepatocytes, indicating successful integrations of at least a few transgenes. One possibility that cannot be discounted is that the HA tag may have interfered with the proper function of the PAH enzyme in an *in vivo* setting, although the *in vitro* studies suggest otherwise. It is also possible that since the GeneRide™ technology fuses the transgene transcript with the albumin mRNA, that the fusion transcript was translated into the rough endoplasmic reticulum destined for Golgi processing and secretion from the cell. PAH does not function extracellularly like albumin. It is a cytosolic enzyme that relies on HSP40 and HSP70 chaperones for proper folding, as well as other PAH monomers and the required co-factor, tetrahydrobiopterin (BH_4), which is continuously recycled in the cytoplasm, to become a stable tetramer. If PAH were secreted, it would likely be quickly degraded and ultimately non-functional.

One positive outcome of this study was the creation of a tagged PAH enzyme that is both detectable and functional in tetrameric form, at least *in vitro*. Future studies are warranted to test whether this is the case in an *in vivo* setting by performing a gene addition therapy experiment using AAV8 LSP-HA-mPAH in *Pah*$^{enu2/enu2}$ mice.

Materials and Methods

Molecular Cloning of pAAV2 LSP_HA-PAH Constructs

The DNA sequence for the HA tag was added to either the N or C terminal of the murine *Pah* gene sequence (*mPah)* and ordered in GeneBlock plasmids. It was cloned into plasmids containing an AAV2 genome sequence with liver specific promoter (LSP) to drive expression using the flanking *NheI* restriction enzyme sites, as well as ampicillin resistance for microbial growth and propagation in DH10B *E. coli* using standard cloning procedures. Plasmids from single colonies were evaluated for overall integrity and proper orientation of HA-PAH by restriction enzyme digests. Further plasmid production was pursued for each construct containing N-term HA-PAH or C-term HA-PAH, referenced as pAAV2 LSP_N-HA-PAH and pAAV2 LSP_C-HA-PAH, respectively and further evaluated in *in vitro* studies.

In vitro evaluation of HA-PAH plasmids: HA Immunofluorescence

Separate wells within a 24-well dish of 80% confluent HEK293 cells were transfected with 2 µg plasmids pAAV2 LSP_N-HA-PAH (indicated as N-HA-PAH), pAAV2 LSP_C-HA-PAH (indicated as C-HA-PAH), p304-GFP (indicated as GFP) using salt-ion DNA-complexing with 10 µM polyethylenimine (PEI). The well transfected with GFP was monitored as an indirect proxy for plasmid gene expression. After 48 hours, approximately 50% cells were GFP-positive. Immunofluorescence for HA was performed at room temperature: fixation in 4% paraformaldehyde 10 minutes, wash 3x PBS, permeabilized in 0.2% Triton-X in

PBS (PBT) for 30 minutes, wash 3x PBS, incubated in blocking solution (10% goat serum, 0.1% BSA, 0.1% Triton X) for 60 minutes, wash 3x PBS, incubated with primary rabbit IgG HA tag antibody (1:200 dilution, MAB0601 from Research & Diagnostic Systems, Inc.) for 60 minutes, wash 3x PBS, incubated with secondary Alexa 488-conjugated goat anti-rabbit IgG secondary antibody (1:200 dilution, A11008 Alexa Fluor 488 goat anti-rabbit IgG (H+L) from Invitrogen) for 60 minutes, and wash 3x PBS. Images were captured on a Nikon H550L fluorescence microscope.

***In vitro* evaluation of HA-PAH plasmids: HA Western Blot**

Separate 10 cm dishes of 80% confluent HEK293 cells were transfected with 12 µg plasmids pAAV2 LSP_N-HA-PAH (indicated as N-HA-PAH), pAAV2 LSP_C-HA PAH (indicated as C-HA-PAH), p304-GFP (indicated as GFP), and pAAV2 LSPmPAH (AAV2 genome containing LSP driving murine PAH cDNA expression, indicated as PAHc) using salt-ion DNA-complexing with 10 µM polyethylenimine (PEI). The dish transfected with GFP was monitored as an indirect proxy for plasmid gene expression. After 48 hours, approximately 50% cells were GFP-positive. Dishes were prepared into cell lysates by washing, scraping, and resuspension in 250 µL lysis buffer. Cell lysate homogenates were diluted in sodium dodecyl sulfate (SDS) sample buffer with added nonyl-phenoxypolyethoxylethanol type 40 (NP-40) nonionic detergent, phenylmethylsulfonyl fluoride (PMSF), and a denaturing dye and heated at 95° for 5 min. 10 µL of ThermoScientific PageRuler ladder and 10 µL of samples (50

µg total protein) were run on a stacked SDS-PAGE gel. The protein was transferred to a polyvinylidene membrane and probed with rabbit IgG HA tag antibody (1:200 dilution, MAB0601 from R&D Systems, Inc.) Membranes were probed with HRP-conjugated goat anti-rabbit IgG secondary antibody (1:1000 dilution, A27034 Goat anti rabbit IgG (H+L) from Thermo Scientific). Bands were visualized using enhanced chemiluminescence (Chemiluminescent Western Blot Detection from ThermoScientific) captured on ThermoScientific Chemiluminescent (CL)-Xposure film.

***In vitro* evaluation of HA-PAH plasmids: PAH Enzyme Activity**

Separate 10 cm dishes of 80% confluent HEK293 cells were transfected with 12 µg plasmids pLSP N-HA-PAH (indicated as N-HA-PAH), pLSP C-HA PAH (indicated as C-HA-PAH), p304-GFP (indicated as GFP), and pLSPmPAH (indicated as PAHc) using salt-ion DNA-complexing with 10 µM polyethylenimine (PEI). The dish transfected with GFP was monitored as an indirect proxy for plasmid gene expression. After 48 hours, approximately 50% cells were GFP-positive. Dishes were prepared into cell lysates by washing, scraping, and resuspension in 250 µL lysis buffer. PAH enzyme activity was determined with 10 µL cell lysate per reaction using an established radioactive chromatography assay [227] with modifications [228].

Molecular Cloning of HA-PAH GR+UHS Construct

We were graciously provided the pAB269-HPD-miRNA plasmid from the Grompe laboratory. The *NheI* restriction enzyme site was used to insert the N-HA-PAH sequence from a custom ordered GeneBlock™ plasmid into the former FIX cDNA site of the pAB269-HPD-miRNA plasmid and referenced as pAAV2 PAH-GR+UHS. Restriction enzyme profiles with *Taq*^{a1} and *AhdI* were performed to determine the overall integrity of the plasmid and AAV ITRs prior to delivery for AAV8 virus production at the OHSU Molecular Virology Core.

AAV Production

The pAAV2 PAH-GR+UHS plasmid was confirmed for overall integrity and intact ITRs by restriction enzyme screening using *Taq1*^{a1} and *Ahd1*, respectively. The OHSU Molecular Virology Core produced large-scale preps of recombinant rAAV2/8 viruses, referenced as rAAV2/8 PAH GR+UHS, using standard triple plasmid transfection procedures into cultured HEK293 cells and purified by iodixanol gradient ultracentrifugation [225]. AAV titers were determined using ITR-based qPCR analysis.

AAV Titer: Dot Blot

Probe preparation: pAAV2-PAH-GR+UHS plasmid was digested with *NheI*. DNA bands at 800bp and 500 bp were gel extracted and made into a radiolabeled probe using dCT^{32}P as nucleotide substrate in the Agilent Prime It II Random Primer Labeling Kit.

Viral preparation: 10 µL of stock rAAV2/8 PAH-GR+UHS was treated with DNase to degrade any unpackaged transgenes, followed by Proteinase K treatment to degrade the protein capsid. Phenol chloroform DNA purification, ethanol and isopropanol wash of ions, and sodium acetate-glycogen precipitation was performed on viral DNA followed by resuspension in 120 µL Tris-ethylenediaminetetraacetic acid (TE) buffer. Viral DNA was made into serial dilutions containing 60 µL, 30 µL, 15 µL, and 7.5 µL of the 120 µL TE-viral DNA solution with the addition of alkali buffer.

Standard preparation: 250 ng of pAAV2 PAH-GR+UHS was linearized with single-cutter restriction enzyme *NotI* and made into serial dilutions ranging from 0.039 ng to 5 ng in alkali buffer.

Hybridization: Standard preparations (in duplicate) and viral preparations (in duplicate) were alkaline hybridized to a zeta membrane through the BioRad Bio-dot 96-well microfiltration vacuum apparatus. The membrane was then briefly washed in saline sodium citrate (SSC) for one minute and DNA UV-crosslinked to the membrane. The probe was then boiled for 10 minutes and placed in a 50 mL hybridization tube with the membrane in a rotisserie hybridization chamber at 65°C for 24 hours. The membrane was then washed 3x in wash buffer (1x SSC, 0.1 % SDS) and exposed to a phosphor screen overnight, imaged by BioRad Personal Molecular Imager (PMI) System, and quantified with BioRad QuantityOne 1-D analysis software.

Titer calculation of vector genomes/ml (vg/mL):

Vg/mL= (DNA mass ng x 10^{-9}g x ($6.022*10^{23}$ /mol)/(MW x volume in µL x 10^{-3} mL)

Where MW (molecular weight) = (number nucleotides transgene) x 330 g/mol.

pAAV2 PAH-GR+UHS = ~4500 nucleotides (1,485,000 M)

Standard quantifications were placed on a linear curve based on known vg/mL concentration and viral quantifications were calculated for vg/mL using linear regression analysis.

Animal Husbandry

Animal care and experimentation were performed in accordance with the guidelines of the Dept. of Comparative Medicine, Oregon Health & Science University and the National Institutes of Health Guide for the Care and Use of Laboratory animals. The mouse model of HT1, homozygous *Fah*$^{\Delta exon5/\Delta exon5}$, denoted as *Fah*$^{-/-}$, was produced by phage-mediated insertional mutagenesis by way of a neomycin-expression cassette into a unique *SphI* site in exon 5 of the *Fah* gene, resulting in a frameshift and overall null allele [242]. This fatal disease causes accumulation of toxic metabolites that cause acute liver failure, but this fatal phenotype can be rescued with constant NTBC treatment in drinking water, which is conveniently transferred *in utero* and through breastmilk to developing progeny. HT1 animals in this study were produced by the breeding of homozygous *Fah*$^{-/-}$ animals that received high energy chow (LabDiet Rodent High Energy Diet 5058, St. Louis, MO) and 8 mg/L NTBC in drinking water. Post-weaning, HT1 animals were provided standard mouse chow (LabDiet Picolab Rodent Diet 5LOD, St. Louis, MO) and received 8 mg/L of NTBC in drinking water until otherwise necessitated for gene therapy selection experimentation.

C57Bl/6-*Pah*$^{enu2/enu2}$ mice ,which are homozygous for a missense c.835T>C (p.F263S) mutation in exon 7 of the murine *Pah* gene, are completely deficient in liver PAH activity, are consequently hyperphenylalaninemic on an unrestricted diet, and are a representative animal model of human PKU [224]. Neonatal *Pah*$^{enu2/enu2}$ mice for these experiments were generated through breeding of rAAV2/8 LSPmPAH gene addition therapy treated *Pah*$^{enu2/enu2}$ sires to *Pah*$^{enu2/enu2}$ dams. Genotyping for the presence of the *Pah*^{enu2} homozygosity was performed by a TaqMan quantitative PCR assay. All mice were fed tap water and standard mouse chow (LabDiet Picolab Rodent Diet 5LOD, St. Louis, MO) *ad libitum* providing approximately 24% protein and 1.04% L-phenylalanine by weight, except breeders that received high energy chow (LabDiet Rodent High Energy Diet 5058, St. Louis, MO) approximately 22% protein and 0.99% L-phenylalanine. Given that adult mice consume approximately 5 g chow per day, daily L-phenylalanine intake is estimated to be approximately 50 mg per day. The animals were housed under a standard 12 hours on, 12 hours off light cycle. All surgical procedures were carried out with inhaled isoflurane general anesthesia to minimize pain and discomfort.

rAAV2/8 PAH-GR+UHS administration and NTBC withdraw in HT1 mice

Neonatal *Fah*$^{-/-}$ mice were injected with either low dose (5.2 x 10^8 vg) or highest possible dose (2.66 x 10^9 vg) rAAV2/8 PAH-GR+UHS through the facial vein on P1 with a maximal volume of 10µL. Animals were provided NTBC throughout development, including maternal NTBC administration and NTBC drinking water

post-weaning. Animals then underwent NTBC withdraw conditioning (40 days of 3 days off NTBC, 4 days on NTBC) followed by NTBC withdraw challenge of continuous NTBC removal until 20% reduction body weight, at which point NTBC was re-administered.

Long Range PCR to detect Targeted Genomic Integrations in High Dose treated *Fah*$^{-/-}$ Mice

Long range PCR of a 2.7 kb fragment using a forward primer preceding the 5' albumin homology arm of the transgene (5'CAACGTCATGGGTGTGACTTTTGAGAATGGAGTAAG) and a reverse primer following the N-terminal HA peptide sequence in the 5' *Pah* cDNA sequence (5'CTTTGGGCAGGAAACAAGTTAC) was performed on liver extracted DNA from one control *Fah-/-* animal (identified as 223) and three high dose treated *Fah-/-* animals (identified as GR4, GR7, and GR10) using the Qiagen Long-range PCR Kit. Lanes of a 1% agar gel were loaded with 1kb DNA ladder, followed by PCR reactions from 223, GR4, GR7, and GR10. DNA bans approximately 2.7kb demonstrate rAAV2/8 PAH-GR+UHS genomic integrations. Smaller bands are non-specific PCR products.

rAAV2/8 PAH-GR+UHS administration and CEHPOBA treatment in *Pah*$^{enu2/enu2}$ Mice

The progeny (5 male and 5 female) from rAAV2/8 LSP-mPAH gene addition therapy treated male *Pah*$^{enu2/enu2}$ and female *Pah*$^{enu2/enu2}$ mice were treated with

high dose rAAV2/8 PAH-GR+UHS via facial vein injections on postnatal day 3. Genotyping of toe clips were performed with the custom made proprietary TaqMan assay to confirm *Pah*$^{enu2/enu2}$ genotype in all progeny. After weaning, animals underwent CEHPOBA intraperitoneal (IP) injections of 1 µmol/g, initiated in waves of 2-4 animals at a time, and body mass recorded at each time of CEHPOBA administration. Animals that were able to withstand CEHPOBA injections for one week were placed on high protein chow to increase dietary intake of tyrosine, thus increasing the HT1-like selective pressure.

Liver HA Immunohistology in rAAV2/8 PAH-GR+UHS treated *Pah*$^{enu2/enu2}$ Mouse

Female 7028 underwent saline-paraformaldehyde perfusion in preparation for liver fixation and immunohistology. Under deep isoflurane inhaled anesthesia, mice were perfused with 0.9% saline via cardiac infusion to clear the hepatic circulation of blood. Excised biopsies from each liver lobule were then fixed for 24 hours in fixation solution (4% paraformaldehyde in phosphate buffered saline) followed by dehydration in 25% buffered sucrose for an additional 24 hours. Tissues were embedded in optimal cutting tissue (OCT) media, sliced into 15 micrometer sections, and mounted on glass slides. Sections were treated (following blocking) with rabbit IgG HA tag antibody (1:200 dilution, MAB0601 from R&D Systems, Inc.) and incubated for 2 hours at room temperature. After appropriate washes, sections were treated with Alexa 488-conjugated goat anti-rabbit IgG secondary antibody (1:150 dilution, A11008 Alexa Fluor 488 goat anti-

rabbit IgG (H+L) from Invitrogen) and incubated for one hour at room temperature. After washing, cover slips were mounted with Vectashield mounting medium containing DAPI. Images were captured on a Nikon H550L fluorescence microscope.

Serum Phenylalanine

Serum phenylalanine was determined using an established fluorometric protocol [226].

Liver PAH Enzyme Activity

PAH enzyme activity was determined using an established radioactive chromatography assay [227] with modifications [228].

Blood Amino Acids

Blood amino acid concentrations were determined using an established protocol [28] by pre-column derivatization with 6-aminoquinolyl-N-hydroxysuccinimidyl carbamate (AQC, Waters AccQ Tag™derivitization system) and separation by ultra-high performance liquid chromatography and UV absorbance detection (Waters Acquity™ UPLC, Milford, MA) using the Waters Masstrak Amino Acid Analysis method.

Acknowledgements

DYR and the experiments were funded by the National PKU Alliance. SRW, SD, COH were funded by NIH R01 NS080866.

We graciously acknowledge the Grompe laboratory for supplying us with GeneRide™ and universal hepatocyte selection expertise and reagents.
We express our sincerest gratitude to the National PKU Alliance for supporting this research.

Author Contributions

D.R. performed the experiments, analyzed data, and wrote the manuscript.
S.W. performed the surgical procedures and assisted with mouse breeding, molecular techniques, and experimental design.
S.D. assisted with mouse breeding and molecular techniques.
S.N. assisted with experimental design and reagents.
M.G. assisted with reagents, experimental design, analyses, data interpretation, manuscript editing, and oversaw D.R. as a Dissertation Advisory Committee member.
C.H. assisted with funding, experimental design, analyses, data interpretation, manuscript editing, and was primary mentor to D.R. during graduate school.

CHAPTER 4:

A Novel Pah-Exon1 Deleted Murine Model of Phenylalanine Hydroxylase (PAH) Deficiency

This work was published in the journal of

Molecular Genetics and Metabolism [246].

Title Page

A novel Pah-exon1 deleted murine model of phenylalanine hydroxylase (PAH) deficiency

Daelyn Y. Richards[1], Shelley R. Winn[1], Sandra Dudley[1], Lev Fedorov[2], Nicole Rimann[3], Beat Thöny[3], and Cary O. Harding[1]

[1]Department of Medical and Molecular Genetics, Oregon Health & Science University, Mailstop L-103, 3181 Sam Jackson Park Rd., Portland, OR 97239, USA

[2]Transgenic Mouse Models Core, Oregon Health & Science University, 3181 Sam Jackson Park Rd., Portland, OR 97239, USA

[3]Department of Pediatrics, University of Zurich, Steinweissstrasse 75, Zurich CH-8032, Switzerland

Correspondence should be addressed to C.O.H. (hardingc@ohsu.edu)

Portland, Oregon, United States of America

Corresponding Author Contact Information:

Address: 3181 SW Sam Jackson Park Road, Mail Code L103, Portland, Oregon 97239

Tel: 503 494-7608

Fax: 503 494-6886

Email: hardingc@ohsu.edu

Abstract

Phenylalanine hydroxylase (PAH) deficiency, colloquially known as phenylketonuria (PKU), is among the most common inborn errors of metabolism and in the past decade has become a target for the development of novel therapeutics such as gene therapy. PAH deficient mouse models have been key to new treatment development, but all prior existing models natively express liver PAH polypeptide as inactive or partially active PAH monomers, which complicates the experimental assessment of protein expression following therapeutic gene, mRNA, protein, or cell transfer. The mutant PAH monomers are able to form hetero-tetramers with and inhibit the overall holoenzyme activity of wild type PAH monomers produced from a therapeutic vector. Preclinical therapeutic studies would benefit from a PKU model that completely lacks both PAH activity and protein expression in liver. In this study, we employed CRISPR/Cas9-mediated gene editing in fertilized mouse embryos to generate a novel mouse model that lacks exon 1 of the *Pah* gene. Mice that are homozygous for the *Pah* exon 1 deletion are viable, severely hyperphenylalaninemic, accurately replicate phenotypic features of untreated human classical PKU and lack any detectable liver PAH activity or protein. This model of classical PKU is ideal for further development of gene and cell biologics to treat PKU.

Keywords: Phenylketonuria; CRISPR/Cas9; Knockout mouse model; Gene therapy

Introduction

Phenylketonuria (PKU) (OMIM # 261600) is among the most well-studied inborn errors of metabolism. PKU is most commonly caused by phenylalanine hydroxylase (PAH, EC 1.14.16.1) deficiency as the result of inherited *PAH* mutations, but can also be caused by mutations in the *DNAJC12* gene, one of the co-chaperones required for proper PAH folding and degradation [50]. PAH deficiency results in hyperphenylalaninemia (HPA) and irreversible neurological consequences if left untreated [46]. The PAH enzyme functions in liver as homo-tetramers to hydroxylate phenylalanine (Phe) into tyrosine and requires the co-factor tetrahydrobiopterin for catalysis [47]. Dietary phenylalanine (Phe) tolerance among PKU patients differs widely depending on the body's ability to maintain Phe homeostasis, resulting in a clinical continuum of phenotypes ranging from chronic mild hyperphenylalaninemia to severe classical PKU.

The *Pah*$^{enu2/enu2}$ mouse model recapitulates classical PKU with toxic hyperphenylalaninemia that causes neurological damage if untreated, and due to this classical PKU phenotype, is the most utilized animal model for testing novel therapeutics. Elevated brain Phe impairs cognitive and behavioral performance, as well as proper monoamine neurotransmitter production [28]. Abundant stable, nonfunctional PAH protein that is recognized by anti-PAH antibodies is expressed in liver [91]. For research that aims to perform preclinical gene therapy studies, the presence of this mutant protein introduces confounding variables and challenges to experimental design, analysis, and interpretation. These

challenges include the inability to distinguish transgene-derived functional enzyme from native mutant PAH by immunohistochemistry, as well as the dominant negative effect of mutant monomers forming hetero-tetramers with functional monomers, thereby lowering the overall activity of the holoenzyme complex [247]. In order to better evaluate genetic therapeutic interventions, a model that is completely void of PAH protein and activity is greatly desired. To accomplish this task, this study sought to delete the entire first exon of the *Pah* gene in C57BL/6 mouse embryos using the CRISPR/Cas9 system [181].

Results

Experimental Design

Guide Validation

Using two *in silico* single guide RNA (sgRNA) design tools, CHOPCHOP and MIT Guide Design, *Streptococcus pyogenes* Cas9 appropriate guides throughout the *Pah* 5' upstream untranslated region (5' UTR), exon 1, and intron 1 (IVS1) were identified (Figure 1A). Six sgRNAs (labeled guides 1, 3, 4, 6, 7 & 8) were selected to test for effective targeted double-stranded DNA breaks (DSB) (Figure 4-1A). Using the Takara *In Vitro* Guide-It assay, sgRNAs 3, 4, 6, 7 & 8 were identified as being effective at inducing a DSB in mouse DNA, provided the remaining necessary gene editing components, in an *in vitro* setting (Figure 4-1B). Guide 4 (5' UTR) and guide 8 (IVS 1) were selected to knockout exon 1 of the *Pah* gene in murine embryos (Figure 4-1C). After CRISPR/Cas9-mediated *Pah* gene targeting, the zygotes were transferred into oviducts of pseudo-pregnant females yielding eighty-five liveborn F0 progeny.

Pah exon1 Deletion Screen

DNA isolated from tail biopsies of 85 potentially genetically altered offspring were analyzed for large deletions. PCR amplification of a 753 bp fragment flanking exon 1 in the *Pah* locus was performed, followed by gel electrophoresis, and screening for the presence of visually discernable deletions spanning approximately 200 bp or more (Figure 4-1D). CRISPR-modified alleles that contained small indels not visually detectable or large deletions greater in span

than the amplicon and that would therefore not be amplified with this screening procedure were not further sought. Apparent heterozygous *Pah* exon 1 deletions were detected in four female pups using this screening procedure, but only two could be confirmed and analyzed upon Sanger sequencing. The first animal carried a 243 bp deletion that was designated as allele a (Figure 4-1C). Unfortunately, this deleted allele was unable to be propagated through breeding and therefore was not further characterized. Fortunately, a 258 bp deletion spanning exon 1 in a second founder animal, confirmed with Sanger sequencing and designated as allele b, was successfully propagated to an F1 generation and bred to homozygosity (Figure 4-1C, 4-1D, 4-1E and 4-1F). Hereafter, we designate this mutant allele $Pah^{\Delta exon1}$, and mice that are homozygous for this deleted allele as $Pah^{\Delta exon1/\Delta exon1}$, heterozygous as $Pah^{+/\Delta exon1}$, and wild type as $Pah^{+/+}$.

Characterization of *Pah*$^{\Delta exon1/\Delta exon1}$ animals

Breeding of C57BL/6-*Pah*$^{\Delta exon1/\Delta exon1}$ Mice

Four $Pah^{+/\Delta exon1}$ X $Pah^{+/\Delta exon1}$ crosses generated 23 pups with the following genotypes obtained at two weeks of life: 6 $Pah^{+/+}$, 12 $Pah^{+/\Delta exon1}$, and 5 $Pah^{\Delta exon1/\Delta exon1}$. This yield of genotypes is consistent with the 1:2:1 ratio expected from Mendelian inheritance of a recessive trait (Chi square = 0.36, df = 2, between the probability of 0.9 - 0.1, and thus the null hypothesis that there is no difference between the observed and expected ratios was not rejected). This result indicates that homozygosity for the $Pah^{\Delta exon1}$ allele is not associated with

embryonic or neonatal lethality. However, beyond 2 weeks age, we have observed spontaneous demise in 10/17 of *Pah*$^{\Delta exon1/\Delta exon1}$ animals during the transition from nursing to dependence upon solid food. *Pah*$^{\Delta exon1/\Delta exon1}$ mice that survive beyond weaning exhibit coat color hypopigmentation on an unrestricted diet (Figure 4-2A), a characteristic phenotype of mouse models of PKU that results from phenylalanine-mediated competitive inhibition of the melanin-synthesizing enzyme tyrosinase [61].

Serum and brain amino acid profiles

Serum and brain amino acid profiles were examined in adult (6-12 week old) *Pah*$^{\Delta exon1/\Delta exon1}$ (N=6, 1 male and 5 female), *Pah*$^{+/\Delta exon1}$ (N=3, 1 male and 2 female), and *Pah*$^{+/+}$ (N=3, 1 male and 2 female) animals (Figure 4-2B). Serum phenylalanine levels in *Pah*$^{\Delta exon1/\Delta exon1}$ mice averaged 2172 ± 275 µM (mean ± SD), consistent with severe PKU, and were significantly elevated in comparison to either *Pah*$^{+/\Delta exon1}$ (80 ± 14 µM) or *Pah*$^{+/+}$ (78 ± 12 µM) mice by one-way ANOVA ($F(2,9) = 156.7$, $P < 0.0001$). There was no difference of hyperphenylalaninemia between male and female *Pah*$^{\Delta exon1/\Delta exon1}$ animals in an unpaired t-test, with an average of 2364 µM in 3 male mice and 2248 µM in 7 female mice (*p*-value 0.7035). Serum tyrosine concentration was statistically different between genotypes by one-way ANOVA ($F(2, 9) = 6.090$, $P = 0.0213$) with *Pah*$^{\Delta exon1/\Delta exon1}$ (49 ± 13 µM) less than *Pah*$^{+/+}$ animals (75 ± 10 µM) but not significantly different from *Pah*$^{+/\Delta exon1}$ (62 ± 5 µM).

Brain homogenates were analyzed for Phe, as well as the amino acid neurotransmitter precursors for dopamine and serotonin, tyrosine and tryptophan, respectively (Figure 4-2C). Brain Phe content was statistically elevated in *Pah*$^{\Delta exon1/\Delta exon1}$ mice (817 ± 90 nmol/g) in comparison to either *Pah*$^{+/\Delta exon1}$ (146 ± 19 nmol/g) or *Pah*$^{+/+}$ animals (114 ± 9 nmol/g) in a one-way ANOVA ($F(2, 9) = 154.2$, $P < 0.0001$). There were no statistical differences in brain tyrosine or tryptophan between the *Pah*$^{\Delta exon1}$ allele genotypes (Figure 4-2C), with brain Tyr of 90 ± 14 nmol/g and brain Trp of 26 ± 4 nmol/g in *Pah*$^{\Delta exon1/\Delta exon1}$ animals. These data are similar to published brain large neutral amino acid profiles in *Pah*$^{enu2/enu2}$ mice (brain Phe 762 ± 17 nmol/g, brain Tyr 85 ± 15 nmol/g, and brain Trp 20 ± 3 nmol/g) [28].

Brain Neurotransmitters

The content of the monoamine neurotransmitters dopamine, 5-hydroxytryptophan (5-HTP), serotonin, and their metabolites homovanillic acid (HVA) and 5-hydroxyindoleacetic acid (5-HIAA) were examined in adult *Pah*$^{\Delta exon1}$ animals. There are two parallel pathways that lead to the synthesis and metabolism of dopamine and serotonin. In dopaminergic neurons, tyrosine hydroxylase converts tyrosine into L-DOPA, which can then be converted into dopamine by L-amino acid decarboxylase (L-AAAD). After dopamine is secreted into the synapse, it can either be taken up by dopamine specific transporter (DAT) or metabolized into HVA. In *Pah*$^{\Delta exon1}$ animals, there was no difference in brain dopamine between *Pah*$^{\Delta exon1/\Delta exon1}$ animals (196.8 ± 38.78 nmol/g protein),

Pah$^{+/\Delta exon1}$ animals (260.6 ± 102.4 nmol/g) and *Pah*$^{+/+}$ animals (234.3 ± 24.13 nmol/g protein) by one-way ANOVA (F (2,8) = 1.129, *P* = 0.3700), (Figure 4-2D). Interestingly, there was a significant difference in brain HVA among the groups (F (2,8) = 9.349, *P* = 0.0081), but *post hoc* intergroup comparison revealed only an unexplained significant increase (*P* = 0.016) in brain HVA of *Pah*$^{+/\Delta exon1}$ animals (28.51 ± 3.74 nmol/ g protein) in comparison to *Pah*$^{+/+}$ animals (19.04 ± 2.03 nmol/g) but no significant difference (*P* = 0.9453) between *Pah*$^{\Delta exon1/\Delta exon1}$ animals (18.36 ± 3.73 nmol/g) and wild type mice (Figure 4-2E).

In the serotonergic neurons, tryptophan hydroxylase converts tryptophan into 5-HTP, which can then be converted by L-AAAD into serotonin. After serotonin is secreted into the synapse, it can either be taken up by serotonin reuptake transporters or metabolized into 5-HIAA. In contrast to dopamine, the brain serotonin content was significantly different among *Pah*$^{+/+}$, *Pah*$^{+/\Delta exon1}$, *Pah*$^{\Delta exon1/\Delta exon1}$ mice (one-way ANOVA F (2,8) = 91.20, *P* < 0.0001), (Figure 4-2F). Brain serotonin content was significantly lower (*P* = 0.0001) in *Pah*$^{\Delta exon1/\Delta exon1}$ animals (47.30 ± 5.79 nmol/g protein) than in wild type animals (90.53 ±3.10 nmol/g). Inexplicably, brain serotonin was somewhat increased (*P* = 0.002) in *Pah*$^{+/\Delta exon1}$ mice (122.1 ± 12.8 nmol/g). Similarly, the brain content of 5-HIAA, a marker of serotonin turnover, was significantly different among the genotypes by one-way ANOVA (F (2, 8) = 22.42, *P* = 0.0005), (Figure 4-2G). Brain 5-HIAA was significantly decreased (*P* = 0.0048) in *Pah*$^{\Delta exon1/\Delta exon1}$ animals (18.95 ± 6.28 nmol/g protein) in comparison to *Pah*$^{+/+}$ animals (73.60 ± 10.11

nmol/g protein). Brain 5-HIAA content was not significantly different ($P = 0.1629$) between wild type and *Pah*$^{+/\Delta exon1}$ animals (100.3 ± 32.24 nmol/g protein).

PAH Enzyme Activity

Liver PAH enzymatic activity was measured in homogenates from *Pah*$^{\Delta exon1/\Delta exon1}$ and *Pah*$^{+/\Delta exon1}$ mice and compared to that of the existing PKU model, *Pah*$^{enu2/enu2}$ along with *Pah*$^{+/enu2}$ mice (Figure 4-3A). Liver PAH enzyme activity is expressed as the percent of wild type C57BL/6 liver activity. As expected, PAH activity was undetectable in liver of either *Pah*$^{\Delta exon1/\Delta exon1}$ or *Pah*$^{enu2/enu2}$ mice. However, there was a surprising difference in the liver PAH activity measured in heterozygous *Pah*$^{+/\Delta exon1}$ (58 ± 7% wild type activity) and *Pah*$^{+/enu2}$ (29 ± 5% wild type activity) mice, with a $P < 0.0001$ *via post-hoc* intergroup comparison analysis with Tukey multiple comparisons test (Figure 4-3A).

PAH Protein Expression

Western blot analysis of bulk liver homogenate revealed no visible band for anti-PAH staining at the expected 50 kDa size in *Pah*$^{\Delta exon1/\Delta exon1}$ animals (Figure 4-3B). There is a strong band for PAH in *Pah*$^{+/+}$ animals, and less intense but visible PAH bands in *Pah*$^{+/\Delta exon1}$ and *Pah*$^{enu2/enu2}$ animals. Bands staining for GAPDH at 37 kDa reveal similar protein loading in all samples.

Liver fluorescent-immunohistochemistry using anti-PAH antibody conjugated to Alexa Fluor 488 (green) and nuclear staining with DAPI (blue), revealed strong

PAH expression in *Pah*$^{+/+}$ mice but complete absence of visible PAH expression in *Pah*$^{\Delta exon1/\Delta exon1}$ animals (Figure 4-3C).

PCR amplification and Sanger sequencing of potential CRISPR/Cas9 off target mutation sites

PCR amplification and Sanger sequencing of the top four predicted off target sites for Cas9-mediated double strand breaks associated with each of the guide RNA sequences used to produce the *Pah* exon 1 deletion detected no deleterious sequence differences (Supplemental figure 4-1).

Gene Addition Therapy in *Pah*$^{\Delta exon1/\Delta exon1}$ animals

Gene Therapy

In order to demonstrate applicability of this model, liver tropic recombinant adeno-associated virus serotype 8 (rAAV8) containing the murine *Pah* (*mPAH*) cDNA (rAAV2/8 LSPmPAH) [140] was administered to three homozygous *Pah*$^{\Delta exon1}$ animals in a small preliminary dose escalation experiment. The highest, middle, and lowest doses (1 X 10^{12} vector genomes (vg), 1 X 10^{11} vg, and 1 X 10^{10} vg of rAAV2/8 LSPmPAH, respectively) were delivered systemically via retro-orbital injection. A control animal received rAAV2/8 vector containing a nonsense frameshift mutation that abolishes PAH expression (1 X 10^{12} vg rAAV2/8 LSPmPAHfs). The phenylalanine levels in the three treated animals showed substantial correction in blood (127 µM, 194 µM, and 235 µM, respectively) and brain (382 nmol/g, 135 nmol/g, and 325 nmol/g, respectively)

14 days post-administration at all three vector doses while the animal that received the frameshift virus maintained elevated blood (1,928 µM) and brain (1,222 nmol/g) Phe levels (Table 4-1). Interestingly, the gene therapy treated animals exhibited liver PAH enzyme activity (96.1%, 42.0%, and 4.8% of wild type C57BL/6 liver activity), rAAV2 vector genome copy number (49.7 ± 2.9 vg, 16.2 ± 3.1 vg, and 2.9 ± 0.2 vg/ diploid liver genome), and intensity of liver fluorescent-immunohistochemical PAH staining that correlated with the vector dose (Table 4-1 and Figure 4-4).

Similar gene addition therapy was administered to *Pah*$^{enu2/enu2}$ animals (3 males and 3 females per dose) systemically through the retro-orbital route with doses of 1 x 10^{11} vg and 1 x 10^{12} vg of rAAV2/8 LSPmPAH, that conferred reduced Phe of 176 ± 52 µM and 99 ± 22 µM, respectively, % WT PAH enzyme activity of 7.7 ± 2.2% and 14.8 ± 3.3%, respectively, and vg/dg of 8-42 vg/dg and 56-291 vg/dg, respectively (Table 4-1).

Figures

Figure 4-1: Experimental Design, Screening, and Sequencing

A. *In silico* guide generation

Guide ID	Target Sequence	PAM	Strand	MIT Score
Guide 1	TGTCTATCCACTGCTACGTC	AGG	Plus	90
Guide 3	CGGGGCTGATGGTTTTAACC	TGG	Minus	87
Guide 4	GTGTTGCCCTGACGTAGCAG	TGG	Minus	84
Guide 6	GTTAGGAAAAGTTTGCACTC	AGG	Minus	75
Guide 7	TGCTCAGGACTCCGTTCTCC	AGG	Minus	74
Guide 8	TTTGGGCAGGTAAGCCTGTT	GGG	Plus	73

B. *In vitro* guide validation

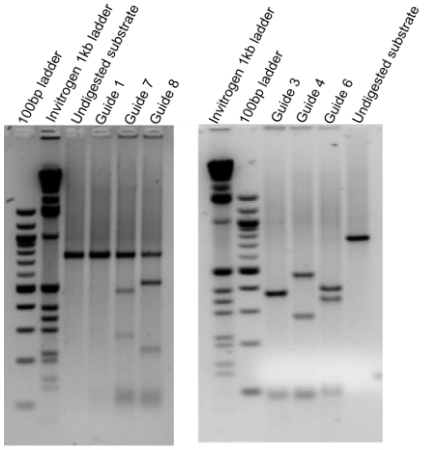

C. *Pah* exon 1 knock-out design

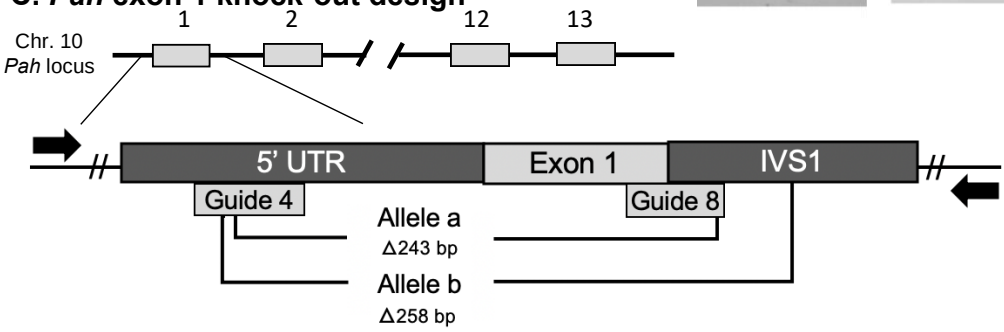

D. Gel electrophoresis of F0 *Pah*$^{+/\Delta exon1}$

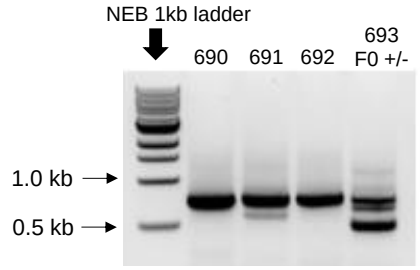

E. Gel electrophoresis of F2 litter

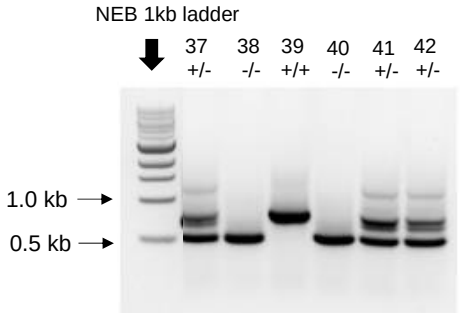

F. *Pah*$^{\Delta exon1}$ Sanger Sequencing

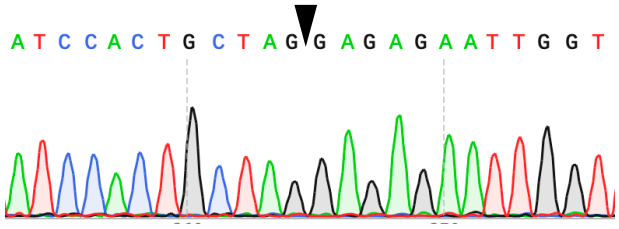

Figure 4-1: **Experimental Design, Screening, and Sequencing.**

A. *In silico* guide generation. The table displays the six guides that were selected for *in vitro* analysis using the MIT Guide Design *in silico* tool. Guide ID, Target Sequence, PAM site, Strand (plus or minus), and MIT Score are displayed, where higher scores indicate an improved prediction for cutting efficiency. **B. *In vitro* guide validation.** Gel electrophoresis of *in vitro* Guide-It Takara Assay performed with the six guides identified in Supplemental 1A and run on a 3% agarose gel. In the left gel, Guide1 displays no cutting of substrate, while guides 7 and 8 display partial cutting of substrate into 300 bp and 500 bp bands and 200 bp and 600 bp bands, respectively. In the right gel, Guides 3, 4, and 6 show complete cutting of substrate, with a doublet of 400 bp bands from guide 3 cutting, 300 bp and 500 bp from guide 4, and 350 bp and 450 bp from guide 6. Of note, guide 1 was the only guide that did not demonstrate substrate cutting. **C. *Pah* exon 1 knockout design.** The diagram illustrates the experimental design to use CRISPR/Cas9 mediated technology with strategically selected sgRNAs to knockout exon 1 of the *Pah* locus. The gene structure of murine *Pah*, located on chromosome 10, is shown with exon 1, exon 2, exon 12, and exon 13 labeled, and // indicates the gene structure containing exons 3-11. Locations of Guide 4 (5' UTR) and Guide 8 (exon1-IVS1 junction) are displayed and placed below the *Pah* structure due to targeting of the minus strand DNA sequence. The PCR design to detect large, 200+ bp deletions in the 5' *Pah* locus is indicated with black arrows to represent primers. Forward primer is located in the 5' UTR and 3' primer is located in IVS1 (where // indicates DNA gap),

resulting in amplification a 753 bp product that flanks exon 1 in the absence of gene modification. Two founder females were identified with deletions spanning exon 1; one animal contained a deletion of 243 bp, designated allele a, and the other animal contained a deletion of 258 bp, designated allele b. **D. Gel electrophoresis of F0 *Pah*$^{+/\Delta exon1}$ female mouse.** Tail biopsy DNA from potential *Pah*$^{+/\Delta exon1}$ founder mice was amplified with the primers described in Figure 1C. All mice have expected the expected wild type ~750 bp band but founder b (693) carries an additional ~500 bp band representing an allele with a ~250 bp deletion. **E. Gel electrophoresis of F2 *Pah*$^{\Delta exon1}$ allele progeny.** Genotyping of the progeny form a *Pah*$^{+/\Delta exon1}$ X *Pah*$^{+/\Delta exon1}$ breeding: Mouse 37 (*Pah*$^{+/\Delta exon1}$), Mouse 38 (*Pah*$^{\Delta exon1/\Delta exon1}$), Mouse 39 (*Pah*$^{+/+}$), Mouse 40 (*Pah*$^{\Delta exon1/\Delta exon1}$), Mouse 41 (*Pah*$^{+/\Delta exon1}$), and Mouse 42 (*Pah*$^{+/\Delta exon1}$). *Pah*$^{+/+}$ contains a single ~750 band, *Pah*$^{+/\Delta exon1}$ contains two bands, a ~750 bp band and a ~500 bp band, and *Pah*$^{\Delta exon1/\Delta exon1}$ contains a single ~500 bp band. **E. Sanger sequencing of *Pah*$^{\Delta exon1}$ allele.** The chromatogram displays 12 nucleotides spanning in either direction from the deleted region in the *Pah*$^{\Delta exon1}$ allele, indicated with the black triangle.

Figure 4-2: Characterization of Amino Acids & Derivatives in *Pah*$^{\Delta exon1}$ Mice

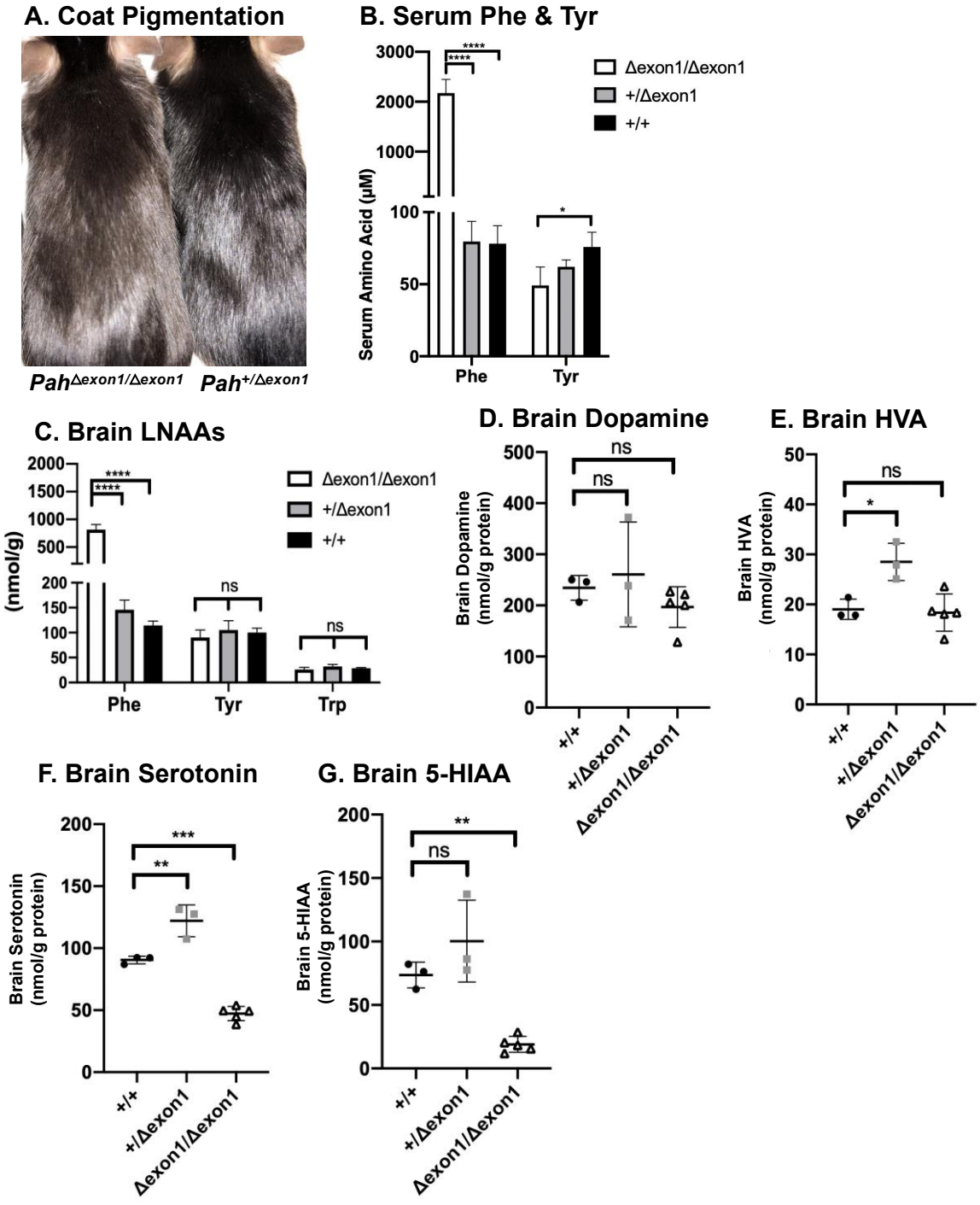

Figure 4-2: Characterization of Amino Acids & Derivatives in *Pah*$^{\Delta exon1}$ Mice

A. Coat pigmentation. Photograph of untreated *Pah*$^{\Delta exon1/\Delta exon1}$ (left) and *Pah*$^{+/\Delta exon1}$ (right) mice on standard mouse chow diet. **B. Serum Phe & Tyr.** Mean serum phenylalanine and tyrosine concentration (± SD) of adult *Pah*$^{\Delta exon1/\Delta exon1}$, *Pah*$^{+/\Delta exon1}$, and *Pah*$^{+/+}$ animals following euthanasia. The left y-axis indicates µM serum amino acid concentration. The average serum Phe was 2172 µM, 80 µM, and 78 µM, respectively. One-way ANOVA revealed significant effects of genotype on serum Phe ($F(2,9) = 156.7$, $P < 0.0001$). The average serum Tyr was 49 µM, 62 µM, and 75 µM, respectively. One-way ANOVA revealed significant effects of genotype on serum Tyr between *Pah*$^{\Delta exon1/\Delta exon1}$ and *Pah*$^{+/+}$ animals ($F(2, 9) = 6.090$, $P = 0.0213$). **C. Brain LNAAs.** Mean brain LNAA concentrations (± SD) of *Pah*$^{\Delta exon1/\Delta exon1}$, *Pah*$^{+/\Delta exon1}$, and *Pah*$^{+/+}$ animals at time of euthanasia. The y-axis indicates amino acid concentration in nmol/g wet weight. The average brain Phe was 817 nmol/g, 146 nmol/g, and 114 nmol/g, respectively. One-way ANOVA revealed significant effects of genotype on brain Phe ($F(2, 9) = 154.2$, $P < 0.0001$). The average brain Tyr was 90 nmol/g, 105 nmol/g, and 100 nmol/g, respectively and brain Trp was 26 nmol/g, 32 nmol/g, 28 nmol/g, respectively. One-way ANOVA revealed no statistical differences in brain Tyr or Trp in *Pah*$^{\Delta exon1}$ allele mice. **D. Brain dopamine.** Brain dopamine concentrations in nmol/g protein (y-axis) of individual animals (represented as single points) in each genotype of *Pah*$^{\Delta exon1}$ allele mice (x-axis). There was no statistical significance in brain dopamine across genotypes by one-way ANOVA ($F(2,8) = 1.129$, $P = 0.3700$). **E. Brain HVA.** Brain HVA concentrations in nmol/g

protein (y-axis) of individual animals (represented as single points) in each genotype of *Pah*$^{\Delta exon1}$ allele mice (x-axis). There was a significant difference in brain HVA across genotypes (one-way ANOVA: $F(2, 8) = 9.349$, $P = 0.0081$) with *post-hoc* multiple comparisons showing a significant increase of HVA in heterozygous animals in comparison to WT animals (adjusted $P = 0.016$) but no difference between homozygous and WT animals (adjusted $P = 0.9453$). **F. Brain serotonin in *Pah*$^{\Delta exon1}$ allele mice.** Brain serotonin concentrations in nmol/g protein (y-axis) of individual animals (represented as single points) in each genotype of *Pah*$^{\Delta exon1}$ allele mice (x-axis). There was a significant difference in brain serotonin across genotypes (one-way ANOVA: $F(2,8) = 91.20$, $P < 0.0001$), with significantly less brain serotonin in *Pah*$^{\Delta exon1/\Delta exon1}$ animals (47.30 nmol/g protein) than wild type (90.53 nmol/g protein) or heterozygous (122.1 nmol/g protein) animals. **G. Brain 5-HIAA.** Brain 5-HIAA concentrations in nmol/g protein (y-axis) of individual animals (represented as single points) in each genotype of *Pah*$^{\Delta exon1}$ allele mice (x-axis). There was a significant difference in brain 5-HIAA across genotypes (one-way ANOVA: $F(2,8) = 22.42$, $P = 0.0005$), with less brain 5-HIAA in *Pah*$^{\Delta exon1/\Delta exon1}$ animals (18.95 nmol/g protein) than wild type (73.6 nmol/g protein) or heterozygous (100.3 nmol/g protein) animals.

Figure 4-3: Characterization of PAH in *Pah*$^{\Delta exon1}$ Mice

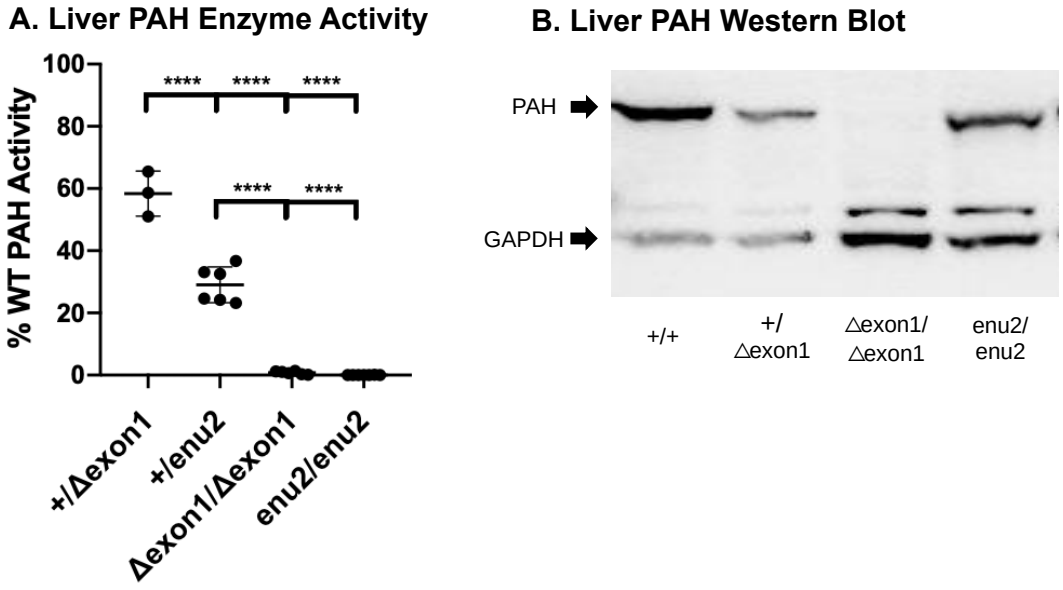

C. Liver PAH Fluorescent Immunohistochemistry

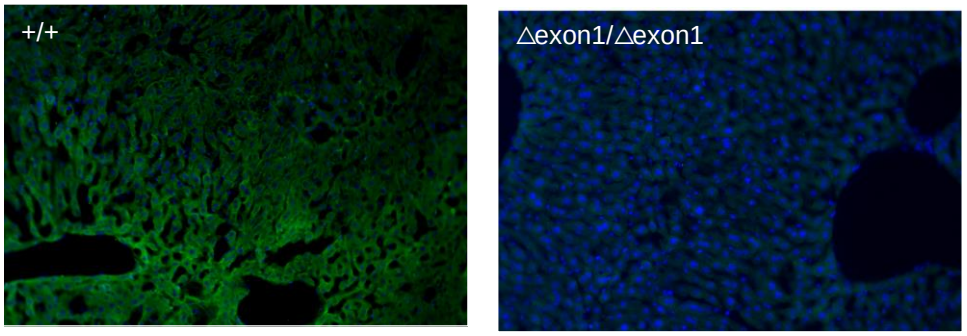

Figure 4-3: Characterization of PAH in *Pah*$^{\Delta exon1}$ Mice

A. Liver PAH enzyme activity. Mean liver PAH enzyme activity (± SD) in homozygous and heterozygous *Pah*$^{\Delta exon1}$ and *Pah*^{enu2} mice. The y-axis indicates liver PAH activity expressed as percent wild type (WT) PAH enzyme activity. The average enzyme activity was 58% in *Pah*$^{+/\Delta exon}$ and 29% in *Pah*$^{+/enu2}$, while all homozygous recessive animals were 0%. One-way ANOVA revealed statistical differences in percent WT PAH enzyme activity across these genotypes ($F(3, 18) = 212.7$, $P < 0.0001$). **B. Liver PAH western blot.** Western blot analysis of anti-PAH and anti-GAPDH in liver homogenates from *Pah*$^{\Delta exon1}$ allele and *Pah*$^{enu2/enu2}$ mice. The arrows on the left of the image indicate band sizes for PAH at 50kDa (top) and GAPDH at 37kDa (bottom). **C. Liver PAH fluorescent immunohistochemistry.** Anti-PAH fluorescent immunohistochemistry in liver tissue samples from *Pah*$^{+/+}$ and *Pah*$^{\Delta exon1/\Delta exon1}$ mice. Green indicates the presence of PAH by anti-PAH antibodies bound by secondary antibodies conjugated with AlexaFluor 488 (green fluorescence) and blue indicates nuclear staining with DAPI. The left image depicts PAH IHC on untreated *Pah*$^{+/+}$ liver tissue with strong green signal and top right image displays PAH IHC of untreated *Pah*$^{\Delta exon1/\Delta exon1}$ liver tissue with absent green signal.

Figure 4-4: Liver PAH Fluorescent Immunohistochemistry of Gene Therapy Treated *Pah*$^{\Delta exon1/\Delta exon1}$ Mice

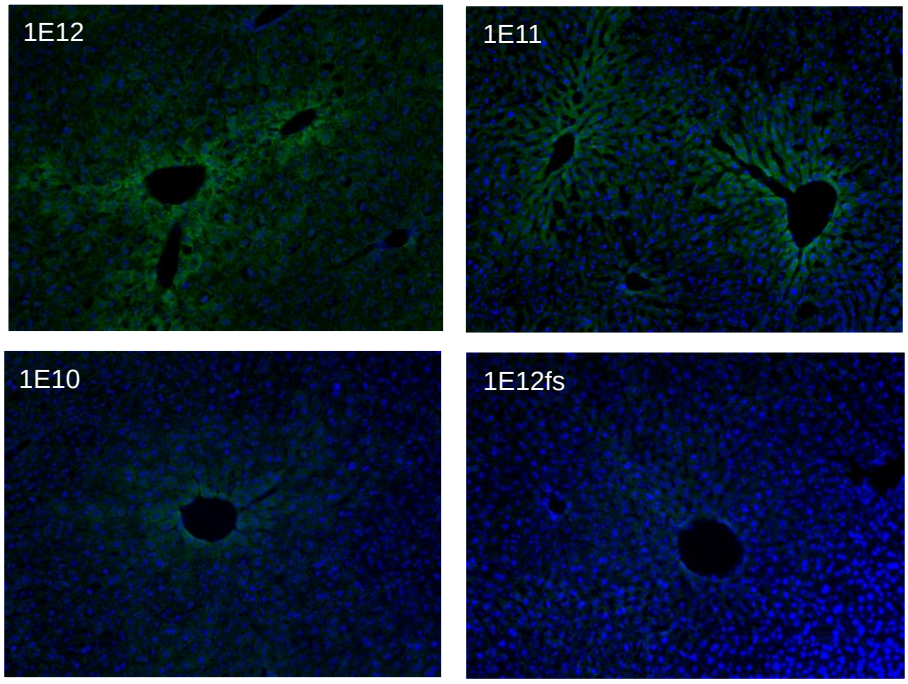

Figure 4-4: Liver PAH Fluorescent Immunohistochemistry of Gene Therapy Treated *Pah*$^{\Delta exon1/\Delta exon1}$ mice. Anti-PAH fluorescent-immunohistochemistry in liver tissue samples from gene addition therapy treated *Pah*$^{\Delta exon1/\Delta exon1}$ mice. Green indicates the presence of PAH by anti-PAH antibodies bound by secondary antibodies conjugated with AlexaFluor 488 (green fluorescence) and blue indicates nuclear staining with DAPI. The four images display the gene therapy treated *Pah*$^{\Delta exon1/\Delta exon1}$ mice as labelled according to dosing of therapeutic vectors of LSPmPAH AAV2/8: 1 X 10^{12} vg (top left image labelled with **1E12**), 1 X 10^{11} vg (top right image labelled with **1E11**), and 1 X 10^{10} vg (bottom left image labelled with **1E10**), followed by 1 X 10^{12} vg of the control vector (LSPmPAHfs) containing a frameshift (bottom right image labelled with **1E12fs**).

Table 4-1: Molecular Analyses of Gene Therapy Treated *Pah*$^{\Delta exon1/\Delta exon1}$ and *Pah*$^{enu2/enu2}$ Mice

Gene Therapy	Blood Phe Pre-GT (μM)	Blood Phe Post-GT (μM)	Blood Tyr Pre-GT (μM)	Blood Tyr Post-GT (μM)	Brain Phe Post-GT (μM	Brain Tyr Post-GT (μM)	Liver PAH activity (%WT)	Vg copy/liver diploid genome
***Pah*$^{\Delta exon1/\Delta exon1}$ mice**								
1E12 AAV2/8 LSPmPAHfs female	2193	1928	38	37	1222	116	0.2%	1.0
1E10 AAV2/8 LSPmPAH male	3095	235	48	117	325	161	4.8%	2.9
1E11 AAV2/8 LSPmPAH female	2677	195	45	115	135	135	42%	16.2
1E12 AAV2/8 LSPmPAH male	1835	127	56	132	382	160	96.1%	50
***Pah*$^{enu2/enu2}$ mice**								
1E11 AAV2/8 LSPmPAH 3 male/3 female	1983 ± 540[a]	176 ± 52 [a]	ND	ND	ND	ND	7.7 ± 2.2% [a]	8-42 [b]
1E12 AAV2/8 LSPmPAH 3 male/3 female	1921 ± 603 [a]	99 ± 22 [a]	ND	ND	ND	ND	14.8 ± 3.3% [a]	56-291[b]

ND – not done. [a] – mean ± SD. [b] - range

Table 4-1: Molecular Analyses of Gene Therapy Treated *Pah*$^{\Delta exon1/\Delta exon1}$ and *Pah*$^{enu2/enu2}$ Mice

Pre- and post- gene therapy (GT) effects in a dose escalation experiment in *Pah*$^{\Delta exon1/\Delta exon1}$ mice, as well as gene addition therapy in *Pah*$^{enu2/enu2}$ animals. The first column indicates the gene therapy administered, including dose and transgene, where rAAV2/8 LSPmPAH indicates a therapeutic virus containing an rAAV2 genome with a transgene cassette containing a Liver Specific Promoter driving murine PAH packaged into an AAV8 capsid. The AAV2/8 LSPmPAHfs contains a frameshift and is used as a control vector.

Supplemental Figure 4-1: sgRNA Off-Target Sanger Sequencing

A. Guide 4 Off-Target Sanger Sequencing

Guide 4 Sequence: GTGTTGCCCTGACGTAGCAGTGG

Location: Chr8:115751069
Sequence: GTGGTGCCTGAGGTAGCAGTGG
COSMID Score: 2.01

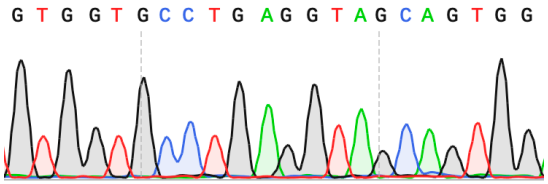

Location: Chr2:33139660
Sequence: TTGTTGCCCTGACATGGCAGTGG
COSMID Score: 3.72

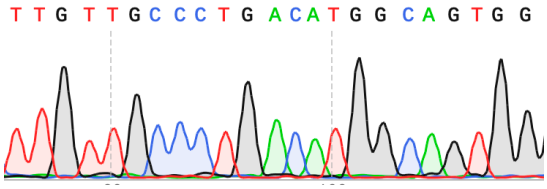

Location: ChrX:57746102
Sequence: GTGTAGCCTGATGTAGCAGAGG
COSMID Score: 2.03
Chromatogram displaying complementary sequence:

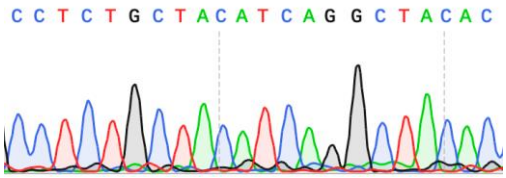

Location: Chr8:86472947
Sequence: GTGTTGTCCCTGAGCTAGCAGTGG
COSMID Score: 3.72
Chromatogram displaying complementary sequence:

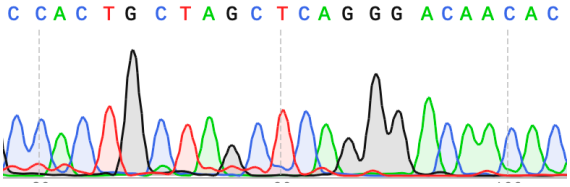

B. Guide 8 Off-Target Sanger Sequencing

Guide 8 Sequence: TTTGGGCAGGTAAGCCTGTTGGG

Location: Chr13:35827032
Sequence: TATGCCAGGTAAGCCTGTTCGG
COSMID Score: 1.02
Chromatogram displaying complementary sequence:

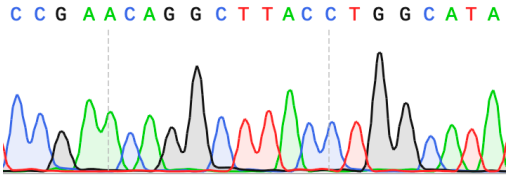

Location: Chr12:95441363
Sequence: TTAGGGAAGGAAGCCTGTTGGG
COSMID Score: 1.59

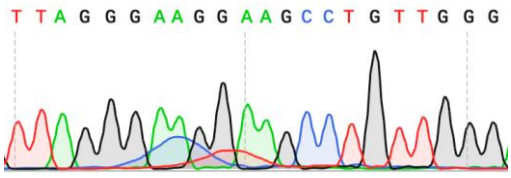

Location: Chr1:22629912
Sequence: TGTGGGTAGGAAGCCTGTTCGG
COSMID Score: 1.57
Chromatogram displaying complementary sequence:

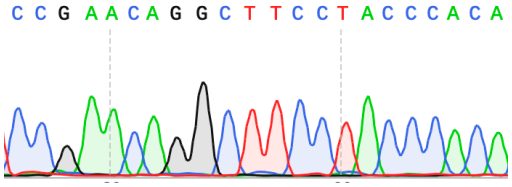

Location: Chr5:110339511
Sequence: TCTGGTCAGGTAAAGCCTGTTGGG
COSMID Score: 1.84
Chromatogram displaying complementary sequence:

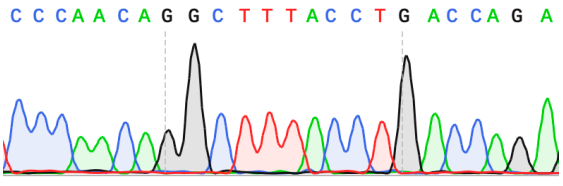

Supplemental Figure 4-1: sgRNA Off-Target Sanger Sequencing

A. Guide 4 off-target Sanger sequencing. Guide 4 sequence with PAM site is displayed at the top, followed by chromatograms displaying the top four Guide 4 off-target sites, including location, sequence (PAM site in red), and COSMID score. **B. Guide 8 off-target Sanger sequencing.** Guide 8 sequence (with PAM site in red) is displayed at the top, followed by chromatograms displaying the top four Guide 8 off-target sites, including location, sequence (PAM site in red), and COSMID score.

Discussion

This study was able to successfully generate a novel murine model for classical PKU completely void of hepatic PAH protein expression. *Pah*$^{+/\Delta exon1}$ x *Pah*$^{+/\Delta exon1}$ mating produced the expected 1:2:1 Mendelian ratios of *Pah*$^{+/+}$ to *Pah*$^{+/\Delta exon1}$ to *Pah*$^{\Delta exon1/\Delta exon1}$ offspring. Additionally, female *Pah*$^{+/\Delta exon1}$ x male *Pah*$^{\Delta exon1/\Delta exon1}$ mating was productive, yielding progeny in a 1:1 ratio of *Pah*$^{+/\Delta exon1}$ to *Pah*$^{\Delta exon1/\Delta exon1}$ animals. Complete PAH deficiency did not cause embryonic or neonatal lethality. However, *Pah*$^{\Delta exon1/\Delta exon1}$ mice struggled to wean from nursing to solid food more frequently than the prior existing *Pah*$^{enu2/enu2}$ model, with increased mortality at weaning. They required more attention to husbandry at this period with delayed separation from their dam and provision of soft food placed directly in the bottom of the cage until they demonstrated consistent ability to reach the chow overhead in the cage lid. The precise reason for this difference in the phenotype at weaning between the *Pah*$^{\Delta exon1/\Delta exon1}$ and *Pah*$^{enu2/enu2}$ models requires further investigation. There were no other obvious differences in the physical phenotype or neurologic performance of the two models to explain the loss of *Pah*$^{\Delta exon1/\Delta exon1}$ mice near weaning. Blood and brain amino acid concentrations including the levels of phenylalanine and tyrosine in adult mice that survived weaning did not differ significantly between the two mouse strains. Brain neurotransmitter evaluation revealed consistent findings with the *Pah*$^{enu2/enu2}$ animals, which showed minimal disruptions in the dopamine pathway, but significant deficiencies in serotonin production [28]. The main biochemical difference between the *Pah*$^{\Delta exon1/\Delta exon1}$ and *Pah*$^{enu2/enu2}$ models is the complete

lack of detectable PAH protein in the knockout mouse. Deleterious CRISPR/Cas9-mediated mutation at an off-target site is a theoretical, low probability event that could adversely affect the phenotype of *Pah*$^{\Delta exon1/\Delta exon1}$ mice. PCR amplification and Sanger sequencing of the top four predicted off-target Cas9 cutting sites for each of the two guides used to develop the mouse detected no genotoxicity at any of those eight locations, however this approach was not comprehensive for the entire genome. To eliminate the possibility of any adverse mutations at alleles other than *Pah*, we are currently outbreeding the *Pah*$^{\Delta exon1}$ allele onto a clean C57BL/6 genetic background.

Prior to this, the available mammalian animal models of PKU consisted of mouse models denoted as *Pah*$^{enu1/enu1}$, *Pah*$^{enu2/enu2}$, and *Pah*$^{enu3/enu3}$, which were created by random N-ethyl-N-nitrosourea (ENU) mutagenesis [91]. The *Pah*^{enu3} allele, which is no longer available due to breeding difficulties and neonatal lethality, contained a frameshift mutation that caused premature termination of the tetramerization domain [92]. *Pah*^{enu1} and *Pah*^{enu2} alleles are missense mutations that result in phenotypes on opposite ends of the hyperphenylalaninemia spectrum and are the predominant models of PKU to date. An additional model of PKU combines *enu1* and *enu2* as a heteroallelic *Pah*$^{enu1/enu2}$ model, recapitulating compound heterozygosity for *PAH* mutations which occurs in approximately 87% of humans with PKU [93, 94]. The *Pah*$^{enu1/enu1}$ and *Pah*$^{enu1/enu2}$ models are less desirable for gene and cell interventions due to their mild phenotype.

The longstanding and most popular mouse model for preclinical PKU gene therapy studies has been the *Pah*$^{enu2/enu2}$ model, which is homozygous for a p.F263S (c.835 T>C) missense mutation in the central catalytic domain of PAH. It produces abundant albeit inactive PAH enzyme and recapitulates classical human PKU, with severe hyperphenylalaninemia, cognitive and behavioral disabilities, hypopigmentation, and occasional seizures. We and other groups have successfully treated adult *Pah*$^{enu2/enu2}$ animals with AAV-mediated gene addition therapy demonstrating robust, long-term efficacy [140, 146, 147, 248]. Additionally, this model has been used in hepatocyte transplant studies [148, 216, 249] and CRISPR/Cas9-mediated gene correction of the *enu2* point mutation in neonatal [187] and adult animals [223]. While these studies have driven the advancements in PKU therapeutic development, there is a significant limitation in this model, specifically the expression of inactive PAH monomer, leading to barriers in both efficacy and molecular analyses of gene and cell therapeutic interventions. The expression of mutant PAH protein makes immuno-based molecular analyses using anti-PAH antibodies following gene therapy uninformative as the ability to quantify or localize transgene-delivered protein is limited. Additionally, it has been proposed that the native mutant PAH monomers interact with and reduce overall activity of wild type monomers, and in this mouse model, pose an additional barrier to efficacy in gene therapy studies.

The possibility that mutant PAH monomers might have a dominant negative effect upon the activity of wild type PAH was first suggested from a study of liver

PAH activities measured in parents of children with PKU [250]. In these individuals who were presumably heterozygous for pathogenic *PAH* mutations (the study occurred prior to cloning of the *PAH* gene), liver PAH activity measured only 4.4-23% of wild type activity rather than the 50% typically expected for a recessively-inherited disorder. In this new study, we now confirm significant differences in liver PAH enzyme activity between $Pah^{+/\Delta exon1}$ and $Pah^{+/enu2}$ heterozygous animals, indicating that the production of mutant F263S monomers in $Pah^{+/enu2}$ heterozygous mice adversely impacted the proper function of wild type PAH. These data provide strong *in vivo* evidence for the dominant negative effect of at least this single missense *Pah* mutation. Further studies are warranted to confirm these findings and extend them to the Pah^{enu1} model. We propose that this phenomenon may extend to multiple human missense *PAH* mutations.

Preliminary results from a small liver-directed AAV8-mediated dose escalation gene addition trial in three $Pah^{\Delta exon1/\Delta exon1}$ mice revealed the utility of this model for liver gene transfer studies particularly in regard to employing anti-PAH immunohistochemistry in the assessment of hepatocyte transduction frequency, a feat that was previously unachievable in existing murine models. Furthermore, comparison of the efficacy in this small trial to the efficacy of $Pah^{enu2/enu2}$ mice corroborates the suspicion that F263S mutant monomers present in the latter model inhibit the activity of wild type transgene-produced PAH and thereby limit treatment efficacy. Despite similar vector genome numbers within hepatocytes of

the *Pah*$^{\Delta exon1/\Delta exon1}$ and *Pah*$^{enu2/enu2}$ animals, PAH enzyme activity was far greater in the *Pah*$^{\Delta exon1/\Delta exon1}$ animals (Figure 3A). More *Pah* $^{\Delta exon1/\Delta exon1}$ animals need to be treated to confirm these findings, but nevertheless we are confident in reporting that this knockout model is more sensitive to therapeutic intervention and is better able to depict a more accurate analysis of vector genome to PAH activity due to the lack of mutant monomer expression, ameliorating the dominant negative effect observed in *Pah*$^{enu2/enu2}$ mice.

In conclusion, we report the development of a novel PAH deficient murine model harboring a recessively inherited deletion of *Pah* exon 1. Because anti-PAH immunohistochemistry can be readily employed to track hepatocyte transduction following gene therapy, in addition to an apparently improved therapeutic threshold in comparison to the existing *Pah*^{enu2} model, we predict that this novel model will find particular utility in the future investigation of gene addition and gene editing methods. Importantly, with AAV-mediated gene addition therapy for PKU now entering human trials, this model provides a platform to more clearly correlate gene therapy treatment with physiological outcomes and aid our understanding of clinical trial results. While creating a model for classical PKU gene therapy with fewer confounding variables and enhanced molecular analyses was the impetus for this project, the overarching goal of generating this model was to add to the experimental tools available for PKU scientists and to advance PKU research.

Materials & Methods

Experimental Design

Guide Design and Validation

Single guide RNAs (sgRNA) were designed using the online guide design tools CHOPCHOP and MIT Guide Design, using nucleotides 87521818-87522107 of the murine GRCm38.p4 C57BL/6J chromosome 10 sequence, which contains the 5' untranslated region (5' UTR) through intervening sequence 1 (IVS 1) of the *Pah* locus. Of eight guides produced (Figure 1A), six were selected for further sgRNA investigation (guides 1,3,4,6,7,8). All guides were tested with the Takara Guide-It sgRNA *In-Vitro* Transcription Kit (Cat. No. 632635) and Screening System (Cat. No. 632639). Guides 3, 4, 6, 7 and 8 proved effective at inducing a targeted double-stranded break in the PCR substrate, and only guide 1 was unable to induce a cut in the target DNA (Figure 4-1B). The sgRNAs 4 and 8, located in the 5' UTR and IVS1, respectively, were selected for *Pah* gene targeting in murine embryos (Figure 4-1C).

Delivery of Cas9/sgRNA to mouse zygotes

Female C57BL/6N JAX® mice at 4-5 weeks of age were super-ovulated, mated with males, and 0.5 day old single cell zygotes were isolated as previously described [251]. Two approaches to accomplish mouse *Pah* exon 1 deletion were performed in this study. In the first approach, a mixture of Cas9 mRNA and sgRNAs were injected into the cytoplasm of the one-cell fertilized eggs [252]. In the second approach, electroporation of Cas9 protein/sgRNA (RNP) complex

using the NEPA21 system (NEPA GENE Co. Ltd, Chiba Japan) was performed on single-cell fertilized eggs [253]. Zygotes from either approach were then transferred into the oviducts of pseudo pregnant recipient CD1/NCrl foster dams (Charles River), and the surviving offspring were screened for sizable deletions in the *Pah* exon 1 region after weaning.

PCR Screen for Deleted Alleles

Tail biopsies were acquired from F0 animals at three weeks of age and screened for visually discernable deletions of 200 bp or more using standard PCR and gel electrophoresis. Forward primer 5'-GGTTGCGGAGAATCCATAC-3' and reverse primer 5'-TGACTAAGGACCAGCCATTTC-3' which are complementary to *Pah* sequences outside the putative Cas9 cleavage sites were used to amplify 753 bp spanning the 5' UTR and 3' IVS1 of exon 1 in the *Pah* locus using standard PCR with Invitrogen Platinum™ Taq DNA polymerase and the following cycling parameters: initial denaturation at 94°C for 5 minutes, followed with 30 cycles of denaturation at 94°C for 30 seconds, primer annealing at 55°C for 30 seconds, and extension at 72°C for 1 minute, and a final extension of 72°C for 5 minutes. Products were analyzed by electrophoresis on a 1% agarose gel with 1kb NEB ladder (Figure 4-1D and 4-1E). Bands approximately 500 bp in size were excised from the gel and purified with the Qiagen QIAQuick Gel Extraction kit (Cat. 28706 x 40) for Sanger sequencing.

Knockout-allele Sanger Sequencing

Purified approximately 500 bp PCR products described above were quantified using the Epoch Microplate Spectrophotometer and analyzed by standard Sanger sequencing with 5'-GGTTGCGGAGAATCCATAC-3' forward primer on an ABI 3130XL sequencer.

Animal studies

Animal husbandry

Animal care and experimentation were performed in accordance with the guidelines of the Dept. of Comparative Medicine, Oregon Health & Science University and the National Institutes of Health Guide for the Care and Use of Laboratory animals. The knockout *Pah*$^{\Delta exon1/\Delta exon1}$ mice were produced through male *Pah*$^{+/\Delta exon1}$ x female *Pah*$^{+/\Delta exon1}$ as well as male *Pah*$^{\Delta exon1/\Delta exon1}$ x female *Pah*$^{+/\Delta exon1}$ crosses. Pups were toe clipped at two weeks for genotyping and identification purposes. All mice were fed tap water and standard mouse chow (LabDiet Picolab Rodent Diet 5LOD, St. Louis, MO) *ad libitum* providing approximately 24% protein and 1.04% L-phenylalanine by weight, except breeders that received high energy chow (LabDiet Rodent High Energy Diet 5058, St. Louis, MO) approximately 22% protein and 0.99% L-phenylalanine. Given that adult mice consume approximately 5 g chow per day, daily L-phenylalanine intake is estimated to be approximately 50 mg per day. The animals were housed under a standard 12 hours on, 12 hours off light cycle. All

surgical procedures were carried out with inhaled isoflurane general anesthesia to minimize pain and discomfort.

Gene Therapy

Three 6-8 week old *Pah*$^{\Delta exon1/\Delta exon1}$ mice (two males and one female) were treated with recombinant liver tropic adeno-associated virus serotype 8 vector containing AAV 2 genome (AAV2/8) that expressed the murine *Pah* cDNA from a strong Liver Specific Promoter (LSPmPAH) at doses of either 1 x 10^{10} vector genomes (vg) (1 male), 1 x 10^{11} vg (1 female), or 1 x 10^{12} vg (1 male) per mouse via retroorbital injection. An additional control female animal was administered 1 x 10^{12} vg of a similar viral vector containing an inactivating frameshift mutation in the transgene, denoted as AAV2/8 LSPmPAHfs. Blood was obtained prior to AAV injection for measurement of blood Phe concentration. Two weeks later animals were harvested for molecular analyses, including serum and brain amino acid analysis, hepatic PAH enzyme activity, liver PAH fluorescent-immunohistochemistry, and quantitative PCR (qPCR) to determine vg copy number in total liver DNA.

A similar gene therapy study was performed in the *Pah*$^{enu2/enu2}$ mouse model. Two cohorts of six adult *Pah*$^{enu2/enu2}$ animals (3 male and 3 female) were administered 1 x 10^{11} vg or 1 x 10^{12} vg AAV2/8 LSPmPAH via retro-orbital injection. Blood was obtained prior to AAV injection for measurement of blood Phe concentration. Two weeks later animals were harvested for molecular

analyses, including serum Phe concentration, hepatic PAH enzyme activity, and quantitative PCR (qPCR) to determine vg copy number in total liver DNA.

Euthanasia and tissue harvest

Animals were sedated using inhaled isoflurane anesthesia. Whole blood was collected by cardiac puncture, allowed to clot in an Eppendorf tube, and serum was separated by centrifugation. The mice were then euthanized by exsanguination and perfused with 20 mL normal saline via the left cardiac ventricle to clear blood from the liver and brain.

Molecular Characterization

Blood and Brain Amino Acids

Blood and brain amino acid concentrations were determined using an established protocol [28] by pre-column derivatization with 6-aminoquinolyl-N-hydroxysuccinimidyl carbamate (AQC, Waters AccQ Tag™ derivatization system) and separation by ultrahigh performance liquid chromatography and UV absorbance detection (Waters Acquity™ UPLC, Milford, MA) using the Waters Masstrak Amino Acid Analysis method (Figure 4-2B and 4-2C).

Brain Neurotransmitters

Mouse half brains were processed as previously described [28, 254] for the measurement of dopamine, homovanillic acid (HVA), 5-hydroxytryptophan (5-HTP), serotonin, and 5-hydroxyindoleacetic acid (5-HIAA) through ultrahigh

performance liquid chromatography (UHPLC) and electrochemical detection basically as previously established [255]. Neurotransmitter concentrations were corrected for the total protein content of brain homogenate and reported as nmol/g protein (Figure 4-2D, 4-2E, 4-2F and 4-2G).

Liver PAH Enzyme Activity

PAH enzyme activity was determined in liver homogenates using a radiometric chromatography assay [227] with modifications [228], corrected for protein content, and normalized to the measured wild type C57Bl/6 liver PAH activity from the same run (Figure 4-3A).

Liver PAH Western Blot

Bulk liver homogenates were prepared by mechanical homogenization of four 10 mg biopsies in 800 µL of cold lysis buffer, followed by centrifugation at 770 rpm for 8 minutes at 4°C. The supernatant was collected and quantified for protein concentration using the Micro BCA™ Protein Assay Kit from ThermoFisher (Cat. 23235). Each lane was loaded with a sample preparation containing 250 ng of protein in 1 µL, NuPage LDS Sample Buffer, 50 mM dithiothreitol, and water up to a total volume of 10 µL and incubated at 70° C for 10 min. 3 µL of Magic Mark™ ladder and 10 µL of each sample were loaded on a NuPage pre-cast gel and separated by electrophoresis in MOPS buffer at 200V for 50 minutes. The protein was transferred to a polyvinylidene fluoride membrane with electrophoresis in NuPage transfer buffer at 100V for 45 minutes. The membrane

was blocked with 5% milk in TBS-T (Tris Buffer Saline-Tween) and probed with rabbit polyclonal anti-PAH antibody (1:200 dilution, BS3704 PAH (R400) from Bioworld, Inc.) and GAPDH loading control antibody (1:200 dilution, MA5-15738 GAPDH loading control antibody from Invitrogen) overnight. The membrane was washed with TBS-T and probed with HRP-conjugated goat anti-rabbit IgG secondary antibody (1:1000 dilution, A27034 Goat anti-rabbit IgG (H+L) from Thermo Scientific and m-IgGκ BP-HRP Sc 506102 from Santa Cruz Biotechnology) for one hour and washed. Bands were visualized using enhanced chemiluminescence (Chemiluminescent Western Blot Detection from ThermoScientific) captured on the Azure Sapphire Biomolecular Imager chemiluminescence detection system (Figure 4-3B).

Quantitative PCR for Vector Genome Copy Number in Total Liver DNA

Total liver genomic DNA from untreated *Pah*$^{\Delta exon1/\Delta exon1}$ mice was spiked with linearized LSPmPAH vector DNA and then sequentially diluted to produce a series of qPCR standards with final concentrations of 0.1 vector genome/diploid liver genome (vg/dg), 1 vg/dg, 3 vg/dg, 10 vg/dg, 30 vg/dg, 100 vg/dg, or 300 vg/dg. Total liver DNA isolated from gene therapy treated animals (three AAV2/8 LSPmPAH animals and one AAV2/8 LSPmPAHfs animal), as well as an untreated *Pah*$^{\Delta exon1/\Delta exon1}$ animal as a negative control, were subjected to qPCR, along with the standard series, using SYBR Select MM (Applied Biosystems), forward primer PAH7.125F, and reverse primer PAH10.12R, to produce fluorescently labeled PCR products. Amplification was carried out and analyzed

on a Qiagen Rotor-Gene Q real-time thermocycler. The number of AAV vg/dg from gene therapy treated mice was then estimated by comparing the C_t values from the unknowns to a linear regression curve of C_t vs. vg/dg generated from the standard series (Table 4-1). Each standard sample was amplified in duplicate to generate the standard curve, while each unknown was amplified in triplicate with the mean vg/dg reported in Table 4-1.

Liver PAH Fluorescent Immunohistochemistry

Select animals of *Pah*$^{+/+}$ and *Pah*$^{\Delta exon1/\Delta exon1}$ genotype, as well as gene therapy treated *Pah*$^{\Delta exon1/\Delta exon1}$ animals, underwent saline-paraformaldehyde perfusion in preparation for liver fixation and immunohistochemistry (Figure 4-3C and Figure 4-4). Under deep isoflurane inhaled anesthesia, mice were perfused with 0.9% saline via cardiac infusion to clear the hepatic circulation of blood. Excised biopsies from each liver lobule were then fixed for 24 hours in fixation solution (4% paraformaldehyde in phosphate buffered saline) followed by immersion in 25% buffered sucrose for an additional 24 hours. Tissues were embedded in optimal cutting temperature media, sliced into 15 µm sections, and mounted on glass slides. Sections were treated (following blocking) with rabbit polyclonal anti-PAH antibody (1:200 dilution, BS3704 PAH (R400) from Bioworld, Inc.) and incubated for 2 hours at room temperature. After appropriate washes, sections were treated with Alexa 488-conjugated goat anti-rabbit IgG secondary antibody (1:150 dilution, A11008 Alexa Fluor 488 goat anti-rabbit IgG (H+L) from Invitrogen) and incubated for one hour at room temperature. After washing, cover

slips were mounted with Vectashield mounting medium containing DAPI. Images were captured on a Nikon H550L fluorescence microscope.

PCR amplification and Sanger sequencing of potential CRISPR/Cas9 off target mutation sites

Possible sites of off-target sgRNA-Cas9 genotoxicity were selected for Sanger sequencing analysis using the *in silico* COSMID tool [230], which used the guide 4 and guide 8 target sequence to determine the top four off-target sites in the mouse reference genome (GRCm38) for each guide. Sanger sequencing was performed for each region with location, off-target sequence, COSMID score (where lower score indicates higher likelihood of sgRNA-Cas9 double strand break lesions) and Sanger sequencing chromatogram displayed in Supplemental Figure 4-1.

Acknowledgements

We gratefully acknowledge Division of Comparative Medicine for mouse colony maintenance and Transgenic Mouse Models Shared Resource of OHSU for the generation of *Pah* mutant mice. We thank the DNA core facility of Vollum Institute at OHSU for sequencing analysis. We thank Anahita Rossi for technical assistance with the neurotransmitter measurements.

DYR and the experiments were funded by the National PKU Alliance. SRW, SD, NR, BT, and COH were funded by NIH R01 NS080866.

We would like to express our sincerest gratitude to the National PKU Alliance for supporting this research.

Author Contributions

D.R. performed the experiments, analyzed data, and wrote the manuscript.

L.F. assisted with experimental design and manuscript editing.

S.W. performed surgical procedures and assisted with experimental design, mouse breeding, molecular techniques, and editing of the manuscript.

S.D. assisted with mouse breeding and molecular techniques.

N.R. and B.T. performed the brain monoamine neurotransmitter analysis, and B.T. edited the manuscript.

C.H. assisted with funding, experimental design, analyses, data interpretation, manuscript editing, and was primary mentor to D.R. during graduate school.

CHAPTER 5: Conclusion

Discussion

PKU gene therapy is a promising approach to pursue life-long alleviation of restrictive dietary therapy without consequences of neurological damage. Previous work evaluating PKU gene addition therapy demonstrated robust and long-term, yet ultimately temporary efficacy in the *Pah*$^{enu2/enu2}$ murine model of classical PKU that expresses abundant mutant PAH protein. The motivation driving the work of this dissertation was to evaluate two distinct genome editing approaches that could theoretically confer permanent, life-long efficacy of PKU gene therapy in the *Pah*$^{enu2/enu2}$ model, and thus be a stepping-stone to the development of a cure for PKU in humans.

The two genome editing approaches evaluated in this work were, first, the use of the CRISPR/Cas9 technology in a dual AAV gene editing system to assist in the correction of a single point mutation that causes PKU in the *Pah*$^{enu2/enu2}$ model (Chapter 2), and second, the combination of two technologies GeneRide™ and universal hepatocyte selection to allow for the integration of *Pah* cDNA into the end of the albumin locus and selection for properly incorporated hepatocytes, respectively (Chapter 3). Unfortunately, neither of these two genome editing approaches achieved full correction of PKU in the *Pah*$^{enu2/enu2}$ mouse model, however, the CRISPR-mediated gene editing approach proved most promising. All animals treated with all of the components for targeted nuclease activity, a repair template containing correction of the point mutation, as well as vanillin, a potent non-homologous end joining inhibitor, achieved therapeutic effects that

reduced their classification from severe, classical PKU down to mild PKU. In addition to the permanent reduction of Phe levels, these animals were physically indistinguishable from their wildtype and heterozygous counterparts, with dark coat color pigmentation throughout life. The impressive nesting and offspring rearing behaviors of the breeding pair in this study was evidence for neurological and cognitive improvements, though behavioral testing was not formally performed. Further studies are warranted to optimize this approach in order to achieve full correction of PKU. The greatest limitation to efficacy using the CRISPR-mediated gene editing is the type of cellular repair that occurs after the double-stranded break of the Cas9 nuclease, specifically, the lack of homology directed repair to incorporate the functional DNA sequence supplied by the repair template. Efforts should therefore be focused on ways to promote HDR cellular repair, including repair template/dual AAV design, Cas9 enzyme utilized, and addition of other HDR promoting proteins. However, even if full correction is achieved by manipulating these aspects of the therapy, there remains an overarching problem to the translation of this approach to human medicine, specifically application.

It is well documented that there are over one thousand known pathogenic mutations throughout the entire *PAH* locus that cause PKU in humans. In fact, most humans with PKU are compound heterozygotes with missense mutations. The only way to translate this approach would be to produce personalized gene therapy for each exon of the *Pah* gene, with emphasis on areas of greatest

mutational burden and higher priority for increased prevalence, starting with the most common mutation, R408W. Yet it is simply not feasible to create such personalized gene editing therapeutics for rare disorders due to barriers in approval and overall financial benefit. For these reasons, an approach that is broadly applicable regardless of genotype would be preferred, as is the case for the second, less successful gene editing approach evaluated in this work.

The integrating and selective PKU gene therapy incorporating the two technologies GeneRide™ and universal hepatocyte selection into a singular combinatorial therapy showed promise in genetic HT1 mice in a proof of concept preliminary study, however it was unsuccessful in PKU animals when HT1 was induced chemically. It is likely that the chemical inhibitor of FAH, CEHPOBA, was toxic to male mice, however it is perplexing that it was not in female mice. Further studies are warranted to evaluate the molecular basis of the male-specific CEHPOBA toxicity. However, even in female mice that underwent CEHPOBA therapy, no therapeutic efficacy was achieved. It is possible that the neonatal animals that received the AAV8 therapy had circulating neutralizing antibodies to the AAV8 capsid from parental gene addition therapy administered to *Pah*$^{enu2/enu2}$ breeders to promote successful progeny production. Regardless, there was evidence of transgene expression in the liver of the longest CEHPOBA treated mouse, visualized by HA-tag immunohistology. Despite initial *in vitro* studies indicating the HA tag would not interrupt PAH function, it is possible this occurred. It is also still possible that the cells staining positive for HA expression

did in fact express functional HA tagged PAH, but that it was trafficked for extracellular secretion from the cell, as is the albumin protein, instead of the required destination for PAH to function properly, the cytoplasm. The HA tag made it possible to determine that any transgene derived expression occurred, yet it may yet still have drawbacks on functionality that warrant further investigation.

Limitations remain in gene therapy studies in the *Pah*$^{enu2/enu2}$ model that make it less desirable for gene therapy research, particularly the expression of non-functional mutant monomers. The dominant negative phenomenon refers to the formation of hetero-tetramers containing a mix of mutant, non-functional PAH monomers and wildtype, functional PAH monomers that results in an overall reduction of PAH holoenzyme activity. This is supported by significantly less PAH enzyme activity in heterozygous *Pah*$^{+/enu2}$ animals from the expected 50% enzyme activity of an animal containing one functional allele and one mutant allele. Thus when gene therapy is administered in this model, the expression of the mutant monomers poses an additional barrier to therapeutic efficacy and confounds the analysis of actual PAH activity provided by the therapy. Furthermore, the normal expression of mutant monomers that are recognized with anti-PAH antibodies makes direct probing of gene therapy derived PAH an impossible task. These limitations of the *Pah*$^{enu2/enu2}$ model inspired the creation of a novel mouse model of classical PKU containing null mutations that confer absent PAH expression. This feat was achieved by knocking-out the first exon of

the *Pah* locus using CRISPR/Cas9 technology in mouse zygotes. The homozygous knockout animals, termed *Pah*$^{\Delta exon1/\Delta exon1}$, were confirmed to have absent PAH expression. A head-to-head comparison of PAH enzyme activity in heterozygous *Pah*$^{+/\Delta exon1}$ and *Pah*$^{+/enu2}$ animals demonstrated, for the first time, strong *in vivo* evidence of the dominant negative phenomenon, with *Pah*$^{+/enu2}$ animals expressing markedly less enzyme activity than the *Pah*$^{+/\Delta exon1}$ animals. Studies evaluating the application of this novel model for gene addition therapy further supported the dominant negative effects as indicated by increased therapeutic efficacy in *Pah*$^{\Delta exon1/\ \Delta exon}$ animals in comparison to similar doses in *Pah*$^{enu2/enu2}$ animals. While this novel model has a lower survival rate of affected progeny, which can be ameliorated with extra care, it shows incontrovertible benefits for the molecular analysis of novel therapeutic development. In terms of gene therapy, transgene derived PAH expression can now be evaluated using antibody-based assays, including Western blot and liver immunohistology, a feat that was previously unachievable. Finally, more precise therapeutic effects can be determined, providing a better understanding of the challenges faced in translation to human medicine.

The overall work in this dissertation using genetic manipulations in murine PKU have advanced the field of genetics by evaluating two gene editing approaches that had the potential to be curative, as well as the development of a novel classical PKU mouse model that eases PKU gene therapy application and evaluation. While neither of the gene editing approaches was fully successful at

correcting PKU, CRISPR/Cas9 showed great promise for the continued efforts to find a cure for PKU. Furthermore, the novel *Pah*$^{\Delta exon1/\Delta exon1}$ mouse model will enhance the ability to evaluate gene editing therapy approaches in the future.

Future Directions

The overarching goal of the work described in this dissertation was to advance our knowledge in the development of a lifelong, curative gene therapy for PKU that would be applicable to all humans regardless of genotype. The next steps in the progress of this work are to further optimize CRISPR/Cas9 gene editing while using an approach that is broadly applicable to human PKU. An AAV-based targeted integration of the *Pah* cDNA into the 5' region of the *Pah* locus with assistance from nuclease activity could achieve this, however the rather large *Pah* cDNA (approximately 1.5 kb) in comparison to a point mutation may be less sterically favorable for HDR and result in reduced integrations. While this could be ameliorated with some form of selective advantage for properly integrated hepatocytes, further efforts to increase the amount of HDR need to be evaluated, including transgene design, Cas9 enzyme utilized, and the addition of HDR promoting proteins. Adjustment of these parameters, including Cas9:template ratios, size of homology arms, modified Cas9 enzymes, and proteins like Rad 51 and Rad 18 warrant further investigation [256]. Now with the advent of the $Pah^{\Delta exon1/\Delta exon1}$ mouse model, these studies can be conducted with simpler, more straightforward molecular analyses.

References

1. AE G. The Croonian Lectures on Inborn Errors of Metabolism. Lancet. 1908;172(4427): 1–7; 172(4428): 73–79; 172(4429): 142–148; 172(4430): 214–230.

2. Garrod AE. About Alkaptonuria. Med Chir Trans. 1902;85:69-78.

3. Knox WE. Sir Archibald Garrod's Inborn Errors of Metabolism. III. Albinism. Am J Hum Genet. 1958;10(3):249-67.

4. Aliu E, Kanungo S, Arnold GL. Amino acid disorders. Ann Transl Med. 2018;6(24):471.

5. Følling IA. Über ausscheidung von phenylbrenztraubensäure in den harn als stoffwechselanomalie in verbindung mit imbezillität. Hoppe-Seylers Z Physiol Chem. 1934;227:169–76.

6. Therrell BL, Padilla CD, Loeber JG, Kneisser I, Saadallah A, Borrajo GJ, Adams J. Current status of newborn screening worldwide: 2015. Semin Perinatol. 2015;39(3):171-87.

7. Følling A, Cass, V., Levy, H. Discovery of Phenylketonuria (PKU) by Dr. Asbjørn Følling. New England Consortium of Metabolic Programs. 1965.

8. Williams RA, Mamotte CD, Burnett JR. Phenylketonuria: an inborn error of phenylalanine metabolism. Clin Biochem Rev. 2008;29(1):31-41.

9. Folling A, Sydnes S. A method for the estimation of phenylpyruvic acid in urine with some examples of its use in dietary treatment of phenylpyruvic oligophrenia. Scand J Clin Lab Invest. 1958;10(4):355-8.

10. Folling A. [Phenylketonuria]. Tidsskr Nor Laegeforen. 1967;87(5):Suppl:451-4.

11. Centerwall SA, Centerwall WR. The discovery of phenylketonuria: the story of a young couple, two retarded children, and a scientist. Pediatrics. 2000;105(1 Pt 1):89-103.

12. Christ SE. Asbjorn Folling and the discovery of phenylketonuria. J Hist Neurosci. 2003;12(1):44-54.

13. Wisniewski HM, Jenkins EC. In memoriam George A. Jervis, M.D., (August 15, 1903-June 5, 1986). J Neuropathol Exp Neurol. 1989;48(1):109-10.

14. Jervis GA. Studies on phenylpyruvic oligophrenia; the position of the metabolic error. J Biol Chem. 1947;169(3):651-6.

15. Jervis GA. Studies on phenylpyruvic oligophrenia; phenylpyruvic acid content on blood. Proc Soc Exp Biol Med. 1952;81(3):715-20.

16. Jervis GA. Phenylpyruvic oligophrenia (phenylketonuria). Res Publ Assoc Res Nerv Ment Dis. 1954;33:259-82.

17. Jervis GA. Excretion of phenylalanine and derivatives in phenylpyruvic oligophrenia. Proc Soc Exp Biol Med. 1950;75(1):83-6.

18. Jervis GA, Drejza EJ. Phenylketonuria: blood levels of phenylpyruvic and ortho-hydroxyphenylacetic acids. Clin Chim Acta. 1966;13(4):435-41.

19. Jervis GA. Detection of heterozygotes for phenylketonuria. Clin Chim Acta. 1960;5:471-6.

20. Penrose L, Quastel JH. Metabolic studies in phenylketonuria. Biochem J. 1937;31(2):266-74.

21. Woolf LI. Excretion of conjugated phenylacetic acid in phenylketonuria. Biochem J. 1951;49(1):ix-x.

22. Woolf LI, Vulliamy DG. Phenylketonuria with a study of the effect upon it of glutamic acid. Arch Dis Child. 1951;26(130):487-94.

23. Bickel H, Gerrard J, Hickmans EM. Influence of phenylalanine intake on phenylketonuria. Lancet. 1953;265(6790):812-3.

24. Bickel H. The effects of a phenylalanine-free and phenylalanine-poor diet in phenylpyruvic oligophrenis. Exp Med Surg. 1954;12(1):114-7.

25. Bickel H. [Diagnosis and therapy of galactosemia and phenylketonuria]. Monatsschr Kinderheilkd. 1955;103(2):81-4.

26. Centerwall WR. Phenylketonuria. J Am Med Assoc. 1957;165(4):392.

27. Konkel L. The Brain before Birth: Using fMRI to Explore the Secrets of Fetal Neurodevelopment. Environ Health Perspect. 2018;126(11):112001.

28. Winn SR, Scherer T, Thony B, Ying M, Martinez A, Weber S, Raber J, Harding CO. Blood phenylalanine reduction corrects CNS dopamine and serotonin deficiencies and partially improves behavioral performance in adult phenylketonuric mice. Mol Genet Metab. 2018;123(1):6-20.

29. Anderson PJ, Leuzzi V. White matter pathology in phenylketonuria. Mol Genet Metab. 2010;99 Suppl 1:S3-9.

30. Dyer CA, Kendler A, Philibotte T, Gardiner P, Cruz J, Levy HL. Evidence for central nervous system glial cell plasticity in phenylketonuria. J Neuropathol Exp Neurol. 1996;55(7):795-814.

31. Koch J. Robert Guthrie— the PKU Story: A Crusade Against Mental Retardation: Hope Publishing House; 1997 1997.

32. Seidenberg M, Martinez RJ, Guthrie R, Minnemeyer H, Tieckelmann H. Phenylalanine metabolism: the production of phenylacetaldehyde by a Proteus species. Arch Biochem Biophys. 1962;97:470-3.

33. Guthrie R, Susi A. A Simple Phenylalanine Method for Detecting Phenylketonuria in Large Populations of Newborn Infants. Pediatrics. 1963;32:338-43.

34. Muldoon K. 50 years of newborn screening pays off with healthier Oregon kids. The Oregonian. 2013.

35. Chace DH, DiPerna JC, Naylor EW. Laboratory integration and utilization of tandem mass spectrometry in neonatal screening: a model for clinical mass spectrometry in the next millennium. Acta Paediatr Suppl. 1999;88(432):45-7.

36. Landau YE, Lichter-Konecki U, Levy HL. Genomics in newborn screening. J Pediatr. 2014;164(1):14-9.

37. Yang L, Chen J, Shen B. Newborn Screening in the Era of Precision Medicine. Adv Exp Med Biol. 2017;1005:47-61.

38. Hanley WB, Clarke JT, Schoonheyt W. Maternal phenylketonuria (PKU)--a review. Clin Biochem. 1987;20(3):149-56.

39. Jervis GA. Phenylpyruvic oligophrenia. Introductory study of fifty cases of mental deficiency associated with excretion of phenylpyruvic acid. *Arch Neurol Psychiatry*. 1937;38:944-63.

40. Dent C. Discussion of Armstrong MD: Relation of biochemical abnormality to development of mental defect in phenylketonuria. In: *Etiologic Factors in Mental Retardation: Report of Twenty-Third Ross Pediatric Research Conference November 8-9, 1956*. Ross Laboratories. 1957;1957:32-3.

41. Richards B. Maternal phenylketonuria. Lancet. 1964;1964(1):829.

42. Levy HL, Ghavami M. Maternal phenylketonuria: a metabolic teratogen. Teratology. 1996;53(3):176-84.

43. Buist NR, Lis EW, Tuerck JM, Murphey WH. Maternal phenylketonuria. Lancet. 1979;2(8142):589.

44. Koch R, Hanley W, Levy H, Matalon K, Matalon R, Rouse B, Trefz F, Guttler F, Azen C, Platt L, Waisbren S, Widaman K, Ning J, Friedman EG, de la Cruz F. The Maternal Phenylketonuria International Study: 1984-2002. Pediatrics. 2003;112(6 Pt 2):1523-9.

45. Maillot F, Lilburn M, Baudin J, Morley DW, Lee PJ. Factors influencing outcomes in the offspring of mothers with phenylketonuria during pregnancy: the importance of variation in maternal blood phenylalanine. Am J Clin Nutr. 2008;88(3):700-5.

46. Blau N. Genetics of Phenylketonuria: Then and Now. Hum Mutat. 2016;37(6):508-15.

47. Flydal MI, Martinez A. Phenylalanine hydroxylase: function, structure, and regulation. IUBMB Life. 2013;65(4):341-9.

48. Uhlen M, Fagerberg L, Hallstrom BM, Lindskog C, Oksvold P, Mardinoglu A, Sivertsson A, Kampf C, Sjostedt E, Asplund A, Olsson I, Edlund K, Lundberg E, Navani S, Szigyarto CA, Odeberg J, Djureinovic D, Takanen JO, Hober S, Alm T, Edqvist PH, Berling H, Tegel H, Mulder J, Rockberg J, Nilsson P, Schwenk JM, Hamsten M, von Feilitzen K, Forsberg M, Persson L, Johansson F, Zwahlen M, von Heijne G, Nielsen J, Ponten F. Proteomics. Tissue-based map of the human proteome. Science. 2015;347(6220):1260419.

49. Lichter-Konecki U, Hipke CM, Konecki DS. Human phenylalanine hydroxylase gene expression in kidney and other nonhepatic tissues. Mol Genet Metab. 1999;67(4):308-16.

50. Jung-Kc K, Himmelreich N, Prestegard KS, Shi TS, Scherer T, Ying M, Jorge-Finnigan A, Thony B, Blau N, Martinez A. Phenylalanine hydroxylase variants interact with the co-chaperone DNAJC12. Hum Mutat. 2019;40(4):483-94.

51. Anikster Y, Haack TB, Vilboux T, Pode-Shakked B, Thony B, Shen N, Guarani V, Meissner T, Mayatepek E, Trefz FK, Marek-Yagel D, Martinez A, Huttlin EL, Paulo JA, Berutti R, Benoist JF, Imbard A, Dorboz I, Heimer G, Landau Y, Ziv-Strasser L, Malicdan MCV, Gemperle-Britschgi C, Cremer K, Engels H, Meili D, Keller I, Bruggmann R, Strom TM, Meitinger T, Mullikin JC, Schwartz G, Ben-Zeev B, Gahl WA, Harper JW, Blau N, Hoffmann GF, Prokisch H, Opladen T, Schiff M. Biallelic Mutations in DNAJC12 Cause Hyperphenylalaninemia, Dystonia, and Intellectual Disability. Am J Hum Genet. 2017;100(2):257-66.

52. Uno Y, Kanda M, Miwa T, Umeda S, Tanaka H, Tanaka C, Kobayashi D, Suenaga M, Hattori N, Hayashi M, Yamada S, Nakayama G, Fujiwara M, Kodera Y. Increased Expression of DNAJC12 is Associated with Aggressive Phenotype of Gastric Cancer. Ann Surg Oncol. 2019;26(3):836-44.

53. He HL, Lee YE, Chen HP, Hsing CH, Chang IW, Shiue YL, Lee SW, Hsu CT, Lin LC, Wu TF, Li CF. Overexpression of DNAJC12 predicts poor response

to neoadjuvant concurrent chemoradiotherapy in patients with rectal cancer. Exp Mol Pathol. 2015;98(3):338-45.

54. Blau N, Martinez A, Hoffmann GF, Thony B. DNAJC12 deficiency: A new strategy in the diagnosis of hyperphenylalaninemias. Mol Genet Metab. 2018;123(1):1-5.

55. Miranda FF, Thorolfsson M, Teigen K, Sanchez-Ruiz JM, Martinez A. Structural and stability effects of phosphorylation: Localized structural changes in phenylalanine hydroxylase. Protein Sci. 2004;13(5):1219-26.

56. Patel MS, Arinze IJ. Phenylketonuria: metabolic alterations induced by phenylalanine and phenylpyruvate. Am J Clin Nutr. 1975;28(2):183-8.

57. Boscott RJ, Bickel H. Detection of some new abnormal metabolites in the urine of phenylketonuria. Scand J Clin Lab Invest. 1953;5(4):380-2.

58. Boscott RJ, Bickel H. Phenylalanine and tyrosine metabolism in patients with phenylketonuria. Biochem J. 1953;56(322nd Meeting):i.

59. Armstrong MD, Robinson KS. On the excretion of indole derivatives in phenylketonuria. Arch Biochem Biophys. 1954;52(1):287-8.

60. Bessman SP, Tada K. Indicanuria in phenylketonuria. Metabolism. 1960;9:377-85.

61. Fitzpatrick TB, Miyamoto M. Competitive inhibition of mammalian tyrosinase by phenylalanine and its relationship to hair pigmentation in phenylketonuria. Nature. 1957;179(4552):199-200.

62. Ding XQ, Fiehler J, Kohlschutter B, Wittkugel O, Grzyska U, Zeumer H, Ullrich K. MRI abnormalities in normal-appearing brain tissue of treated adult PKU patients. J Magn Reson Imaging. 2008;27(5):998-1004.

63. White DA, Connor LT, Nardos B, Shimony JS, Archer R, Snyder AZ, Moinuddin A, Grange DK, Steiner RD, McKinstry RC. Age-related decline in the microstructural integrity of white matter in children with early- and continuously-treated PKU: a DTI study of the corpus callosum. Mol Genet Metab. 2010;99 Suppl 1:S41-6.

64. Fisch RO, Torres F, Gravem HJ, Greenwood CS, Anderson JA. Twelve years of clinical experience with phenylketonuria. A statistical evaluation of symptoms, growth, mental development, electroencephalographic records, serum phenylalanine levels, and results of dietary management. Neurology. 1969;19(7):659-66.

65. Koff E, Kammerer B, Boyle P, Pueschel SM. Intelligence and phenylketonuria: effects of diet termination. J Pediatr. 1979;94(4):534-7.

66. Murphy D. Termination of dietary treatment of phenylketonuria. Ir J Med Sci. 1969;8(4):177-83.

67. Clayton BE, Moncrieff AA, Pampiglione G, Shepherd J. Biochemical and EEG studies in phenylketonuric children during phenylalanine tolerance testc. Arch Dis Child. 1966;41(217):267-72.

68. Statement NIoHPCDC. Phenylketonuria: Screening and Management. National Institutes of Health PKU Consensus Statement. 2000.

69. van Calcar SC, Ney DM. Food products made with glycomacropeptide, a low-phenylalanine whey protein, provide a new alternative to amino Acid-based medical foods for nutrition management of phenylketonuria. J Acad Nutr Diet. 2012;112(8):1201-10.

70. Berry SA, Brown C, Grant M, Greene CL, Jurecki E, Koch J, Moseley K, Suter R, van Calcar SC, Wiles J, Cederbaum S. Newborn screening 50 years later: access issues faced by adults with PKU. Genet Med. 2013;15(8):591-9.

71. Bartholome K. Letter: A new molecular defect in phenylketonuria. Lancet. 1974;2(7896):1580.

72. Kaufman S, Milstien S, Bartholome K. Letter: New forms of phenylketonuria. Lancet. 1975;2(7937):708.

73. Bartholome K, Byrd DJ, Kaufman S, Milstien S. Atypical phenylketonuria with normal phenylalanine hydroxylase and dihydropteridine reductase activity in vitro. Pediatrics. 1977;59(5):757-61.

74. Bartholome K, Byrd DJ. Letter: L-dopa and 5-hydroxytryptophan therapy in phenylketonuria with normal phenylalanine-hydroxylase activity. Lancet. 1975;2(7943):1042-3.

75. Schaub J, Daumling S, Curtius HC, Niederwieser A, Bartholome K, Viscontini M, Schircks B, Bieri JH. Tetrahydrobiopterin therapy of atypical phenylketonuria due to defective dihydrobiopterin biosynthesis. Arch Dis Child. 1978;53(8):674-6.

76. Danks DM, Cotton RG, Schlesinger P. Letter: Tetrahydrobiopterin treatment of variant form of phenylketonuria. Lancet. 1975;2(7943):1043.

77. Burton BK, Grange DK, Milanowski A, Vockley G, Feillet F, Crombez EA, Abadie V, Harding CO, Cederbaum S, Dobbelaere D, Smith A, Dorenbaum A. The response of patients with phenylketonuria and elevated serum phenylalanine to treatment with oral sapropterin dihydrochloride (6R-tetrahydrobiopterin): a phase II, multicentre, open-label, screening study. J Inherit Metab Dis. 2007;30(5):700-7.

78. Levy HL, Milanowski A, Chakrapani A, Cleary M, Lee P, Trefz FK, Whitley CB, Feillet F, Feigenbaum AS, Bebchuk JD, Christ-Schmidt H, Dorenbaum A, Sapropterin Research G. Efficacy of sapropterin dihydrochloride (tetrahydrobiopterin, 6R-BH4) for reduction of phenylalanine concentration in patients with phenylketonuria: a phase III randomised placebo-controlled study. Lancet. 2007;370(9586):504-10.

79. Burnett JR. Sapropterin dihydrochloride (Kuvan/phenoptin), an orally active synthetic form of BH4 for the treatment of phenylketonuria. IDrugs. 2007;10(11):805-13.

80. Longo N, Dimmock D, Levy H, Viau K, Bausell H, Bilder DA, Burton B, Gross C, Northrup H, Rohr F, Sacharow S, Sanchez-Valle A, Stuy M, Thomas J, Vockley J, Zori R, Harding CO. Evidence- and consensus-based recommendations for the use of pegvaliase in adults with phenylketonuria. Genet Med. 2018.

81. Brown CS. Family reflections on phenylketonuria. Pediatr Res. 2018;84(6):797-8.

82. Bilder DA, Noel JK, Baker ER, Irish W, Chen Y, Merilainen MJ, Prasad S, Winslow BJ. Systematic Review and Meta-Analysis of Neuropsychiatric Symptoms and Executive Functioning in Adults With Phenylketonuria. Dev Neuropsychol. 2016;41(4):245-60.

83. Christ SE, Moffitt AJ, Peck D, White DA, Hilgard J. Decreased functional brain connectivity in individuals with early-treated phenylketonuria: evidence from resting state fMRI. J Inherit Metab Dis. 2012;35(5):807-16.

84. Brown CS, Lichter-Konecki U. Phenylketonuria (PKU): A problem solved? Mol Genet Metab Rep. 2016;6:8-12.

85. Woo SL, Lidsky AS, Guttler F, Chandra T, Robson KJ. Cloned human phenylalanine hydroxylase gene allows prenatal diagnosis and carrier detection of classical phenylketonuria. Nature. 1983;306(5939):151-5.

86. Konecki DS, Wang Y, Trefz FK, Lichter-Konecki U, Woo SL. Structural characterization of the 5' regions of the human phenylalanine hydroxylase gene. Biochemistry. 1992;31(35):8363-8.

87. Scriver CR, Waters PJ, Sarkissian C, Ryan S, Prevost L, Cote D, Novak J, Teebi S, Nowacki PM. PAHdb: a locus-specific knowledgebase. Hum Mutat. 2000;15(1):99-104.

88. Scriver CR, Hurtubise M, Konecki D, Phommarinh M, Prevost L, Erlandsen H, Stevens R, Waters PJ, Ryan S, McDonald D, Sarkissian C. PAHdb 2003: what a locus-specific knowledgebase can do. Hum Mutat. 2003;21(4):333-44.

89. Blau N, Shen N, Carducci C. Molecular genetics and diagnosis of phenylketonuria: state of the art. Expert Rev Mol Diagn. 2014;14(6):655-71.

90. Hillert A, Anikster Y, Belanger-Quintana A, Burlina A, Burton BK, Carducci C, Chiesa AE, Christodoulou J, Dordevic M, Desviat LR, Eliyahu A, Evers RAF, Fajkusova L, Feillet F, Bonfim-Freitas PE, Gizewska M, Gundorova P, Karall D, Kneller K, Kutsev SI, Leuzzi V, Levy HL, Lichter-Konecki U, Muntau AC, Namour F, Oltarzewski M, Paras A, Perez B, Polak E, Polyakov AV, Porta F, Rohrbach M, Scholl-Burgi S, Specola N, Stojiljkovic M, Shen N, Santana-da Silva LC,

Skouma A, van Spronsen F, Stoppioni V, Thony B, Trefz FK, Vockley J, Yu Y, Zschocke J, Hoffmann GF, Garbade SF, Blau N. The Genetic Landscape and Epidemiology of Phenylketonuria. Am J Hum Genet. 2020;107(2):234-50.

91. Shedlovsky A, McDonald JD, Symula D, Dove WF. Mouse models of human phenylketonuria. Genetics. 1993;134(4):1205-10.

92. Haefele MJ, White G, McDonald JD. Characterization of the mouse phenylalanine hydroxylase mutation Pah(enu3). Mol Genet Metab. 2001;72(1):27-30.

93. Sarkissian CN, Boulais DM, McDonald JD, Scriver CR. A heteroallelic mutant mouse model: A new orthologue for human hyperphenylalaninemia. Molecular genetics and metabolism. 2000;69(3):188-94.

94. Zurfluh MR, Zschocke J, Lindner M, Feillet F, Chery C, Burlina A, Stevens RC, Thony B, Blau N. Molecular genetics of tetrahydrobiopterin-responsive phenylalanine hydroxylase deficiency. Hum Mutat. 2008;29(1):167-75.

95. Lagler FB, Gersting SW, Zsifkovits C, Steinbacher A, Eichinger A, Danecka MK, Staudigl M, Fingerhut R, Glossmann H, Muntau AC. New insights into tetrahydrobiopterin pharmacodynamics from Pah enu1/2, a mouse model for compound heterozygous tetrahydrobiopterin-responsive phenylalanine hydroxylase deficiency. Biochem Pharmacol. 2010;80(10):1563-71.

96. Poncet IB, Berry HK, Butcher RE, Kazmaier KJ. Biochemical effects of induced phenylketonuria in rats. Biol Neonate. 1975;26(1-2):88-101.

97. McKean CM, Lieberman R, Webb RB. Experimental phenylketonuria in infant pigs. Dev Med Child Neurol. 1967;9(5):541-3.

98. Allen K, Nicolas, C., Carlson, D., Du, Z., Kaiser, R., Hickey, R., Harding, C., Lillegard, J. Development and Characterization of a Humanized Porcine Model of Phenylketonuria. American Society of Gene & Cell Therapy (ASGCT) 21st Annual Meeting. 2018.

99. Nicholls R, Phil, D. A PKU Swine Model. 5th National PKU Alliance Conference: Advancing the Dream for PKU. 2018.

100. Koppes EA, Redel BK, Johnson MA, Skvorak KJ, Ghaloul-Gonzalez L, Yates ME, Lewis DW, Gollin SM, Wu YL, Christ SE, Yerle M, Leshinski A, Spate LD, Benne JA, Murphy SL, Samuel MS, Walters EM, Hansen SA, Wells KD, Lichter-Konecki U, Wagner RA, Newsome JT, Dobrowolski SF, Vockley J, Prather RS, Nicholls RD. A porcine model of phenylketonuria generated by CRISPR/Cas9 genome editing. JCI Insight. 2020;5(20).

101. Rhesus Macaque Genome S, Analysis C, Gibbs RA, Rogers J, Katze MG, Bumgarner R, Weinstock GM, Mardis ER, Remington KA, Strausberg RL, Venter JC, Wilson RK, Batzer MA, Bustamante CD, Eichler EE, Hahn MW, Hardison RC, Makova KD, Miller W, Milosavljevic A, Palermo RE, Siepel A, Sikela JM, Attaway T, Bell S, Bernard KE, Buhay CJ, Chandrabose MN, Dao M, Davis C, Delehaunty KD, Ding Y, Dinh HH, Dugan-Rocha S, Fulton LA, Gabisi RA, Garner TT, Godfrey J, Hawes AC, Hernandez J, Hines S, Holder M, Hume J, Jhangiani SN, Joshi V, Khan ZM, Kirkness EF, Cree A, Fowler RG, Lee S, Lewis LR, Li Z,

Liu YS, Moore SM, Muzny D, Nazareth LV, Ngo DN, Okwuonu GO, Pai G, Parker D, Paul HA, Pfannkoch C, Pohl CS, Rogers YH, Ruiz SJ, Sabo A, Santibanez J, Schneider BW, Smith SM, Sodergren E, Svatek AF, Utterback TR, Vattathil S, Warren W, White CS, Chinwalla AT, Feng Y, Halpern AL, Hillier LW, Huang X, Minx P, Nelson JO, Pepin KH, Qin X, Sutton GG, Venter E, Walenz BP, Wallis JW, Worley KC, Yang SP, Jones SM, Marra MA, Rocchi M, Schein JE, Baertsch R, Clarke L, Csuros M, Glasscock J, Harris RA, Havlak P, Jackson AR, Jiang H, Liu Y, Messina DN, Shen Y, Song HX, Wylie T, Zhang L, Birney E, Han K, Konkel MK, Lee J, Smit AF, Ullmer B, Wang H, Xing J, Burhans R, Cheng Z, Karro JE, Ma J, Raney B, She X, Cox MJ, Demuth JP, Dumas LJ, Han SG, Hopkins J, Karimpour-Fard A, Kim YH, Pollack JR, Vinar T, Addo-Quaye C, Degenhardt J, Denby A, Hubisz MJ, Indap A, Kosiol C, Lahn BT, Lawson HA, Marklein A, Nielsen R, Vallender EJ, Clark AG, Ferguson B, Hernandez RD, Hirani K, Kehrer-Sawatzki H, Kolb J, Patil S, Pu LL, Ren Y, Smith DG, Wheeler DA, Schenck I, Ball EV, Chen R, Cooper DN, Giardine B, Hsu F, Kent WJ, Lesk A, Nelson DL, O'Brien W E, Prufer K, Stenson PD, Wallace JC, Ke H, Liu XM, Wang P, Xiang AP, Yang F, Barber GP, Haussler D, Karolchik D, Kern AD, Kuhn RM, Smith KE, Zwieg AS. Evolutionary and biomedical insights from the rhesus macaque genome. Science. 2007;316(5822):222-34.

102. Strange BA, Witter MP, Lein ES, Moser EI. Functional organization of the hippocampal longitudinal axis. Nat Rev Neurosci. 2014;15(10):655-69.

103. Winn SR, Scherer T, Thony B, Harding CO. High dose sapropterin dihydrochloride therapy improves monoamine neurotransmitter turnover in murine phenylketonuria (PKU). Mol Genet Metab. 2016;117(1):5-11.

104. Griffith F. The Significance of Pneumococcal Types. J Hyg (Lond). 1928;27(2):113-59.

105. Avery OT, Macleod CM, McCarty M. Studies on the Chemical Nature of the Substance Inducing Transformation of Pneumococcal Types : Induction of Transformation by a Desoxyribonucleic Acid Fraction Isolated from Pneumococcus Type Iii. J Exp Med. 1944;79(2):137-58.

106. Zinder ND, Lederberg J. Genetic exchange in Salmonella. J Bacteriol. 1952;64(5):679-99.

107. Szybalska EH, Szybalski W. Genetics of human cess line. IV. DNA-mediated heritable transformation of a biochemical trait. Proc Natl Acad Sci U S A. 1962;48:2026-34.

108. Szybalski W, Szybalska EH. Drug sensitivity as a genetic marker for human cell lines. Med Bull (Ann Arbor). 1962;28:277-93.

109. Szybalski W. The 50th anniversary of gene therapy: beginnings and present realities. Gene. 2013;525(2):151-4.

110. Rogers S, Pfuderer P. Use of viruses as carriers of added genetic information. Nature. 1968;219(5155):749-51.

111. Rosenberg SA, Packard BS, Aebersold PM, Solomon D, Topalian SL, Toy ST, Simon P, Lotze MT, Yang JC, Seipp CA, et al. Use of tumor-infiltrating lymphocytes and interleukin-2 in the immunotherapy of patients with metastatic melanoma. A preliminary report. N Engl J Med. 1988;319(25):1676-80.

112. Rosenberg SA. Gene therapy for cancer. JAMA. 1992;268(17):2416-9.

113. Rosenberg SA, Anderson WF, Blaese M, Hwu P, Yannelli JR, Yang JC, Topalian SL, Schwartzentruber DJ, Weber JS, Ettinghausen SE, et al. The development of gene therapy for the treatment of cancer. Ann Surg. 1993;218(4):455-63; discussion 63-4.

114. Administration USFaD. Long Term Follow-Up After Administration of Human Gene Therapy Products: Guidance for Indsustry. 2018.

115. High KA, Roncarolo MG. Gene Therapy. N Engl J Med. 2019;381(5):455-64.

116. Anguela XM, High KA. Entering the Modern Era of Gene Therapy. Annu Rev Med. 2019;70:273-88.

117. Wirth T, Parker N, Yla-Herttuala S. History of gene therapy. Gene. 2013;525(2):162-9.

118. Blaese RM, Culver KW, Chang L, Anderson WF, Mullen C, Nienhuis A, Carter C, Dunbar C, Leitman S, Berger M, et al. Treatment of severe combined immunodeficiency disease (SCID) due to adenosine deaminase deficiency with

CD34+ selected autologous peripheral blood cells transduced with a human ADA gene. Amendment to clinical research project, Project 90-C-195, January 10, 1992. Hum Gene Ther. 1993;4(4):521-7.

119. Blaese RM, Culver KW, Miller AD, Carter CS, Fleisher T, Clerici M, Shearer G, Chang L, Chiang Y, Tolstoshev P, Greenblatt JJ, Rosenberg SA, Klein H, Berger M, Mullen CA, Ramsey WJ, Muul L, Morgan RA, Anderson WF. T lymphocyte-directed gene therapy for ADA- SCID: initial trial results after 4 years. Science. 1995;270(5235):475-80.

120. Candotti F, Shaw KL, Muul L, Carbonaro D, Sokolic R, Choi C, Schurman SH, Garabedian E, Kesserwan C, Jagadeesh GJ, Fu PY, Gschweng E, Cooper A, Tisdale JF, Weinberg KI, Crooks GM, Kapoor N, Shah A, Abdel-Azim H, Yu XJ, Smogorzewska M, Wayne AS, Rosenblatt HM, Davis CM, Hanson C, Rishi RG, Wang X, Gjertson D, Yang OO, Balamurugan A, Bauer G, Ireland JA, Engel BC, Podsakoff GM, Hershfield MS, Blaese RM, Parkman R, Kohn DB. Gene therapy for adenosine deaminase-deficient severe combined immune deficiency: clinical comparison of retroviral vectors and treatment plans. Blood. 2012;120(18):3635-46.

121. Wilson JM. Lessons learned from the gene therapy trial for ornithine transcarbamylase deficiency. Mol Genet Metab. 2009;96(4):151-7.

122. Atchison RW, Casto BC, Hammon WM. Adenovirus-Associated Defective Virus Particles. Science. 1965;149(3685):754-6.

123. Donsante A, Miller DG, Li Y, Vogler C, Brunt EM, Russell DW, Sands MS. AAV vector integration sites in mouse hepatocellular carcinoma. Science. 2007;317(5837):477.

124. Russell DW, Grompe M. Adeno-associated virus finds its disease. Nat Genet. 2015;47(10):1104-5.

125. Nault JC, Datta S, Imbeaud S, Franconi A, Mallet M, Couchy G, Letouze E, Pilati C, Verret B, Blanc JF, Balabaud C, Calderaro J, Laurent A, Letexier M, Bioulac-Sage P, Calvo F, Zucman-Rossi J. Recurrent AAV2-related insertional mutagenesis in human hepatocellular carcinomas. Nat Genet. 2015;47(10):1187-93.

126. Nault JC, Mami I, La Bella T, Datta S, Imbeaud S, Franconi A, Mallet M, Couchy G, Letouze E, Pilati C, Verret B, Blanc JF, Balabaud C, Calderaro J, Laurent A, Letexier M, Bioulac-Sage P, Calvo F, Zucman-Rossi J. Wild-type AAV Insertions in Hepatocellular Carcinoma Do Not Inform Debate Over Genotoxicity Risk of Vectorized AAV. Mol Ther. 2016;24(4):660-1.

127. Boutin S, Monteilhet V, Veron P, Leborgne C, Benveniste O, Montus MF, Masurier C. Prevalence of serum IgG and neutralizing factors against adeno-associated virus (AAV) types 1, 2, 5, 6, 8, and 9 in the healthy population: implications for gene therapy using AAV vectors. Hum Gene Ther. 2010;21(6):704-12.

128. Louis Jeune V, Joergensen JA, Hajjar RJ, Weber T. Pre-existing anti-adeno-associated virus antibodies as a challenge in AAV gene therapy. Hum Gene Ther Methods. 2013;24(2):59-67.

129. Rabinowitz J, Chan YK, Samulski RJ. Adeno-associated Virus (AAV) versus Immune Response. Viruses. 2019;11(2).

130. Therapeutics A. Letter to the MTM Disease Community. 2020.

131. Samulski RJ, Muzyczka N. AAV-Mediated Gene Therapy for Research and Therapeutic Purposes. Annu Rev Virol. 2014;1(1):427-51.

132. Srivastava A, Lusby EW, Berns KI. Nucleotide sequence and organization of the adeno-associated virus 2 genome. J Virol. 1983;45(2):555-64.

133. Grimm D, Buning H. Small But Increasingly Mighty: Latest Advances in AAV Vector Research, Design, and Evolution. Hum Gene Ther. 2017;28(11):1075-86.

134. Earley LF, Powers JM, Adachi K, Baumgart JT, Meyer NL, Xie Q, Chapman MS, Nakai H. Adeno-associated Virus (AAV) Assembly-Activating Protein Is Not an Essential Requirement for Capsid Assembly of AAV Serotypes 4, 5, and 11. J Virol. 2017;91(3).

135. Deyle DR, Russell DW. Adeno-associated virus vector integration. Curr Opin Mol Ther. 2009;11(4):442-7.

136. Carpentier AC, Frisch F, Labbe SM, Gagnon R, de Wal J, Greentree S, Petry H, Twisk J, Brisson D, Gaudet D. Effect of alipogene tiparvovec (AAV1-LPL(S447X)) on postprandial chylomicron metabolism in lipoprotein lipase-deficient patients. J Clin Endocrinol Metab. 2012;97(5):1635-44.

137. Russell S, Bennett J, Wellman JA, Chung DC, Yu ZF, Tillman A, Wittes J, Pappas J, Elci O, McCague S, Cross D, Marshall KA, Walshire J, Kehoe TL, Reichert H, Davis M, Raffini L, George LA, Hudson FP, Dingfield L, Zhu X, Haller JA, Sohn EH, Mahajan VB, Pfeifer W, Weckmann M, Johnson C, Gewaily D, Drack A, Stone E, Wachtel K, Simonelli F, Leroy BP, Wright JF, High KA, Maguire AM. Efficacy and safety of voretigene neparvovec (AAV2-hRPE65v2) in patients with RPE65-mediated inherited retinal dystrophy: a randomised, controlled, open-label, phase 3 trial. Lancet. 2017;390(10097):849-60.

138. Al-Zaidy SA, Kolb SJ, Lowes L, Alfano LN, Shell R, Church KR, Nagendran S, Sproule DM, Feltner DE, Wells C, Ogrinc F, Menier M, L'Italien J, Arnold WD, Kissel JT, Kaspar BK, Mendell JR. AVXS-101 (Onasemnogene Abeparvovec) for SMA1: Comparative Study with a Prospective Natural History Cohort. J Neuromuscul Dis. 2019;6(3):307-17.

139. Nathwani AC, Davidoff AM, Tuddenham EGD. Gene Therapy for Hemophilia. Hematol Oncol Clin North Am. 2017;31(5):853-68.

140. Harding CO, Gillingham MB, Hamman K, Clark H, Goebel-Daghighi E, Bird A, Koeberl DD. Complete correction of hyperphenylalaninemia following

liver-directed, recombinant AAV2/8 vector-mediated gene therapy in murine phenylketonuria. Gene Ther. 2006;13(5):457-62.

141. Homology Medicines I. Homology Medicines Announces Presentation of Positive Data from the Dose-Escalation Phase of the pheNIX Gene Therapy Trial for Adults with PKU2020. Available from: https://www.globenewswire.com/news-release/2020/11/06/2122133/0/en/Homology-Medicines-Announces-Presentation-of-Positive-Data-from-the-Dose-Escalation-Phase-of-the-pheNIX-Gene-Therapy-Trial-for-Adults-with-PKU.html.

142. BioMarin. BioMarin, Pioneer in Phenylketonuria (PKU) and Gene Therapy, Doses First Participant in Global PHEARLESS Phase 1/2 Study of BMN 307 Gene Therapy2020. Available from: https://investors.biomarin.com/2020-09-24-BioMarin-Pioneer-in-Phenylketonuria-PKU-and-Gene-Therapy-Doses-First-Participant-in-Global-PHEARLESS-Phase-1-2-Study-of-BMN-307-Gene-Therapy.

143. Corless JK, Middleton HM, 3rd. Normal liver function. A basis for understanding hepatic disease. Arch Intern Med. 1983;143(12):2291-4.

144. Angler N. The Liver: A 'Blob' That Runs the Body. The New York Times. 2017.

145. Baruteau J, Waddington SN, Alexander IE, Gissen P. Gene therapy for monogenic liver diseases: clinical successes, current challenges and future prospects. J Inherit Metab Dis. 2017;40(4):497-517.

146. Rebuffat A, Harding CO, Ding Z, Thony B. Comparison of adeno-associated virus pseudotype 1, 2, and 8 vectors administered by intramuscular injection in the treatment of murine phenylketonuria. Hum Gene Ther. 2010;21(4):463-77.

147. Ding Z, Harding CO, Rebuffat A, Elzaouk L, Wolff JA, Thony B. Correction of murine PKU following AAV-mediated intramuscular expression of a complete phenylalanine hydroxylating system. Mol Ther. 2008;16(4):673-81.

148. Hamman K, Clark H, Montini E, Al-Dhalimy M, Grompe M, Finegold M, Harding CO. Low therapeutic threshold for hepatocyte replacement in murine phenylketonuria. Mol Ther. 2005;12(2):337-44.

149. Barzel A, Paulk NK, Shi Y, Huang Y, Chu K, Zhang F, Valdmanis PN, Spector LP, Porteus MH, Gaensler KM, Kay MA. Promoterless gene targeting without nucleases ameliorates haemophilia B in mice. Nature. 2015;517(7534):360-4.

150. Nygaard S, Barzel A, Haft A, Major A, Finegold M, Kay MA, Grompe M. A universal system to select gene-modified hepatocytes in vivo. Sci Transl Med. 2016;8(342):342ra79.

151. Watson JD, Crick FH. Molecular structure of nucleic acids; a structure for deoxyribose nucleic acid. Nature. 1953;171(4356):737-8.

152. Franklin RE, Gosling RG. Evidence for 2-chain helix in crystalline structure of sodium deoxyribonucleate. Nature. 1953;172(4369):156-7.

153. Sanger F, Nicklen S, Coulson AR. DNA sequencing with chain-terminating inhibitors. Proc Natl Acad Sci U S A. 1977;74(12):5463-7.

154. Mullis K, Faloona F, Scharf S, Saiki R, Horn G, Erlich H. Specific enzymatic amplification of DNA in vitro: the polymerase chain reaction. Cold Spring Harb Symp Quant Biol. 1986;51 Pt 1:263-73.

155. McPherson JD, Marra M, Hillier L, Waterston RH, Chinwalla A, Wallis J, Sekhon M, Wylie K, Mardis ER, Wilson RK, Fulton R, Kucaba TA, Wagner-McPherson C, Barbazuk WB, Gregory SG, Humphray SJ, French L, Evans RS, Bethel G, Whittaker A, Holden JL, McCann OT, Dunham A, Soderlund C, Scott CE, Bentley DR, Schuler G, Chen HC, Jang W, Green ED, Idol JR, Maduro VV, Montgomery KT, Lee E, Miller A, Emerling S, Kucherlapati, Gibbs R, Scherer S, Gorrell JH, Sodergren E, Clerc-Blankenburg K, Tabor P, Naylor S, Garcia D, de Jong PJ, Catanese JJ, Nowak N, Osoegawa K, Qin S, Rowen L, Madan A, Dors M, Hood L, Trask B, Friedman C, Massa H, Cheung VG, Kirsch IR, Reid T, Yonescu R, Weissenbach J, Bruls T, Heilig R, Branscomb E, Olsen A, Doggett N, Cheng JF, Hawkins T, Myers RM, Shang J, Ramirez L, Schmutz J, Velasquez O, Dixon K, Stone NE, Cox DR, Haussler D, Kent WJ, Furey T, Rogic S, Kennedy S, Jones S, Rosenthal A, Wen G, Schilhabel M, Gloeckner G, Nyakatura G, Siebert R, Schlegelberger B, Korenberg J, Chen XN, Fujiyama A, Hattori M, Toyoda A, Yada T, Park HS, Sakaki Y, Shimizu N, Asakawa S, Kawasaki K, Sasaki T, Shintani A, Shimizu A, Shibuya K, Kudoh J, Minoshima S, Ramser J, Seranski P, Hoff C, Poustka A, Reinhardt R, Lehrach H, International

Human Genome Mapping C. A physical map of the human genome. Nature. 2001;409(6822):934-41.

156. Bentley DR, Balasubramanian S, Swerdlow HP, Smith GP, Milton J, Brown CG, Hall KP, Evers DJ, Barnes CL, Bignell HR, Boutell JM, Bryant J, Carter RJ, Keira Cheetham R, Cox AJ, Ellis DJ, Flatbush MR, Gormley NA, Humphray SJ, Irving LJ, Karbelashvili MS, Kirk SM, Li H, Liu X, Maisinger KS, Murray LJ, Obradovic B, Ost T, Parkinson ML, Pratt MR, Rasolonjatovo IM, Reed MT, Rigatti R, Rodighiero C, Ross MT, Sabot A, Sankar SV, Scally A, Schroth GP, Smith ME, Smith VP, Spiridou A, Torrance PE, Tzonev SS, Vermaas EH, Walter K, Wu X, Zhang L, Alam MD, Anastasi C, Aniebo IC, Bailey DM, Bancarz IR, Banerjee S, Barbour SG, Baybayan PA, Benoit VA, Benson KF, Bevis C, Black PJ, Boodhun A, Brennan JS, Bridgham JA, Brown RC, Brown AA, Buermann DH, Bundu AA, Burrows JC, Carter NP, Castillo N, Chiara ECM, Chang S, Neil Cooley R, Crake NR, Dada OO, Diakoumakos KD, Dominguez-Fernandez B, Earnshaw DJ, Egbujor UC, Elmore DW, Etchin SS, Ewan MR, Fedurco M, Fraser LJ, Fuentes Fajardo KV, Scott Furey W, George D, Gietzen KJ, Goddard CP, Golda GS, Granieri PA, Green DE, Gustafson DL, Hansen NF, Harnish K, Haudenschild CD, Heyer NI, Hims MM, Ho JT, Horgan AM, Hoschler K, Hurwitz S, Ivanov DV, Johnson MQ, James T, Huw Jones TA, Kang GD, Kerelska TH, Kersey AD, Khrebtukova I, Kindwall AP, Kingsbury Z, Kokko-Gonzales PI, Kumar A, Laurent MA, Lawley CT, Lee SE, Lee X, Liao AK, Loch JA, Lok M, Luo S, Mammen RM, Martin JW, McCauley PG, McNitt P, Mehta P, Moon KW, Mullens JW, Newington T, Ning Z, Ling Ng B, Novo SM, O'Neill MJ,

Osborne MA, Osnowski A, Ostadan O, Paraschos LL, Pickering L, Pike AC, Pike AC, Chris Pinkard D, Pliskin DP, Podhasky J, Quijano VJ, Raczy C, Rae VH, Rawlings SR, Chiva Rodriguez A, Roe PM, Rogers J, Rogert Bacigalupo MC, Romanov N, Romieu A, Roth RK, Rourke NJ, Ruediger ST, Rusman E, Sanches-Kuiper RM, Schenker MR, Seoane JM, Shaw RJ, Shiver MK, Short SW, Sizto NL, Sluis JP, Smith MA, Ernest Sohna Sohna J, Spence EJ, Stevens K, Sutton N, Szajkowski L, Tregidgo CL, Turcatti G, Vandevondele S, Verhovsky Y, Virk SM, Wakelin S, Walcott GC, Wang J, Worsley GJ, Yan J, Yau L, Zuerlein M, Rogers J, Mullikin JC, Hurles ME, McCooke NJ, West JS, Oaks FL, Lundberg PL, Klenerman D, Durbin R, Smith AJ. Accurate whole human genome sequencing using reversible terminator chemistry. Nature. 2008;456(7218):53-9.

157. Mansour SL, Thomas KR, Capecchi MR. Disruption of the proto-oncogene int-2 in mouse embryo-derived stem cells: a general strategy for targeting mutations to non-selectable genes. Nature. 1988;336(6197):348-52.

158. Rudin N, Sugarman E, Haber JE. Genetic and physical analysis of double-strand break repair and recombination in Saccharomyces cerevisiae. Genetics. 1989;122(3):519-34.

159. Plessis A, Perrin A, Haber JE, Dujon B. Site-specific recombination determined by I-SceI, a mitochondrial group I intron-encoded endonuclease expressed in the yeast nucleus. Genetics. 1992;130(3):451-60.

160. Rouet P, Smih F, Jasin M. Introduction of double-strand breaks into the genome of mouse cells by expression of a rare-cutting endonuclease. Mol Cell Biol. 1994;14(12):8096-106.

161. Kameshima W, Ishizuka T, Minoshima M, Yamamoto M, Sugiyama H, Xu Y, Komiyama M. Conjugation of peptide nucleic acid with a pyrrole/imidazole polyamide to specifically recognize and cleave DNA. Angew Chem Int Ed Engl. 2013;52(51):13681-4.

162. Jabalameli HR, Zahednasab H, Karimi-Moghaddam A, Jabalameli MR. Zinc finger nuclease technology: advances and obstacles in modelling and treating genetic disorders. Gene. 2015;558(1):1-5.

163. Joung JK, Sander JD. TALENs: a widely applicable technology for targeted genome editing. Nat Rev Mol Cell Biol. 2013;14(1):49-55.

164. Ishino Y, Shinagawa H, Makino K, Amemura M, Nakata A. Nucleotide sequence of the iap gene, responsible for alkaline phosphatase isozyme conversion in Escherichia coli, and identification of the gene product. J Bacteriol. 1987;169(12):5429-33.

165. Mojica FJ, Diez-Villasenor C, Soria E, Juez G. Biological significance of a family of regularly spaced repeats in the genomes of Archaea, Bacteria and mitochondria. Mol Microbiol. 2000;36(1):244-6.

166. Mojica FJ, Diez-Villasenor C, Garcia-Martinez J, Soria E. Intervening sequences of regularly spaced prokaryotic repeats derive from foreign genetic elements. J Mol Evol. 2005;60(2):174-82.

167. Makarova KS, Wolf YI, Alkhnbashi OS, Costa F, Shah SA, Saunders SJ, Barrangou R, Brouns SJ, Charpentier E, Haft DH, Horvath P, Moineau S, Mojica FJ, Terns RM, Terns MP, White MF, Yakunin AF, Garrett RA, van der Oost J, Backofen R, Koonin EV. An updated evolutionary classification of CRISPR-Cas systems. Nat Rev Microbiol. 2015;13(11):722-36.

168. Makarova KS, Grishin NV, Shabalina SA, Wolf YI, Koonin EV. A putative RNA-interference-based immune system in prokaryotes: computational analysis of the predicted enzymatic machinery, functional analogies with eukaryotic RNAi, and hypothetical mechanisms of action. Biol Direct. 2006;1:7.

169. Barrangou R, Fremaux C, Deveau H, Richards M, Boyaval P, Moineau S, Romero DA, Horvath P. CRISPR provides acquired resistance against viruses in prokaryotes. Science. 2007;315(5819):1709-12.

170. Brouns SJ, Jore MM, Lundgren M, Westra ER, Slijkhuis RJ, Snijders AP, Dickman MJ, Makarova KS, Koonin EV, van der Oost J. Small CRISPR RNAs guide antiviral defense in prokaryotes. Science. 2008;321(5891):960-4.

171. Marraffini LA, Sontheimer EJ. CRISPR interference limits horizontal gene transfer in staphylococci by targeting DNA. Science. 2008;322(5909):1843-5.

172. Garneau JE, Dupuis ME, Villion M, Romero DA, Barrangou R, Boyaval P, Fremaux C, Horvath P, Magadan AH, Moineau S. The CRISPR/Cas bacterial immune system cleaves bacteriophage and plasmid DNA. Nature. 2010;468(7320):67-71.

173. Deltcheva E, Chylinski K, Sharma CM, Gonzales K, Chao Y, Pirzada ZA, Eckert MR, Vogel J, Charpentier E. CRISPR RNA maturation by trans-encoded small RNA and host factor RNase III. Nature. 2011;471(7340):602-7.

174. Sapranauskas R, Gasiunas G, Fremaux C, Barrangou R, Horvath P, Siksnys V. The Streptococcus thermophilus CRISPR/Cas system provides immunity in Escherichia coli. Nucleic Acids Res. 2011;39(21):9275-82.

175. Gasiunas G, Barrangou R, Horvath P, Siksnys V. Cas9-crRNA ribonucleoprotein complex mediates specific DNA cleavage for adaptive immunity in bacteria. Proc Natl Acad Sci U S A. 2012;109(39):E2579-86.

176. Jinek M, Chylinski K, Fonfara I, Hauer M, Doudna JA, Charpentier E. A programmable dual-RNA-guided DNA endonuclease in adaptive bacterial immunity. Science. 2012;337(6096):816-21.

177. Cong L, Ran FA, Cox D, Lin S, Barretto R, Habib N, Hsu PD, Wu X, Jiang W, Marraffini LA, Zhang F. Multiplex genome engineering using CRISPR/Cas systems. Science. 2013;339(6121):819-23.

178. Uyhazi KE, Bennett J. A CRISPR view of the 2020 Nobel Prize in Chemistry. J Clin Invest. 2020.

179. Khan S, Mahmood MS, Rahman SU, Zafar H, Habibullah S, Khan Z, Ahmad A. CRISPR/Cas9: the Jedi against the dark empire of diseases. J Biomed Sci. 2018;25(1):29.

180. Ceccaldi R, Rondinelli B, D'Andrea AD. Repair Pathway Choices and Consequences at the Double-Strand Break. Trends Cell Biol. 2016;26(1):52-64.

181. Doudna JA, Charpentier E. Genome editing. The new frontier of genome engineering with CRISPR-Cas9. Science. 2014;346(6213):1258096.

182. Pawelczak KS, Gavande NS, VanderVere-Carozza PS, Turchi JJ. Modulating DNA Repair Pathways to Improve Precision Genome Engineering. ACS Chem Biol. 2018;13(2):389-96.

183. Hustedt N, Durocher D. The control of DNA repair by the cell cycle. Nat Cell Biol. 2016;19(1):1-9.

184. National Academies of Sciences E, and Medicine. Human Genome Editing: Science, Ethics, and Governance. Washington D.C.: The National Academies Press; 2017.

185. Li JR, Walker S, Nie JB, Zhang XQ. Experiments that led to the first gene-edited babies: the ethical failings and the urgent need for better governance. J Zhejiang Univ Sci B. 2019;20(1):32-8.

186. Zhou M, Greenhill S, Huang S, Silva TK, Sano Y, Wu S, Cai Y, Nagaoka Y, Sehgal M, Cai DJ, Lee YS, Fox K, Silva AJ. CCR5 is a suppressor for cortical plasticity and hippocampal learning and memory. Elife. 2016;5.

187. Richards DY, Winn SR, Dudley S, Nygaard S, Mighell TL, Grompe M, Harding CO. AAV-Mediated CRISPR/Cas9 Gene Editing in Murine Phenylketonuria. Mol Ther Methods Clin Dev. 2020;17:234-45.

188. Cazzorla C, Bensi G, Biasucci G, Leuzzi V, Manti F, Musumeci A, Papadia F, Stoppioni V, Tummolo A, Vendemiale M, Polo G, Burlina A. Living with phenylketonuria in adulthood: The PKU ATTITUDE study. Mol Genet Metab Rep. 2018;16:39-45.

189. Lichter-Konecki U, Vockley J. Phenylketonuria: Current Treatments and Future Developments. Drugs. 2019.

190. Vockley J, Andersson HC, Antshel KM, Braverman NE, Burton BK, Frazier DM, Mitchell J, Smith WE, Thompson BH, Berry SA, American College of Medical G, Genomics Therapeutics C. Phenylalanine hydroxylase deficiency: diagnosis and management guideline. Genet Med. 2014;16(2):188-200.

191. Singh RH, Cunningham AC, Mofidi S, Douglas TD, Frazier DM, Hook DG, Jeffers L, McCune H, Moseley KD, Ogata B, Pendyal S, Skrabal J, Splett PL, Stembridge A, Wessel A, Rohr F. Updated, web-based nutrition management guideline for PKU: An evidence and consensus based approach. Mol Genet Metab. 2016;118(2):72-83.

192. Greene CL, Longo N. National Institutes of Health (NIH) review of evidence in phenylalanine hydroxylase deficiency (phenylketonuria) and recommendations/guidelines for therapy from the American College of Medical Genetics (ACMG) and Genetics Metabolic Dietitians International (GMDI). Mol Genet Metab. 2014;112(2):85-6.

193. Lichter-Konecki U, Vockley J. Phenylketonuria: Current Treatments and Future Developments. Drugs. 2019;79(5):495-500.

194. Feldmann R, Osterloh J, Onon S, Fromm J, Rutsch F, Weglage J. Neurocognitive functioning in adults with phenylketonuria: Report of a 10-year follow-up. Mol Genet Metab. 2018.

195. Stone WL, Los E. Phenylketonuria. StatPearls. Treasure Island (FL)2019.

196. Gupta S, Lau K, Harding CO, Shepherd G, Boyer R, Atkinson JP, Knight V, Olbertz J, Larimore K, Gu Z, Li M, Rosen O, Zoog SJ, Weng HH, Schweighardt B. Association of immune response with efficacy and safety outcomes in adults with phenylketonuria administered pegvaliase in phase 3 clinical trials. EBioMedicine. 2018;37:366-73.

197. Harding CO, Amato RS, Stuy M, Longo N, Burton BK, Posner J, Weng HH, Merilainen M, Gu Z, Jiang J, Vockley J, Investigators P-. Pegvaliase for the treatment of phenylketonuria: A pivotal, double-blind randomized discontinuation Phase 3 clinical trial. Mol Genet Metab. 2018;124(1):20-6.

198. Thomas J, Levy H, Amato S, Vockley J, Zori R, Dimmock D, Harding CO, Bilder DA, Weng HH, Olbertz J, Merilainen M, Jiang J, Larimore K, Gupta S, Gu Z, Northrup H, investigators P. Pegvaliase for the treatment of phenylketonuria: Results of a long-term phase 3 clinical trial program (PRISM). Mol Genet Metab. 2018;124(1):27-38.

199. Mingozzi F, High KA. Therapeutic in vivo gene transfer for genetic disease using AAV: progress and challenges. Nat Rev Genet. 2011;12(5):341-55.

200. Embury JE, Charron CE, Martynyuk A, Zori AG, Liu B, Ali SF, Rowland NE, Laipis PJ. PKU is a reversible neurodegenerative process within the nigrostriatum that begins as early as 4 weeks of age in Pah(enu2) mice. Brain Res. 2007;1127(1):136-50.

201. Hsu PD, Lander ES, Zhang F. Development and applications of CRISPR-Cas9 for genome engineering. Cell. 2014;157(6):1262-78.

202. Yang Y, Wang L, Bell P, McMenamin D, He Z, White J, Yu H, Xu C, Morizono H, Musunuru K, Batshaw ML, Wilson JM. A dual AAV system enables the Cas9-mediated correction of a metabolic liver disease in newborn mice. Nat Biotechnol. 2016;34(3):334-8.

203. Paulk NK, Loza LM, Finegold MJ, Grompe M. AAV-mediated gene targeting is significantly enhanced by transient inhibition of nonhomologous end joining or the proteasome in vivo. Hum Gene Ther. 2012;23(6):658-65.

204. Fiori E, Oddi D, Ventura R, Colamartino M, Valzania A, D'Amato FR, Bruinenberg V, van der Zee E, Puglisi-Allegra S, Pascucci T. Early-onset behavioral and neurochemical deficits in the genetic mouse model of phenylketonuria. PLoS One. 2017;12(8):e0183430.

205. Chuah MK, Petrus I, De Bleser P, Le Guiner C, Gernoux G, Adjali O, Nair N, Willems J, Evens H, Rincon MY, Matrai J, Di Matteo M, Samara-Kuko E, Yan B, Acosta-Sanchez A, Meliani A, Cherel G, Blouin V, Christophe O, Moullier P, Mingozzi F, VandenDriessche T. Liver-specific transcriptional modules identified by genome-wide in silico analysis enable efficient gene therapy in mice and non-human primates. Mol Ther. 2014;22(9):1605-13.

206. Nair N, Rincon MY, Evens H, Sarcar S, Dastidar S, Samara-Kuko E, Ghandeharian O, Man Viecelli H, Thony B, De Bleser P, VandenDriessche T, Chuah MK. Computationally designed liver-specific transcriptional modules and hyperactive factor IX improve hepatic gene therapy. Blood. 2014;123(20):3195-9.

207. McDonald JD, Dyer CA, Gailis L, Kirby ML. Cardiovascular defects among the progeny of mouse phenylketonuria females. Pediatr Res. 1997;42(1):103-7.

208. Cunningham SC, Spinoulas A, Carpenter KH, Wilcken B, Kuchel PW, Alexander IE. AAV2/8-mediated Correction of OTC Deficiency Is Robust in Adult but Not Neonatal Spfash Mice. Mol Ther. 2009;17(8):1340-6.

209. Wang L, Bell P, Lin J, Calcedo R, Tarantal AF, Wilson JM. AAV8-mediated hepatic gene transfer in infant rhesus monkeys (Macaca mulatta). Mol Ther. 2011;19(11):2012-20.

210. Platt LD, Koch R, Hanley WB, Levy HL, Matalon R, Rouse B, Trefz F, de la Cruz F, Guttler F, Azen C, Friedman EG. The international study of pregnancy outcome in women with maternal phenylketonuria: report of a 12-year study. Am J Obstet Gynecol. 2000;182(2):326-33.

211. Zeile WL, McCune HC, Musson DG, O'Donnell B, O'Neill CA, Tsuruda LS, Zori RT, Laipis PJ. Maternal phenylketonuria syndrome: studies in mice suggest a potential approach to a continuing problem. Pediatr Res. 2018;83(4):889-96.

212. Chang HHY, Pannunzio NR, Adachi N, Lieber MR. Non-homologous DNA end joining and alternative pathways to double-strand break repair. Nat Rev Mol Cell Biol. 2017;18(8):495-506.

213. Ohmori T, Nagao Y, Mizukami H, Sakata A, Muramatsu SI, Ozawa K, Tominaga SI, Hanazono Y, Nishimura S, Nureki O, Sakata Y. CRISPR/Cas9-mediated genome editing via postnatal administration of AAV vector cures haemophilia B mice. Scientific reports. 2017;7(1):4159.

214. Yin H, Xue W, Chen S, Bogorad RL, Benedetti E, Grompe M, Koteliansky V, Sharp PA, Jacks T, Anderson DG. Genome editing with Cas9 in adult mice corrects a disease mutation and phenotype. Nat Biotechnol. 2014;32(6):551-3.

215. Tham KC, Kanaar R, Lebbink JHG. Mismatch repair and homeologous recombination. DNA Repair (Amst). 2016;38:75-83.

216. Hamman KJ, Winn SR, Harding CO. Hepatocytes from wild-type or heterozygous donors are equally effective in achieving successful therapeutic liver repopulation in murine phenylketonuria (PKU). Molecular genetics and metabolism. 2011;104(3):235-40.

217. Duncan AW, Taylor MH, Hickey RD, Hanlon Newell AE, Lenzi ML, Olson SB, Finegold MJ, Grompe M. The ploidy conveyor of mature hepatocytes as a source of genetic variation. Nature. 2010;467(7316):707-10.

218. Duncan AW. Aneuploidy, polyploidy and ploidy reversal in the liver. Semin Cell Dev Biol. 2013;24(4):347-56.

219. Kurinna S, Stratton SA, Coban Z, Schumacher JM, Grompe M, Duncan AW, Barton MC. p53 regulates a mitotic transcription program and determines ploidy in normal mouse liver. Hepatology. 2013;57(5):2004-13.

220. Trefts E, Gannon M, Wasserman DH. The liver. Curr Biol. 2017;27(21):R1147-R51.

221. Bell P, Wang L, Gao G, Haskins ME, Tarantal AF, McCarter RJ, Zhu Y, Yu H, Wilson JM. Inverse zonation of hepatocyte transduction with AAV vectors between mice and non-human primates. Mol Genet Metab. 2011;104(3):395-403.

222. Himmelreich N, Shen N, Okun JG, Thiel C, Hoffmann GF, Blau N. Relationship between genotype, phenylalanine hydroxylase expression and in vitro activity and metabolic phenotype in phenylketonuria. Mol Genet Metab. 2018;125(1-2):86-95.

223. Villiger L, Grisch-Chan HM, Lindsay H, Ringnalda F, Pogliano CB, Allegri G, Fingerhut R, Haberle J, Matos J, Robinson MD, Thony B, Schwank G. Treatment of a metabolic liver disease by in vivo genome base editing in adult mice. Nat Med. 2018;24(10):1519-25.

224. McDonald JD, Bode VC, Dove WF, Shedlovsky A. Pahhph-5: a mouse mutant deficient in phenylalanine hydroxylase. Proc Natl Acad Sci U S A. 1990;87(5):1965-7.

225. Kleven MD, Gomes MM, Wortham AM, Enns CA, Kahl CA. Ultrafiltered recombinant AAV8 vector can be safely administered in vivo and efficiently transduces liver. PLoS One. 2018;13(4):e0194728.

226. McCaman MW RE. Fluorimetric method for the determination of phenylalanine in serum. J Lab Clin Med 1962;59:885–90.

227. Ledley FD, Hahn T, Woo SL. Selection for phenylalanine hydroxylase activity in cells transformed with recombinant retroviruses. Somat Cell Mol Genet. 1987;13(2):145-54.

228. Harding CO, Wild K, Chang D, Messing A, Wolff JA. Metabolic engineering as therapy for inborn errors of metabolism--development of mice

with phenylalanine hydroxylase expression in muscle. Gene Ther. 1998;5(5):677-83.

229. Bae S, Park J, Kim JS. Cas-OFFinder: a fast and versatile algorithm that searches for potential off-target sites of Cas9 RNA-guided endonucleases. Bioinformatics. 2014;30(10):1473-5.

230. Cradick TJ, Qiu P, Lee CM, Fine EJ, Bao G. COSMID: A Web-based Tool for Identifying and Validating CRISPR/Cas Off-target Sites. Mol Ther Nucleic Acids. 2014;3:e214.

231. Zhang J, Kobert K, Flouri T, Stamatakis A. PEAR: a fast and accurate Illumina Paired-End reAd mergeR. Bioinformatics. 2014;30(5):614-20.

232. Martin M. Cutadapt removes adapter sequences from high-throughput sequencing reads. EMBnet 2011;17:10–2.

233. Mighell TL, Evans-Dutson S, O'Roak BJ. A Saturation Mutagenesis Approach to Understanding PTEN Lipid Phosphatase Activity and Genotype-Phenotype Relationships. Am J Hum Genet. 2018;102(5):943-55.

234. Pinello L, Canver MC, Hoban MD, Orkin SH, Kohn DB, Bauer DE, Yuan GC. Analyzing CRISPR genome-editing experiments with CRISPResso. Nat Biotechnol. 2016;34(7):695-7.

235. Nakai H, Yant SR, Storm TA, Fuess S, Meuse L, Kay MA. Extrachromosomal recombinant adeno-associated virus vector genomes are

primarily responsible for stable liver transduction in vivo. J Virol. 2001;75(15):6969-76.

236. Overturf K, Al-Dhalimy M, Tanguay R, Brantly M, Ou CN, Finegold M, Grompe M. Hepatocytes corrected by gene therapy are selected in vivo in a murine model of hereditary tyrosinaemia type I. Nat Genet. 1996;12(3):266-73.

237. Miller DG, Wang PR, Petek LM, Hirata RK, Sands MS, Russell DW. Gene targeting in vivo by adeno-associated virus vectors. Nat Biotechnol. 2006;24(8):1022-6.

238. Kietzmann T. Metabolic zonation of the liver: The oxygen gradient revisited. Redox Biol. 2017;11:622-30.

239. Paulk NK, Wursthorn K, Haft A, Pelz C, Clarke G, Newell AH, Olson SB, Harding CO, Finegold MJ, Bateman RL, Witte JF, McClard R, Grompe M. In vivo selection of transplanted hepatocytes by pharmacological inhibition of fumarylacetoacetate hydrolase in wild-type mice. Mol Ther. 2012;20(10):1981-7.

240. Paulk NK, Wursthorn K, Wang Z, Finegold MJ, Kay MA, Grompe M. Adeno-associated virus gene repair corrects a mouse model of hereditary tyrosinemia in vivo. Hepatology. 2010;51(4):1200-8.

241. Al-Dhalimy M, Overturf K, Finegold M, Grompe M. Long-term therapy with NTBC and tyrosine-restricted diet in a murine model of hereditary tyrosinemia type I. Mol Genet Metab. 2002;75(1):38-45.

242. Grompe M, al-Dhalimy M, Finegold M, Ou CN, Burlingame T, Kennaway NG, Soriano P. Loss of fumarylacetoacetate hydrolase is responsible for the neonatal hepatic dysfunction phenotype of lethal albino mice. Genes Dev. 1993;7(12A):2298-307.

243. Chinsky JM, Singh R, Ficicioglu C, van Karnebeek CDM, Grompe M, Mitchell G, Waisbren SE, Gucsavas-Calikoglu M, Wasserstein MP, Coakley K, Scott CR. Diagnosis and treatment of tyrosinemia type I: a US and Canadian consensus group review and recommendations. Genet Med. 2017;19(12).

244. Morrow G, Tanguay RM. Biochemical and Clinical Aspects of Hereditary Tyrosinemia Type 1. Adv Exp Med Biol. 2017;959:9-21.

245. Tanguay RM, Angileri F, Vogel A. Molecular Pathogenesis of Liver Injury in Hereditary Tyrosinemia 1. Adv Exp Med Biol. 2017;959:49-64.

246. Richards DY, Winn SR, Dudley S, Fedorov L, Rimann N, Thony B, Harding CO. A novel Pah-exon1 deleted murine model of phenylalanine hydroxylase (PAH) deficiency. Mol Genet Metab. 2020.

247. Waters PJ, Scriver CR, Parniak MA. Homomeric and heteromeric interactions between wild-type and mutant phenylalanine hydroxylase subunits: evaluation of two-hybrid approaches for functional analysis of mutations causing hyperphenylalaninemia. Mol Genet Metab. 2001;73(3):230-8.

248. Grisch-Chan HM, Schlegel A, Scherer T, Allegri G, Heidelberger R, Tsikrika P, Schmeer M, Schleef M, Harding CO, Haberle J, Thony B. Low-Dose

Gene Therapy for Murine PKU Using Episomal Naked DNA Vectors Expressing PAH from Its Endogenous Liver Promoter. Mol Ther Nucleic Acids. 2017;7:339-49.

249. Harding CO, Gibson KM. Therapeutic liver repopulation for phenylketonuria. J Inherit Metab Dis. 2010;33(6):681-7.

250. Kaufman S, Max EE, Kang ES. Phenylalanine hydroxylase activity in liver biopsies from hyperphenylalaninemia heterozygotes: deviation from proportionality with gene dosage. Pediatr Res. 1975;9(8):632-4.

251. Hogan B BR, Costantini F, Lacy E. Recovery, culture, and transfer of embryos and germ cells. Cold Spring Harbor Press. 1994;Manipulating the Mouse Embryo: A Laboratory Manual. :p. 127–88.

252. Qin W, Kutny PM, Maser RS, Dion SL, Lamont JD, Zhang Y, Perry GA, Wang H. Generating Mouse Models Using CRISPR-Cas9-Mediated Genome Editing. Curr Protoc Mouse Biol. 2016;6(1):39-66.

253. Remy S, Chenouard V, Tesson L, Usal C, Menoret S, Brusselle L, Heslan JM, Nguyen TH, Bellien J, Merot J, De Cian A, Giovannangeli C, Concordet JP, Anegon I. Generation of gene-edited rats by delivery of CRISPR/Cas9 protein and donor DNA into intact zygotes using electroporation. Sci Rep. 2017;7(1):16554.

254. Elzaouk L, Leimbacher W, Turri M, Ledermann B, Burki K, Blau N, Thony B. Dwarfism and low insulin-like growth factor-1 due to dopamine depletion in

Pts-/- mice rescued by feeding neurotransmitter precursors and H4-biopterin. J Biol Chem. 2003;278(30):28303-11.

255. Blau N, Thony B, Renneberg A, Penzien JM, Hyland K, Hoffmann GF. Variant of dihydropteridine reductase deficiency without hyperphenylalaninaemia: effect of oral phenylalanine loading. J Inherit Metab Dis. 1999;22(3):216-20.

256. Yeh CD, Richardson CD, Corn JE. Advances in genome editing through control of DNA repair pathways. Nat Cell Biol. 2019;21(12):1468-78.

Biography

Education

Washington State University Elson S. Floyd College of Medicine 2019-2023

Medical Doctor

Main campus (MS1 & MS2): Spokane, Washington

Clinical campus (MS3 & MS4): Vancouver, Washington

Oregon Health & Science University 2014-2020

Doctor of Philosophy in Molecular & Medical Genetics

Portland, Oregon

Portland State University 2012-2014

Bachelor of Science in Microbiology and Chemistry, with Honors

Portland, Oregon

Portland Community College 2010-2012

Associates of Arts-Oregon Transfer, Dean's List

Portland, Oregon

Research Experience

Oregon Health & Science University – **Harding Lab** (Genetics) 2014-2020

Focus: Advancing the field of PKU gene therapy by testing novel genome modifying technologies in PKU mice and generating a superior mouse model to test PKU gene therapy technologies.

Oregon Health & Science University – **Nakai Lab** (Virology) 2014-2016

Focus: Adeno-associated virus (AAV) virology research aimed at identifying a stealth AAV capsid capable of evading human AAV-neutralizing antibodies by using mutant AAV libraries with the barcode technology in directed-evolution with collated human intravenous immunoglobulin (IVIg).

Portland State University – **Lutterschmidt Lab** (Endocrinology) 2013-2014

Focus: Behavioral endocrinology research looking at the neuromodulatory effects of Neuropeptide Y (NPY) and Arginine Vasotocin (AVT) on seasonal behavioral life transitions in the red-sided garter snake, *Thamnophis sirtalis*.

Portland Community College – **DeGrauw** (Herpetology) 2011

Focus: Field ecology herpetology research in the Alvord Desert in Southeast Oregon and Nevada's Great Basin region studying sexual dimorphic characteristics in the desert horned lizard, *Phrynosoma platyrhinos*.

Publications

Richards, Daelyn Y., Winn, Shelley R., Dudley, S., Nygaard, S., Mighell, Taylor L., Grompe, M., Harding, Cary O. *AAV-Mediated CRISPR/Cas9 Gene Editing in Murine Phenylketonuria.* Molecular Therapy: Methods and Clinical Development, 2020. 17: p. 234-245.

Richards, Daelyn Y., Winn, Shelley R., Dudley, S., Fedorov, L., Rimann, N., Thöny, B., Harding, Cary O. *A novel Pah-exon1 deleted murine model of phenylalanine hydroxylase (PAH) deficiency.* Molecular Genetics and Metabolism, 2020. 131(3): p. 306-315.

Lucas, Ashley R., **Richards, Daelyn Y.,** Ramirez, Lucy M., Lutterschmidt, Deborah I. *Arginine vasotocin and neuropeptide Y vary with seasonal life-history transitions in garter snakes.* Integrative and Comparative Biology, 2017. 57(6): p. 1166-1183.

First-Author Posters and Abstracts

Abstract

Richards, Daelyn Y., Winn, Shelley R., Dudley, Sandra., Nygaard, Sean., Grompe, Markus**.,** Harding, Cary O. 2019. **"**Therapeutic CRISPR/Cas9-Mediated Gene Editing in Murine Phenylketonuria (PKU)." Japan Society for Inherited Metabolic Disorders Annual Conference. Akita, Japan

Abstract

Richards, Daelyn Y., Winn, Shelley R., Dudley, Sandra., Nygaard, Sean., Grompe, Markus**.,** Harding, Cary O. 2019. **"**Successful CRISPR/Cas9-Mediated Gene Editing in Murine Phenylketonuria (PKU)." Society for Inherited Metabolic Disorders Annual Conference. Bellevue, Washington.

Poster

Richards, Daelyn Y., Winn, Shelley R., Dudley, Sandra., Nygaard, Sean., Mighell, Taylor., O'Roak, Brian., Grompe, Markus., Harding, Cary O. 2018. "CRISPR/Cas9 in Murine Phenylketonuria (PKU)." Oregon Health & Science University. PMCB Recruitment. Portland, Oregon.

Poster

Richards, Daelyn Y., Winn, Shelley R., Dudley, Sandra., Nygaard, Sean., Grompe, Markus., Harding, Cary O. 2018. **"**Successful CRISPR/Cas9-Mediated Gene Editing in Murine Phenylketonuria (PKU)." Oregon Health & Science University Gene Therapy Symposium. Portland, Oregon.

Abstract

Richards, Daelyn Y., Winn, Shelley R., Dudley, Sandra., Nygaard, Sean., Grompe, Markus**.,** Harding, Cary O. 2018. **"**Successful CRISPR/Cas9-Mediated Gene Editing in Murine Phenylketonuria (PKU)." American Society for Gene and Cell Therapy Annual Conference. Chicago, Illinois.

Poster

Richards, Daelyn Y., Winn, Shelley R., Dudley, Sandra., Harding, Cary O. 2017. "Progress on CRISPRcas9 Gene Correction in Pah^{enu2} mice." Oregon Health & Science University Gene Therapy Symposium. Portland, Oregon.

Poster

Richards, Daelyn Y., Winn, Shelley R., Dudley, Sandra., Harding, Cary O. 2017. "Adeno-associated viral gene therapy to treat murine PKU." Oregon Health & Science University Program in Molecular & Cellular Biosciences Recruitment & Research Week. Portland, Oregon.

Poster

Richards, Daelyn Y., Adachi, K., Chang, X. L., Nakai, H. 2015. Approach to design knowledge-based neutralizing antibody-escaping adeno-associated virus vectors. Oregon Health & Science University Gene Therapy Symposium. Portland, Oregon.

Poster

Richards, Daelyn Y., Maine, Ashley R., Lutterschmidt, Deborah I. 2014. "Neuropeptide Y: A potential marker for a life-history transition in red-sided garter snakes (*T. sirtalis*)." Portland State University Undergraduate Research Conference. Portland, Oregon.

Co-Author Poster

Bagget, H., Chang, X., **Richards, Daelyn Y.,** Adachi, K., Nakai, H. 2019. "Mapping Anti-AAV2 Antibody Epitopes Using an IP-Seq Barcode Analysis." Oregon Health & Science University Gene Therapy Symposium. Portland, Oregon.

Academic and Professional Presentations

Japan Society of Inherited Metabolic Disorders- Honorarium 2019

Society of Inherited Metabolic Disorders (SIMD) Recommended Lecture.

"Therapeutic CRISPR/Cas9-mediated gene editing in murine phenylketonuria (PKU)." Akita, Japan

PKU Family Camp- Research Update 2019

"Promising Gene Editing for PKU" and "Upcoming PKU Research"

Washington Family Ranch, Antelope, Oregon

Society for Inherited Metabolic Disorders- Oral Presentation 2019

"Successful CRISPR/Cas9-Mediated Gene Editing in Murine Phenylketonuria"

Downtown Hyatt Seattle-Bellevue, Bellevue, Washington

PMCB Recruitment Department Seminar 2019

"Successful CRISPR/Cas9 Gene Editing in Murine PKU"

Oregon Health & Science University, Portland, Oregon

Lift the Limits for PKU New York City- Fundraising Keynote 2018

"Promising Gene Editing for PKU" 7-minute talk raised $100,000

New York Athletic Club, New York City, New York

Molecular & Medical Genetics Departmental Seminar 2019

"Successful CRISPR/Cas9 Gene Editing in Murine PKU"

Oregon Health & Science University, Portland, Oregon

Lift the Limits for PKU New York City- Fundraising Keynote 2018

"Promising Gene Editing for PKU" 7-minute talk raised $200,000

New York Athletic Club, New York City, New York

PKU Family Camp- Research Update 2018

"Promising PKU Gene Editing in a Preclinical Model"

Washington Family Ranch, Antelope, Oregon

National PKU Alliance Annual Meeting- Research Update 2018

"Promising PKU Gene Editing in a Preclinical Model"

Downtown Hilton, Atlanta, Georgia

Research Week Fast Pitch Competition 2018

"No Regerts." 1st Place

Oregon Health & Science University, Portland, Oregon

American Society for Gene and Cell Therapy- Oral Presentation 2018

"Successful CRISPR/Cas9-Mediated Gene Editing in Murine Phenylketonuria"

Downtown Hilton, Chicago, Illinois

Lift the Limits for PKU Denver- Fundraising Keynote 2018

"Promising Gene Editing for PKU" 7-minute talk raised $180,000

Denver Performing Arts Center, Denver, Colorado

OSU Honors Class HC 299: Topics in Health Sciences Research 2018

"PKU Gene Therapy"

Oregon State University, Corvallis, Oregon

PKU Organization of Illinois Annual Meeting- Keynote Address 2017

"AAV Gene Therapy for the Treatment of Rare Disorders"

DoubleTree Suites by Hilton Downers Grove, Chicago, Illinois

Molecular & Medical Genetics Departmental Seminar 2017

"Updates on PKU Gene Therapy"

Oregon Health & Science University, Portland, Oregon

PKU Family Camp- Research Update 2017

"AAV Gene Therapy for PKU"

Washington Family Ranch, Antelope, Oregon

3 Minute Thesis- Statewide Finals 2017

"Microsurgery to Repair PKU Mutations"

University of Oregon, Eugene, Oregon

3 Minute Thesis- OHSU Research Week Competition 2017

"Microsurgery to Repair PKU Mutations"

Oregon Health & Science University Research Week, Portland, Oregon

UO Honors College Class 441H: Current Biomedical Research Topics 2017

"AAV Gene Therapy for the Treatment of Rare Disorders"

University of Oregon, Eugene, Oregon

Molecular & Medical Genetics Departmental Seminar 2017

"Adeno-Associated Viral Gene Therapy to Treat Murine Phenylketonuria"

Oregon Health & Science University, Portland, Oregon

3 Minute Thesis- OHSU Research Week Competition 2016

"PKU Gene Therapy: Pursuing a Cure"

Oregon Health & Science University Research Week, Portland, Oregon

Graduate Awards

2019 Japan Society of Inherited Metabolic Disorders Honorarium

2019 Graduate Student Organization Leadership Award

2019 Molecular & Medical Genetics Travel Award

2019 Society for Inherited Metabolic Disorders Travel Award

2018-2019 OHSU Research Leadership Scholar

2018 1st Place Poster, OHSU Annual Gene Therapy Symposium

2018 1st Place Fast Pitch Competition- OHSU Research Week

2018 Molecular & Medical Genetics Travel Award

2018 American Society for Gene and Cell Therapy Travel Award

2018 Nicholas L. Tartar Research Fellowship

2017 3 Minute Thesis Statewide Finalist

2016 Nicholas L. Tartar Research Fellowship

2015 1st Place Poster, OHSU Annual Gene Therapy Symposium

2014 Program in Molecular and Cellular Biosciences Student Highlight